ADDIS ABABA UNIVERSITY

COLLEGE OF NATURAL AND COMPUTATIONAL SCIENCE

SCHOOL OF EARTH SCIENCE

IMPACTS OF LAND-USE AND LAND-COVER CHANGES ON LAND SURFACE TEMPERATURE DISTRIBUTION IN BAHIR DAR TOWN AND ITS SURROUNDINGS USING REMOTE SENSING

By

ABEL BALEW

(GSR/3946/09)

Advisor

Dr. TESFAYE KORME

A thesis submitted to

The School of Graduate Studies of Addis Ababa University in Partial Fulfillment of the Requirements for the Degree of Masters of Science in Remote Sensing and Geo-informatics

Addis Ababa University

June 2018

IMPACTS OF LAND-USE AND LAND-COVER CHANGES ON LAND SURFACE TEMPERATURE DISTRIBUTION IN BAHIR DAR TOWN AND ITS SURROUNDINGS USING REMOTE SENSING

By

ABEL BALEW BIMREW

(GSR/3946/09)

A thesis submitted to

The School of Graduate Studies of Addis Ababa University in Partial Fulfillment of the Requirements for the Degree of Masters of Science in Remote Sensing and Geo-informatics

Addis Ababa University

June 2018

Addis Ababa University
School of Graduate Studies

This is to certify that thesis prepared by **ABEL BALEW BIMREW**, entitled: "***Impacts of Land-use and Land-cover Changes on Land Surface Temperature Distribution in Bahir Dar Town and its Surroundings Using Remote Sensing***" and submitted in partial fulfillment of the requirements for the degree of Masters of Science in Remote sensing and Geo-informatics complies with the regulations of the University and meets the accepted standards with respect to the originality and quality.

Signed by the Examining committee:

Dr. Tesfaye Korme	_____	_____/_____/_____
Advisor	Signature	Date
Dr. K.V.Suryabhagavan	_____	_____/_____/_____
Chairperson	Signature	Date
Dr. K.V.Suryabhagavan	_____	_____/_____/_____
Examiner	Signature	Date
Prof. M.Balakrishnan	_____	_____/_____/_____
Examiner	Signature	Date

Dedication

I dedicate my thesis work to my little brother, Denberu Balew, who gave his life to educate me. I also dedicate this thesis to my loving friend Alubel Arega, to his encouragement.

Acknowledgment

First, I would like to thank the "**Almighty God**" who gives me strength, patience and trust to complete my study fruitfully.

I express my heartfelt appreciation to my advisor Dr. Tesfaye Korme (Associate Professor), who supported me from the beginning of this research to its compilation and for valuable discussions and advising throughout the study.

My gratitude goes to Dr. Mersha Alemu for his kindly advise and support. I also thank to Dr. Binyam Tesfaw for his generous support at the beginning of this research.

I thank my father Ato Balew Bimrew, and mother Tinagn Belete, and brothers Bayu Balew and Sendeku Balew, for their special supports from lower grade education up to now. I also thank my sister Bethlehem Getie for her strong support. Special thank also goes to all my other family members.

Finally, I have a great gratefulness to Bahir Dar town Municipality and Ethiopian Meteorology Agency Bahir Dar Branch for providing me the necessary data and information for this study. I also appreciate Secretary of Bahir Dar town Municipality and meteorology experts.

Table of Contents

List of Tables

List of Figures

List Appendices

List of Acronyms

6S	Second Simulation of a Satellite Signal in the Solar Spectrum
AVHRR	Advanced Very High Resolution Radiometer
CSA	Central Statistical Agency
DAIS	Digital Airborne Imaging Spectrometer
DEM	Digital Elevation Model
DIP	Digital Image Processing
DN	Digital Number
EFAP	Ethiopian Forest Action Program
ENVI	Environment for Visualizing Images
EPA	Environmental Protection Agency
ERDAS	Earth Resources Data Analysis System
ETM+	Enhanced Thematic Mapper Plus
FAO	Food and Agriculture Organization
GHG	Greenhouse Gasses
GPS	Global Positioning System
HRG	High-resolution Geometrical,
IPCC	Intergovernmental Panel on Climate Change
LP DAAC	Land Processes Distributed Active Archive Center
LSE	Land Surface emissivity
LST	Land Surface Temperature
LULC	Land-use and land-cover
MODIS	Moderate Resolution Imaging Spectroradiometer
MS	Multispectral
MSS	Multispectral Sensor
MWA	Mono Window Algorithm
NASA	National Aeronautics and Space Administration
NDVI	Normalized Difference Vegetation Index
NMA	National Meteorology Agency
NOAA	National Oceanic and Atmospheric Administration
OLI	Operational Land Imagery

PAN	Panchromatic
PV	Proportion of Vegetation
QUAC	Quick Atmospheric Correction
SPOT	Système Pour l'Observation de la Terre
SRTM	Shuttle Radar Topography Mission
SWA	Split Window Algorithm
TIR	Thermal Infrared
TIRS	Thermal Infrared Sensor
TM	Thematic Mapper
TOA	Top of Atmosphere
UHI	Urban Heat Island
UN	United Nations
USGS	United States Geological Survey

Abstract

Spatio-temporal Land-Use and Land-Cover (LULC) changes has been affecting geo-environmental and climate change globally. These extreme changes affect Land Surface Temperature (LST). The present study analyzed the impacts of LULC changes on the distribution of LST in Bahir Dar town and its surrounding. Land-use and land-cover, Normalized Difference Vegetation Index (NDVI) and LST were analyzed from Landsat 5 TM (1987), Landsat 7 ETM+ (2002) and Landsat 8 OLI/TIRS (2017) using remote sensing techniques. Land-use and land-cover changes between 1987 to 2017 were analyzed using remote sensing techniques and the results were validated using ground truth data. Land surface temperature from Landsat 5 TM (1987) and Landsat 7 ETM+ (2002) was analyzed using a Mono-Window Algorithm (MWA). Split-Window Algorithm (SWA) used to generate LST from Landsat 8 TIRS (2017). The result indicates that LULC has been changing in space and time. During 1987-2017, cropland was the dominant land-use which was covered more than 50%. Settlement areas increased from 3.3% in 1987 to 9.13% in 2017. Service, industrial and paved surfaces areas also increased. However, wetland vegetation, shrubland, grassland, forest and water body are degraded. This study shows that LST has been increasing from 1987 to 2017 and its distribution varies spatially due to LULC variation, proximity to Lake Tana and Abay River, wind direction, and nature of topography and elevation. During the study periods, LST of Bahir Dar town and its surrounding varies from 12.35℃-43.01℃. Normalized difference vegetation index and LST have indirect relationship. Cropland located in the east, west, south and southwest parts of Bahir Dar town have high LST. Settlement areas located along Lake Tana and Abay River, and some places in Deq Istifanos Island and Kibran Gebriel Island have low LST. Most central parts of Bahir Dar town and Deq Istifanos Island relatively have high temperature. Land-use and land-cover is a serious problem and it cause raise in LST, particularly rapidly urban expansion increase urban heat island (UHI). Therefore, there should be sound environmental management and thermal refreshing mechanisms.

Keywords: Remote Sensing, Bahir Dar Town, LULC change, NDVI, LST, MWA, SWA

CHAPTER ONE

1. INTRODUCTION

1.1 Background of the Study

Currently, more than half of the world's population live in urban areas, and is expected to be 66% in the year of 2050 (United Nations, 2014). This figure indicates that the urban dwellers have been increasing from time to time. Developing countries especially Africa and Asia contribute more to this rapid increase of urbanization (UN-HABITAT, 2010, 2013). Mainly, from 2010-2015 urbanization in Africa is continuously increasing and predicted to be 56% with the annual increment of 1.1%. In the same way, Ethiopia is one of the nations in Africa where urban dwellers have been increasing from 19% in 2014 and expected to be 38% in 2050. According to 2014 UN report, the urban growth rate of Ethiopia between 2010-2015 was 2.3% (United Nations, 2014).

Such a fast human population growth in urban area (Peter, 1994) has been increasing land-use and land-cover (LULC) changes globally from time to time in magnitude and spatial extent (Defries et al., 2004; Hansen et al., 2013; Lambin et al., 2001; Lambin and Meyfroidt, 2011; Mustard et al., 2012). Because as the population increase the demand for resource utilization increases proportionally and put pressure on natural resources and damage them. Besides, the land has been continuously and extremely depleting due to anthropogenic factors (Brink et al., 2014; Niamir-Fuller et al., 2012) since people could not take care of their land. Besides, rapid population growth exploitation both natural and manmade resources (Bhattacharjee and Nayak, 2003; Sarma et al., 2008).

Changes in land-use and land-cover affect the overall functioning of the earth system at local, regional, and global levels (Defries et al., 2004; Foly et al., 2005; Lambin et al., 2001; Lambin and Meyfroidt, 2011). This in turn brings global change (Feddema et al., 2005; Foly et al., 2005; Kueppers and Snyder, 2012), particularly temperature (IPCC, 2007; Wang et al., 2013) and rainfall (Woldemichael et al., 2012). This is because of global changes affects many parts of geo-environmental systems. In addition to this, changes in the condition and composition of land-cover affect climate, bio-geochemical cycles and energy fluxes, and livelihoods of people. Consequently, such kinds of problems contribute to the climate change (McCarthy et al., 2010) like global warming and absolute change of environmental landscape (Donato et al., 2016).

In most Eastern African countries, LULC has been happening due to the increase of both human and livestock population (Pomeroy et al., 2003). For instance, overpopulation damaging land through overutilizing of land for agricultural activities such as cropping and grazing by their livestock. As a result, land covered by natural vegetation is converted to urban area and built-up lands, farmlands, and grazing lands. Consequently, these cause soil erosion, deforestation, land degradation, loss of biodiversity, (Maitima et al., 2009) and climate change and contributing more to global warming.

As Ethiopia is one of the East Africa countries, the problem of LULC change is very high and it has been increasing from year to year. This is mainly due to population growth (Hurni et al., 2005) and perceptions of local communities towards land management (Belay et al., 2014) which contributes a lot for conversion of landscape and depletion of resources, for instance, forest and its biodiversity, water and soil resources. Furthermore, the country is vulnerable to surface runoff and flooding, and sedimentation (Hurni et al., 2005). Therefore, the land is very dynamic in all parts of the country particularly in Amhara regional state the problem is very severe because the land is not sufficient to support the population of the region. Because of this, forest, shrubland, bushland and grasslands has been heavily damaged and depleted to obtain additional land for settlement, farmland and grazing land.

Therefore, to ensure sustainable LULC and maintain global climate changes, it is crucial to monitor paths of land-use and land-cover change and its dynamism, and predict their possible future conditions (Aadil et al., 2014; Reenberg, 2006). Landscape analysis is, therefore, a suitable approach for monitoring distinct LULC patterns and their changes (Arvor et al., 2013; Defries et al., 2004). Assessing LULC changes is also very significant to analyze its impacts on the Earth's surface, for example, land surface temperature (LST) changes and distributions.

This could be done using remote sensing technology since it is capable of acquiring satellite imageries that help in conducting LULC change detection analysis. It is also capable of acquiring surface temperature synchronously over large areas and allows to assess spatio-temporal distribution of LST. Satellite-based surface thermal information also efficient to analyze spatial and temporal variations between LST and LULC, and their relationships through analyzing data obtained from sensors spectral reflectance (Feyisa et al., 2016; Gluch et al., 2006; Mundia and

Aniya, 2005; Pham and Yamaguchi, 2011; Weng, 2001; Zhao et al., 2016; Zhou et al., 2014). Remote sensing is also very crucial to predict the future conditions of land-use and land-cover and land surface temperature and their resultant effect on the earth's environment.

1.2 Statement of the Problem

The patterns of land-use and the types of land-cover of Bahir Dar town and its surrounding has been changing from time to time due to anthropogenic factors. Land-use and land-cover change particularly rapid increase of built-up areas and impervious surfaces such as asphalt and parking lots at the expense of other land-covers like grassland, forest, shrubland, marshlands and agricultural land of the surrounding areas, increases solar radiation absorption and thermal conductivity. This high radiation on the biophysical surface material makes the town warmer and warmer from time to time. These are the driving cause for the variations of LST, which is very vital to the study of urban climates (Voolgt and Oke, 2003; Wei et al., 2015) like UHI.

Thus, such higher surface temperatures in the urban area increase the demands for air conditioning, and consumptions of both water and electricity, and may change precipitation patterns that lead to alterations to biotic communities. An excess amount of heat may also affect the comfort of urban dwellers and lead to greater health risks (Claus and Mushtaq, 2011). Land surface temperature also modifies the air temperature of the atmospheric boundary layer and is a key component in the surface energy balance of the town and the surrounding areas even though it is influenced by the Lake Tana breathe. Change in urban LST, therefore, can have significant effects on local weather and climate (Claus and Mushtaq, 2011) of Bahir Dar town. This is because the land surface temperature is highly correlated with the patterns of the land-use and, land-cover types their changes (Barsi et al., 2014; Sobrino et al., 2004a; Wang et al., 2015; Weng et al., 2004). These changes, in turn, can have negative effects on landscape aesthetics, energy efficiency, human health and quality of living in urban environments (Yue et al., 2007).

Hence, for sustainable environmental resource management, assessing the land-use practice and the types of land-cover and its impacts is very significant to analyze LST and monitoring and assessing climate change and its related problems. This is because LULC is the most important variable of global changes which affects ecological systems. As a result, the characteristics of LULC and its patterns have imperative impacts on climate, biogeochemistry, hydrology, the

diversity and abundance of terrestrial species, and peoples' livelihoods (Sandra et al., 2017). Moreover, LULC change has become a central component in current plans for monitoring environmental changes and managing natural resources. The study on LULC change, therefore, provides precise information on the spread and status of the world's water bodies, wildlife, forest, grassland, and agricultural resources.

Therefore, in order to alleviate these problems and forwarding better solutions, analyzing LULC change and LST using remote sensing technology is very significant. This is due to the fact that remote sensing is very capable to retrieve LST, land surface emissivity (LSE) and normalized difference vegetation index (NDVI) using different algorithms and analyze the relationship between these parameters as well as the impacts of LULC change on earth's ecosystem. Currently, advanced remote sensing technologies especially provide high-resolution satellite imageries, that enable the system to be powerful in environmental resources monitoring and management. So, by doing this research, it is possible to show the degree to which the environment and climate in Bahir Dar town and its surrounding have changed. Thus, this study aims at assessing the impacts of LULC changes on land surface temperature distribution and changes in Bahir Dar town and its surroundings from 1987-2017.

1.3 Objectives of the Study

1.3.1 General Objective

The general objective of this study is to assess land-use and land-cover changes in Bahir Dar town and its surroundings and to analyze its impact on the distribution and changes of land surface temperature from 1987 to 2017 using remote sensing techniques.

1.3.2 Specific Objectives

The specific objectives of the study were

- To assess land-use and land-cover changes of Bahir Dar Town and its surrounding;
- To examine spatio-temporal variations of land surface temperature of Bahir Dar town and its surrounding;
- To analyze the impacts of land-use and land-cover changes on land surface temperature changes in Bahir Dar town and its neighboring places.

1.4 Significance of the Study

As Bahir Dar town is the fastest growing town in the Amhara Regional State, the pattern and the type of land-use and land-cover changes have been proportionally rapid. Such fast changes on landscape affect LULC of the area and cause land surface temperature increase; and therefore, they entail different land-use and land-use planning, and LST mitigation, adaptation strategies and options. In order to see the change in LST, the types of LULC and their changes have to primarily analyze through applying change detection analysis. Here, satellite data and remote sensing techniques play a great role. Thus, preparing up-to-date LULC map helps for proper land-use and land-use planning, and environmental protection. The result of this study will also be used in decision making and planning with regard to mitigation measures of the impacts of LULC change. Furthermore, the study is significant to analyze spatio-temporal variations of LST, how it may change and why it changes; examine the relationship between LST with NDVI. Information obtained from this study may also be used for spatial planning especially land management and hydrology. Therefore, the result of the study can be used by researchers, environmental and hydrologic expert, policymakers and other stakeholders.

1.5 Scope of the Study

The focus of this study is Bahir Dar town and its surrounding, in the Amhara Regional State of Ethiopia. This area is chosen because on one hand for the past decades Lake Tana and its catchments have been seriously affected by severe and continuous LULC changes. On another hand, Bahir Dar town is currently a rapidly growing town and there is an expansion of built-up areas and impervious surfaces at the expense of other LULC types. Due to the process of urbanization and improper land-use and management and its related problems, LST has been increasing and this causes various socio-economic, environmental and climatic problems. Thus, this study can provide information about the impacts of LULC change on the change and distribution of LST through give emphasis only for the year 1987 to 2017.

1.6 Limitation of the Study

This study made an effort in acquiring all the necessary data collection and processing, interpretation and analysis. However, the thesis work has encountered some restrictions. Google Earth image resolution in 1987 and 2002 were one of the challenges in image classification of the study. However, to solve this problem, Bahir Dar town master plan map and aerial photograph were used as an aid for

image classification. Taking ground control points and observing the type of LULC around the secured place was also another limitation. The tedious process to get data from different governmental organizations was also another limitation of the study.

1.7 Organization of the Thesis

This thesis is organized into six chapters. The first chapter presents the introduction part of the study including the background of the study, statement of the problem, objectives of the study, significance of the study, scope, and limitation of the study. The second chapter describe literature review which give emphasis on concepts about LULC change and their impacts, NDVI, and LST and its algorithms. Chapter three explain the data needed for the research and methods followed to obtain results from the input data. The fourth chapter explains about the major LULC types and their change, spatial and temporal distribution and change of NDVI and LST, and influence of Lake Tana and River Abay for LST distribution. The relationship between LULC with NDVI and LULC with LST, and the correlation between NDVI and LST also present in this chapter. The fifth chapter explains the main discussion on LULC changes, distribution and change of NDVI and LST, and influence of Lake Tana and Abay River to the distribution of LST in the study area. The final chapter presents conclusions and recommendations.

CHAPTER TWO

2. LITERATURE REVIEW

2.1 Basic Concepts of Land-use and Land-cover Changes

According to FAO (2000) and Gregorio (2005), land cover refers to the biophysical cover of the surface of the earth or land, for instance, vegetation covers such as forest, shrub/bushland, and grassland and water. Land cover can also be defined as the attributes of the earth's land surface covered by vegetation, desert, water bodies like lake, sea, ocean, bare soil and ice (Chrysoulakis et al., 2004 and Lambin et al., 2003). Whereas land-use is characterized by the activities, arrangements and inputs people undertake in a certain land cover type to produce, change, modify or maintain it (Gregorio, 2005). Land-use also refers to land is used by humans for different purposes, for example, settlement, industrial area, cropping and grazing. According to Chrysoulakis et al. (2004) and Zubair (2006), land use is the land which employed by human beings for their various needs and exploiting of land cover for different activities like residential and industrial zones, farm and grazing land and mining.

Land-use and land-cover change is, therefore, the modification of Earth's surface (both water bodies and terrestrial areas) through human activities. Land-use and land-cover change can also be expressed as any biophysical change of land-cover like vegetation cover and waterbodies and improper use of land for different activities; for example, for grazing, cropping and irrigation (Quentin et al., 2006). Changes in land-use and land-cover can be grouped into two categories as conversion and modification (FAO, 2000; Gregorio, 2005). Land-use and land-cover conversion refers to change from one land-use and land-cover to another, for example, wetland and water bodies to agricultural fields, forest to residential and industrial areas, cropland and grassland. Modification of LULC refers to some alteration of on the same land-use and land-cover or it is a gradual change of land-use and land-cover; for instance, dense forest to open forest, open forest to scattered tree.

Furthermore, land-use and land-cover changes vary in spatial extent and time. The spatial extent of land-use and land-cover change indicate the location or place where there is a change whereas temporal change refers to the variation of changes from time to time with their attribute.

2.2 Causes and Impacts of Land-use and Land-cover Change

Land-use and land-cover changes occurred due to natural and anthropogenic factors. As the United States Environmental Protection Agency (EPA) (1999) states there were three main driving causes for land-use and land-cover changes. These are (1) natural processes, such as wildfire, climate and atmospheric changes, and pest infestation; (2) direct effects of human activity such as deforestation, soil erosion and reduction of biodiversity which brings land degradation, and construction like road and buildings.; and (3) indirect effects of human activities, like depletion or lowering of water table and contamination of groundwater.

Anthropogenic factors are the major driving forces of land-use and land-cover changes (Brink et al., 2014; Niamir-Fuller et al., 2012) even though there is also a contribution from the natural processes. Land-use and land-cover change is a very complex process (Abate, 2011; Belay, 2002) because its causes and impacts are very closely related; for example, land degradation. Currently, the human-related causes of land-use and land-cover changes are very serious (Agarwal et al., 2002). There are many types of human induced problems for the changes of the surface of the earth.

For example, expansion of agricultural land (Bongers and Tennigkeit, 2010; Brink et al., 2014, Cotula, 2009; Maitima et al., 2009) due to rapid population growth responsible for massive collapse of natural vegetation, loss of biodiversity and land degradation (Donato et al., 2016; Sandra et al., 2017; William and Turner, 1992). Exhausted land is also vulnerable for soil erosion which causes for declining of organic matter in the soil, soil structure degradation and reduction in soil nutrients (Sandra et al., 2017; Shukla et al., 1990; William and Turner, 1992). Extreme land degradation has a severe impact on the productivity of agricultural fields (Aadil et al., 2014). Extreme transformation of forests, grassland, bushland and shrubland brings a reduction of plant species diversity and continuously shrinking of natural wildlife. Intensification of agriculture such as crop and pastoral land towards the natural ecosystem which is related to population growth also contribute for extreme changes of LULC and environment (Lambin and Meyfroidt, 2011).

Moreover, rapid population growth reduces forest areas (since they use as fuelwood and timber) and woodlands (grazing by their livestock). This destruction affects biological diversities and functions ecosystems (Peter, 1994) and causes for climate change which raises the risk for wildfire

(Donato et al., 2016). Yadvinder et al. (2008) also agreed that population expansion causes deforestation and create pressure on forest resilience. This extreme destruction of forestland is a root for climate change at local, regional and global level (Peter, 1994). Deforestation also affects the process of atmosphere and thermodynamics at the earth-atmosphere interface and water storage capacity and soil hydraulic conductivity (Shukla et al., 1990). Besides, changes in land-use and land-cover affect hydrological cycles and its parameters (Shukla et al., 1990; Zhenglei et al., 2009).

Population growth and economic development also destructing wetlands (Zhenglei et al., 2009), which strongly influence hydrological cycles (Yanagi, 2008; Zhao and Lai, 2007), and cause for environmental change (H. Liu et al., 2004; Y. Liu et al., 2004). Furthermore, the hydrological condition of the earth surface changes the physicochemical property of wetland. The scarcity of water, drop of the freshwater source and depletion of the existing groundwater are also problems related to land-use and land-cover changes. These directly or indirectly affect food production, human health, and economic development (Zhenglei et al., 2009).

Moreover, exhaustive use of land and change of land-cover and its patterns vulnerable to soil and land degradation (Temesgen et al., 2014; William and Turner, 1992). This leads for increasing poverty and migration, failure of land productivity, damage of biodiversity and natural resources, deterioration of groundwater recharge and carbon storage capacity, change in population size, and spatial distribution (Abate, 2011). Land-use and land-cover changes also have consequences of soil and land degradation, soil erosion, salinization and desertification (Abbas et al., 2010; William and Turner, 1992). According to William and Turner (1992), soil and land degradation results in soil erosion, salinization, compaction, acidification, nutrient impoverishment, waterlogging and dehumification

Desertification is also another effect of extreme land-use and land-cover. It increases the concentration of carbon-di-oxide in the atmosphere and brings wildfire. Therefore, incidences of forest fire related to land-use and land-cover degradation/change increase the emission of toxic gasses (GHG) such as carbon monoxide and nitric oxide which alter the chemistry of the atmosphere causing air pollution, affecting energy balance and climate and global warming (Peter, 1994). Land-use and land-cover change have impacts on hydrology. It changes the quality of water and water flows, cause surface water pollution, depletion of groundwater aquifers. Land-use and

land-cover changes also increase the frequency and severity of flooding which is due to continuous and serious deforestation (William and Turner, 1992).

In addition, urban expansion due to rapid population growth is another factor for LULC change since it brings a dramatic change of landscape patterns and types (Fenglei et al., 2009; Jianga and Tiana, 2010). This dynamics has been changing the availability of different biophysical resources and lead to decreased availability of different products and services for human, livestock, and damage the environment (Hussien, 2009). Liu et al. (2002) and Wilson et al. (2003) also agreed that the rapid urban expansion is the result of population growth and socio-economic development. Therefore, such kind of enlargement around urban areas and the surroundings has massive impacts on the environment (Jianga and Tiana, 2010), for instance cause for the warming of urban and its surrounding areas (Jianga and Tiana, 2010; Qijiao and Zhixiang, 2015).

Rapid and uncontrolled urbanization causes many environmental problems, such as air pollution (Wu et al., 2013), urban heat island effect (Jianga and Tiana, 2010; Qijiao and Zhixiang, 2015; Wu et al., 2013), and vegetation loss (Jianga and Tiana, 2010; Taubenböck et al., 2012; Weng, 2012). These result in the degradation of the environment and affect the quality of human settlements (Goldewijk and Ramankutty, 2004). Increase in the population and built-up areas brings trouble on the carrying capacity. Expansion of built-up areas due to urbanization cause destruction of the ecological environment (Jianga and Tiana, 2010; Zhu et al., 2016).

Further, LULC change due to urban expansion causes urban heat island (UHI) (Jianga and Tiana, 2010) that has adverse social, economic and environmental effects both at local, regional and global scale (Du et al., 2007, Luber and McGeehin, 2008 and Zheng et al., 2014). Thus, higher urban temperatures increase the demand for air conditioning, change urban thermal environments and ultimately lead to thermal discomforts and incidence of heat-related illnesses (Qijiao and Zhixiang, 2015).

2.3 Land-use and Land-cover Change in Ethiopia

Land-use dynamics is one of the major environmental problems in Ethiopia (Berhan, 2010). Land-use and land-cover changes in Ethiopia, particularly in the highland areas caused by a combination of various factors though it depends on the conditions of the area (Eyayu et al., 2009; Hassen et

al., 2015; Mohammed, 2011; Woldeamlak, 2002; Woldeamlak and Sterk, 2005; Yeshaneh et al., 2013). Even tough causes of LULC changes varies from place to place human-induced factors are the main driving forces, and create a complex system and troubles (Agarwal et al., 2002; Verheye, 2007). This complexity ranges from biophysical attributes to social and economic drivers of changes. (Veldkamp and Lambin, 2001). These driving forces change the landscape patterns and land-cover types, for instance, change and modification of topography, climate, vegetation and soil characteristics. Cultural factors such as habits of logging vegetation cover, exposing of soil for erosion and degrading land may also trigger LULC changes (Lambin et al., 2003). Besides these, institutional causes like political, legal, economic, and traditional factors and their interaction with individual decision making are important for LULC change and management (Lambin et al., 2003).

In Ethiopia, vegetation cover is decreasing due to the expansion of cultivated land (Abate, 2011; Belay, 2002; Gessesse and Kleman, 2007; Gete and Hurni, 2001). Estimates of deforestation in Ethiopia, which is mainly for expansion of rain-fed agriculture that varies from 80,000 to 200,000 ha per annum (EPA , 1997). As EFAP (1993) stated that the extent of the forest was much higher from 40% at the beginning of the twentieth century, 16% in the 1950s, 3.1% by 1982, only 2–3% in 1990s, and 3.56% in 2004 (Badege, 2001; Wubalem, 2012). Accordingly, some remnant stands of natural forests are mainly restricted to religious sites, along rivers and streams, and on peaks of hills where crop cultivation is difficult in the highlands of Ethiopia (Warra et al., 2013). This is due to the rapid expansion of agriculture and rural and urban settlement.

Therefore, rapid increase in deforestation as well as poor practices of managing farmlands accelerating soil erosion and land degradation in the Ethiopian highlands (Hassen et al., 2015, Hurni et al., 2005; Mohammed et al., 2005), principally common where high population exist and their livelihoods directly depend on the exploitation of natural resources (Woldeamlak and Sterk, 2005). Such fast rates of vegetation conversion, unsustainable agricultural land-use and severe soil erosion are the effects of LULC changes and land degradation in the highlands of Ethiopia (Mekuria, 2005). Because of population pressures, economic factors and policy issues, settlements, farmland and degraded lands have been expanding while grasslands and forest areas have been diminishing largely (Alemu et al., 2015; Eleni et al., 2013; Getachew et al., 2011; Hassen et al.,

2015; Tsehaye and Mohammed, 2013; Woldeamlak, 2002). Further, there is an expansion of urban built-up areas at the expense of forest, grass and shrublands (Mohammed, 2011).

Moreover, LULC changes are associated with deforestation, biodiversity loss and land degradation (Maitima et al., 2009). Land-use and land-cover change is a serious problem in changing the environment (Abate, 2011). Similarly, land-use and land-cover change aggravate soil erosion and its related problems (Belay, 2002; Desta et al., 2000; Tilahun et al., 2001). The major causes of land degradation in Ethiopia are rapid population increase, severe soil loss, deforestation, low vegetative cover and unbalanced crop and livestock production (Girma, 2001). In this case, the Ethiopian highlands are highly affected by land degradation, which has eroded the natural resource bases of the area (Tilahun et al., 2001).

Therefore, LULC changes have diverse impacts on soil quality, water supply, reservoir storage capacity, agricultural productivity and ecology of a region (Sharma et al., 2011). Land-use and land-cover changes affect life and human livelihoods (Lambin et al., 2003, 2001; Lambin and Geist, 2006; Lambin and Meyfroidt, 2011).

2.4 Land Surface Temperature and its Algorithm

According to Srivastava et al. (2010), land surface temperature (LST) is defined as the surface radiometric temperature corresponding to the instantaneous field of view of the sensor. Land surface temperature can also define as the temperature emitted by the surface and measured in kelvin (Rajeshwari and Mani, 2014). Moreover, LST is the temperature measured at the Earth's surface and is regarded as its skin temperature (Dash et al., 2002). Land surface temperature is defined as the surface radiometric temperature corresponding to the instantaneous field-of-view of the sensor (Prata et al., 1995) or the ensemble directional radiometric surface temperature (Norman and Becker, 1995). land surface temperature can be defined as the temperature felt when the land surface is touched with the hands or it is the skin temperature of the ground.

land surface temperature is a key parameter for many environmental models, for example, energy and water exchange between atmosphere and surface (Yuan and Bauer, 2007); numerical weather prediction; global ocean circulation; climatic variability (Valor and Caselles, 1996). It represents the combined result of all energy exchange processes between the atmosphere and the land surface (Albin et al., 2017 and Voolgt and Oke, 2003). Thus, LST has become a basic requirement for

model validation or model constraining in surface energy and water budget modeling on various scales (Kalma et al., 2008; Kustas and Anderson, 2009). It serves as a metric for soil moisture and vegetation condition in ecological and hydrological modeling and environmental monitoring (Czajkowski et al., 2000; Kustas and Anderson, 2009). Further, LST has been used in the area of thermal anomalies and high temperature events detection (Sobrino et al., 2009). Land surface temperature is also useful to predict the energy and water exchanges between land surface and atmosphere, which plays an important role in human-environment interactions (Qijiao and Zhixiang, 2015).

Furthermore, LST is widely used in urban climate studies to quantify the surface urban heat island and to explore its relationship with urban surface properties and air temperature variability as well as for surface-atmosphere exchange processes in urban environments (Voolgt and Oke, 2003; Weng, 2009). Land surface temperature is a vital variable in the physical processes of land surface energy and water balance on regional and global scales, is widely used in a range of hydrological, meteorological, and climatological applications (Duan et al., 2014; Karnieli et al., 2010; Li et al., 2009; Vlassova et al., 2014). Land surface temperature is also one of the key parameters controlling the chemical, physical and biological processes of the earth surface and is an important factor for the study of urban climate (Pu et al., 2006).

Therefore, LST can be easily derived from remotely sensed data (Lazzarini et al., 2013; Li et al., 2013; Mohan and Kandya, 2015) such as Landsat, NOAA-AVHRR, MODIS. For a given sensor viewing direction, LST depends on the distribution of temperature and emissivity within a pixel and the spectral channel of measurement (Becker and Li, 1995). In order to obtain LST from space radiometry images, there should be atmospheric, angular and emissivity correction. Absorption, upward atmospheric emission, and the downward atmospheric irradiance reflected from the surface are the main effects of the atmosphere (Franca and Cracknell, 1994).

Several atmospheric correction approaches have been established depending on sensor characteristics though mono-window and split-window algorithm is commonly used for retrieving land surface temperature.

Mono-window algorism: Mono-window algorism use radiance measurements in one infrared window channel and correct the atmospheric effects to determine land surface temperature (Price,

1983; Susskind et al., 1984). Therefore, single-channel methods can be applied to sensors with only one infrared channel thought it is also used for multi-channel thermal sensors. For example, Atmospheric correction for Landsat TM is done based on Landsat TM 5 (Qin et al., 2001a; Sobrino et al., 2004a), DAIS (Digital Airborne Imaging Spectrometer) (Sobrino et al., 2004b). The method requires that the vertical and horizontal distribution of temperature and water vapor in the atmosphere is accurately known (Dash et al., 2002; Ottle' and Vidal-Madjar, 1992). To estimate land surface temperature through mono-window algorithm, ground emissivity, atmospheric transmittance and effective mean atmospheric temperature are critical parameters (Qin et al., 2001a).

Split-window algorism: The split window technique is used for multi-channel sensors (Becker and Li, 1990; Price, 1984; Sobrino et al., 1991), in which radiance differences observed by each atmospheric window of the respective thermal infrared channel. The SWA uses differential absorption between two channels within one atmospheric window in order to eliminate the atmospheric influence and calculates the temperature at the sensor as a linear combination of two brightness temperatures (Dash et al., 2002). For example in Landsat-8 (Du et al., 2014; Jimenez-Munoz et al., 2014; Meijun et al., 2015; Rozenstein et al., 2014; Xiaolei et al., 2014), DAIS (Sobrino et al., 2004b) and NOAA-AVHRR (Qin et al., 2001b). The algorithm assumes that the land surface emissivity values in both thermal infrared channels are Known (Meijun et al., 2015).

2.5 Normalized Difference Vegetation Index

Normalized difference vegetation index (NDVI) is an index based on spectral reflectance of the ground surface feature. Each feature has its own characteristic reflectance varying according to the wavelength. Normalized difference vegetation index can be developed using near-infrared and red bands of the remote sensing data and value ranges between -1 to +1. A Higher value of NDVI (close to +1) infers the presence of healthy vegetation in the area while its lower value (-1) is the indicator of the absence of vegetation. Hence, the NDVI is very crucial induces for assessing the health of vegetation, the greenness of the earth surface, crop monitoring and yield forecasting, and forest cover assessment and deforestation and desertification. Normalized difference vegetation index is very essential used for analyzing and mapping land-use and land-cover (Ahl et al., 2006; De Boer, 2000; Huang and Siegert, 2006; Lunetta et al., 2006; Woodcock et al., 2002).

Furthermore, NDVI is very essential for analyzing urban green environment and urban climate since it indicates the level of dryness and warmness of the area.

2.6 Relationship of Land-use and Land-cover Types with Normalized Difference Vegetation Index and Land Surface Temperature

Land surface temperature, normalized difference vegetation index and land surface emissivity are significant factors in energy budget assessment, land cover valuation, and other related studies to earth surface characteristics (Fei et al., 2016). This provides a better understanding of the overall land-use and land-cover classes and environmental studies (Biro et al., 2013; Mallick et al., 2012). Normalized difference vegetation index and land surface emissivity can be used to assess and evaluate the spatial relationship between LST and different LULC in urban areas and environments (Amiri et al., 2009; Maimatiyiming et al., 2014).

As the land surface temperature is sensitive to the vegetation and the content of moisture in the soil, it can be used to detect the LULC changes (Dash et al., 2002). Land surface temperature varies in LULC types (Jianga and Tiana, 2010; Sun et al., 2012; Weng et al., 2004; Yue et al., 2007), for instance urban green spaces has high NDVI and low LST than industrial zone. Land surface temperature has inversely related with NDVI (Jianga and Tiana, 2010; Sobrino and Raissouni, 2000; Sun et al., 2012; Yue et al., 2007). This means that the higher the NDVI value the lower in the value of surface temperature and the lower the NDVI the higher the LST. This indicates that spatial distribution of LST and NDVI vary with the variation of LULC types (Sobrino and Raissouni, 2000; Weng et al., 2004; Wilson et al., 2003; Yue et al., 2007). For example, LST increases with the expansion of built-up areas (Jianga and Tiana, 2010; Sun et al., 2012) while normalized difference vegetation index is lower. Therefore quantifying and assessing the interrelationship of LST and NDVI is very important for evaluating environmental zonal influences in urban ecosystems (Wilson et al., 2003).

2.7 Impacts of Land-use and Land-cover Change on Land Surface Temperature Distribution

Population expansion and its spatial distribution have an impact on the destruction of land-cover and exhaustive use of land (Jianga and Tiana, 2010; Small, 2004). This affects the ecosystem of the earth surface and reduction in plant species biodiversity. Land-use and land-cover change, therefore, has a great impact on the change and distribution of land surface temperature. Because the surface composition of the types of LULC varies which determine materials emissivity, means the surface is very hot and reemit high amount of energy when it exposed for the incoming radiation due to high surface reflectance. For instance, because of low evaporative cooling and low heat transfer capacity of bare land especially salinized soil domination has a high surface temperature. Besides, the modification and change of vegetation cover, agricultural and grazing land, and water bodies have a great influence on the changes and variation of the earth's surface temperature (Fei et al., 2016). Such extreme kinds of LULC change contribute to the variation of climate change and influence the distribution and changes of LST.

Though forests have an extensive influence on local, regional and global climates, loss of forest due to deforestation results in increased insolation; decreased cloudiness and approximately compensating the effect of cloud; amplified reflectance of land surface; change the large-scale convergence of atmospheric moisture which influence precipitation and modify rainfall patterns; and changes in surface roughness and wind speeds and direction (Yadvinder et al., 2008). Deforestation also contributes directly and indirectly to the loss of terrestrial marine ecosystems. Therefore, it accelerates diminution forest area, loss of complexity and diversity (Donato et al., 2016) as well as affect volume of water, increase surface water heat due to sedimentation and rise evaporation. Besides, it increases in soil and land degradation, desertification (Abbas et al., 2010, Temesgen et al., 2014, 2009; William and Turner, 1992), wetland degradation (Zhenglei et al., 2009) and cause for fluctuation of rainfall and humidity, and change surface temperature. This instability affects the thermodynamic processes at the earth-atmosphere interface and the dynamic processes in the atmosphere (Shukla et al., 1990).

Deforestation also increases greenhouse gases (GHG) emission, for instance, carbon-di-oxide, methane nitrous oxide and others into the atmosphere (Rajeshwari and Mani, 2014), increases albedo and decreases canopy roughness (Peter, 1994), minimize rainfall availability and increase

surface temperatures (William and Turner, 1992). This increase land surface temperature of the surface of the earth. Consequently, the change in the value of land surface temperature changes the climate and its elements.

Rapid urban expansion and industrialization increase buildings, gases released from vehicles and industries (Manea et al., 2013), non-evaporating impervious surfaces like concrete and asphalt (Jianga and Tiana, 2010; Qijiao and Zhixiang, 2015; Tang et al., 2014), which heats up the urban environment directly. Subsequently, urbanization leads to the reduction of green spaces in urban areas (Jianga and Tiana, 2010), which modifies urban surface water content and vegetation cover (Qijiao and Zhixiang, 2015; Tang et al., 2014). Physical change of the urban surface (albedo, thermal capacity, heat conductivity) can affect urban surface temperatures by altering the sensible and latent heat exchange between the urban surface and boundary layers (Frey and Parlow, 2012; Mohan and Kandya, 2015). Therefore, these urban biophysical changes increase UHI (Fenglei et al., 2009; William and Turner, 1992) a phenomenon of higher atmospheric and surface temperatures occurring in urban areas than in surrounding rural areas (Gluch et al., 2006; Voolgt and Oke, 2003). These are responsible for climate change (Du et al., 2007; Luber and McGeehin, 2008; Zheng et al., 2014) and increasing energy consumption (Sevgi et al., 2009) finally, these bring global warming at local, regional and global scales.

2.8 The Importance of Remote Sensing for Land-Use and Land-Cover and Land Surface Temperature Analysis

The land is becoming degraded and the pattern and types of land cover are changed at local, regional and global levels. Therefore, efficient way of analyzing what, why, where and when land-use and land-cover are changed is very essential for sustainable land management and economic development. Furthermore, assessing and mapping the consequences of LULC change and the possible solution is very significant. Monitoring temporal land-use and land-cover changes is also very important for environmental management.

In this regard, remote sensing has been playing a crucial role in provides satellite imageries assess natural resources and monitor environmental changes. For example, Landsat is one of the satellites which providing synoptic, repetitive and global coverage data freely since 1972. Landsat imageries have been used for the various terrestrial application. Therefore, Remote Sensing allows analyzing

land-use and land-cover change dynamics using time series of remotely sensed data by integrating it with socio-economic or biophysical data. Remote sensing is also efficient in land-cover mapping, detecting and monitoring land-cover change over time and space, identifying land use attributes and land cover change hot spots (Abate, 2011; Abbas et al., 2010; Temesgen et al., 2014). With the advancement of technology, reduction in data cost, availability of historic spatio-temporal data and high-resolution satellite images, remote sensing technologies are now very useful for conducting land cover change detection analysis and predicting the future scenario (Agarwal et al., 2002).

Moreover, land surface temperature and NDVI can be easily computed by using satellite data specifically thermal remote sensing is very crucial for assessing and measuring urban thermal environment (Sun et al., 2012; Yue et al., 2007). It also provides a tool for analyzing thermal variation (Weng, 2003) measurements of physical, environmental and socioeconomic variables in urban settings (Small, 2004). Remote sensing data is also significance for analyzing the relationship of LULC change with LST and NDVI. Therefore remote sensing is very useful for studying urban environment (Yue et al., 2007) and rural environment As a result, it possible to extract information about the earth's surface from the satellite imageries and analyze and make an informed decision.

CHAPTER THREE

3. MATERIAL AND METHODS

3.1 Description of Study Area

3.1.1 Location and Area

This research was conducted in Bahir Dar town and its surroundings which is the capital of Amhara National Regional State. The geographical location of the study area extends from latitude 11° 30' 11" to 11° 58' 11"N and longitude 37° 2' 2" to 37° 29' 4"E. It has a total of 1,073.53 km^2, from which the terrestrial part was about 243.07 km^2 (215.57 km^2 was an area of Bahir Dar town, and 27.41 and 0.09 km^2 was Deq Istifanos and Kibran Gebriel Islands, respectively). An area of 830.46 km^2 was covered from Lake Tana. Bahir Dar town is far from Addis Ababa at the distances of 567 km along Bure road and 465 km along Motta road (Figure 3.1).

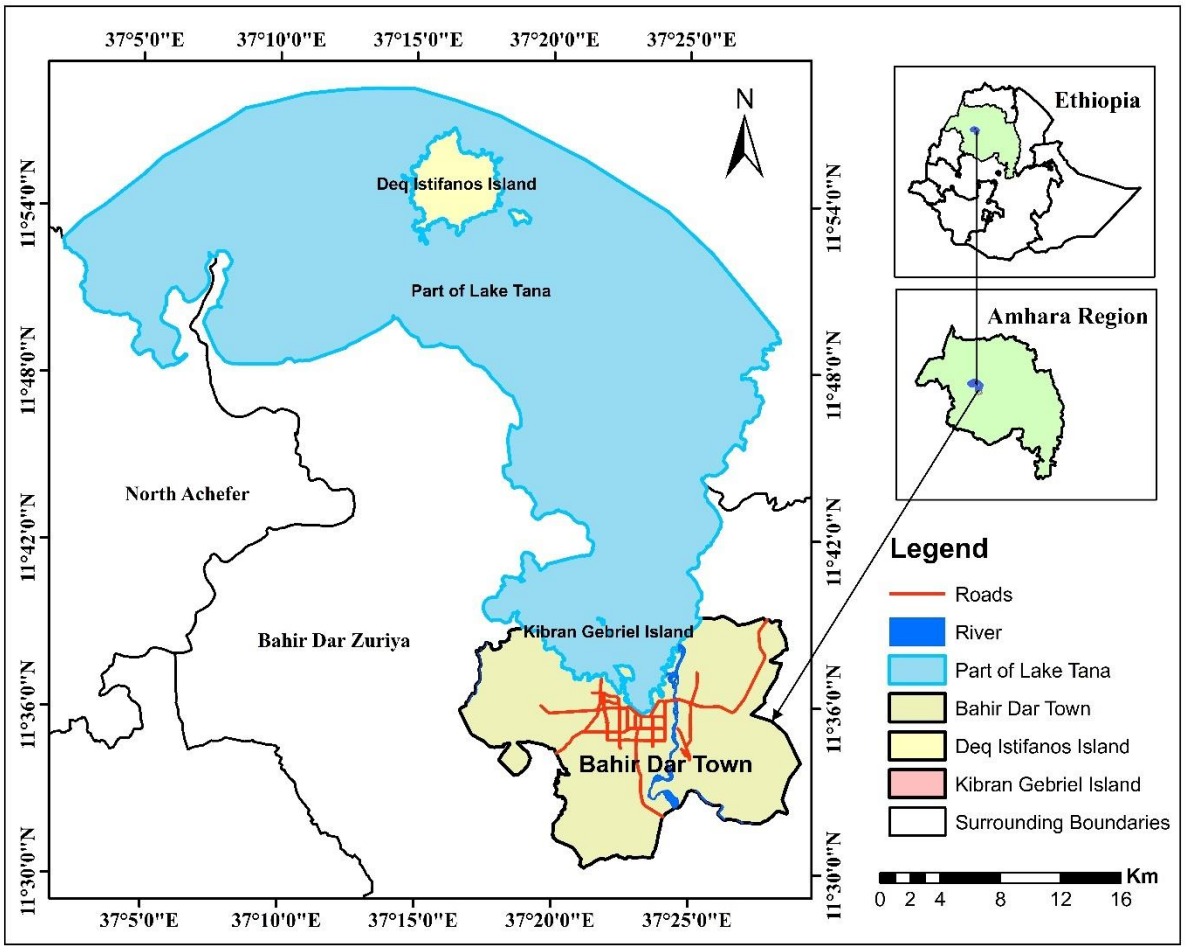

Figure 3.1: Geographical location of the study area

3.1.2 Topography

Bahir Dar town is bounded by Lake Tana from the north. The topography of Bahir Dar town and its surroundings is relatively flat. The elevation of the study area varies from 1,708 m in the southeast to 2,007 m in eastern and western peripheries of the town (Figure 3.2).

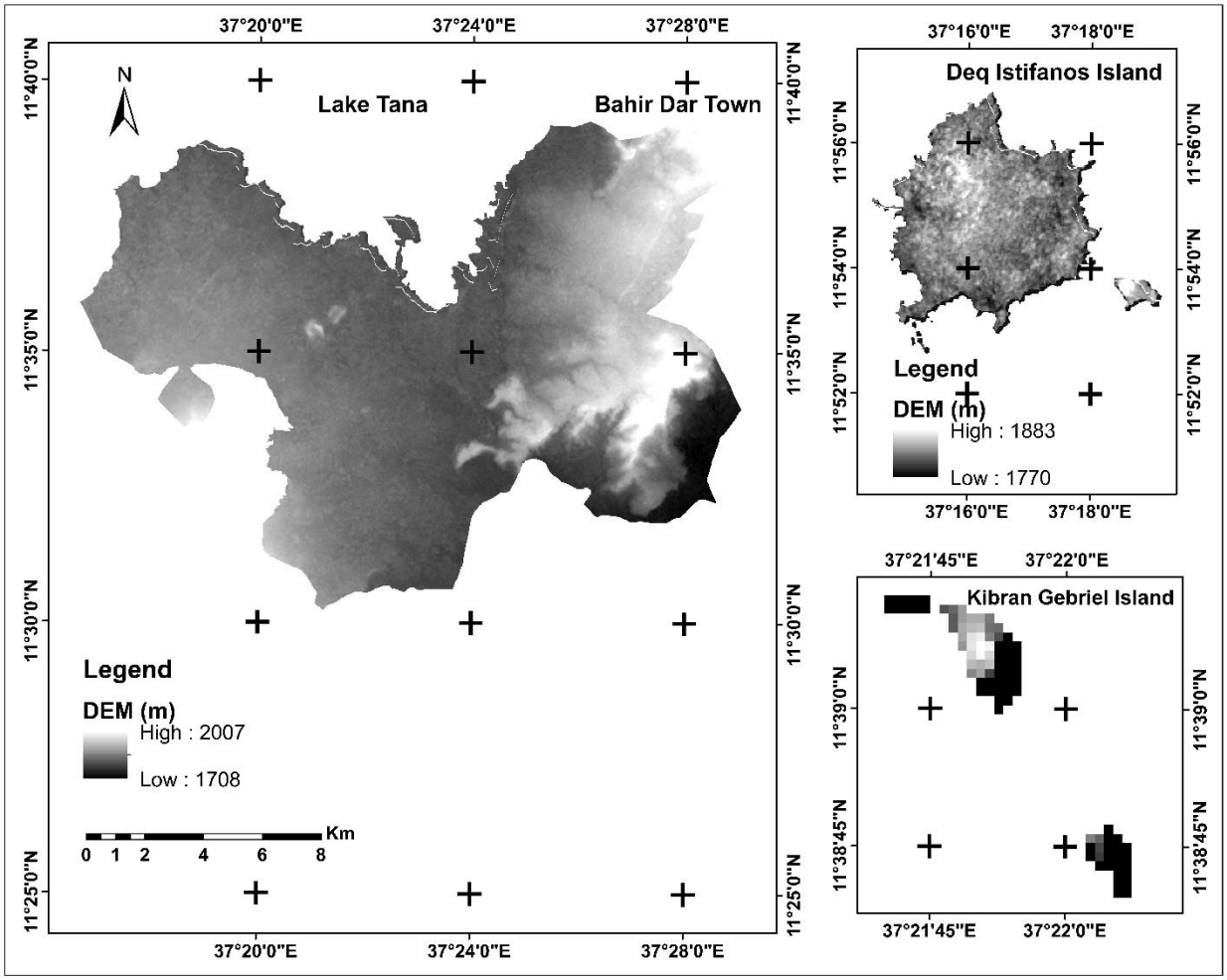

Figure 3.2: Elevation map of the study area

Even though the topography of the study area is relatively flat, there are some places which are characterized by deep river gorge. Therefore, the slope of the area abruptly increases to more than 20% towards southeast following the drainage of River Abay. However, most of the areas of the town, as well as Deq Istifanos Island, has a slope in the range of 3-10% and the slope of some places in the town and Island varies from 13-24% (Figure 3.3).

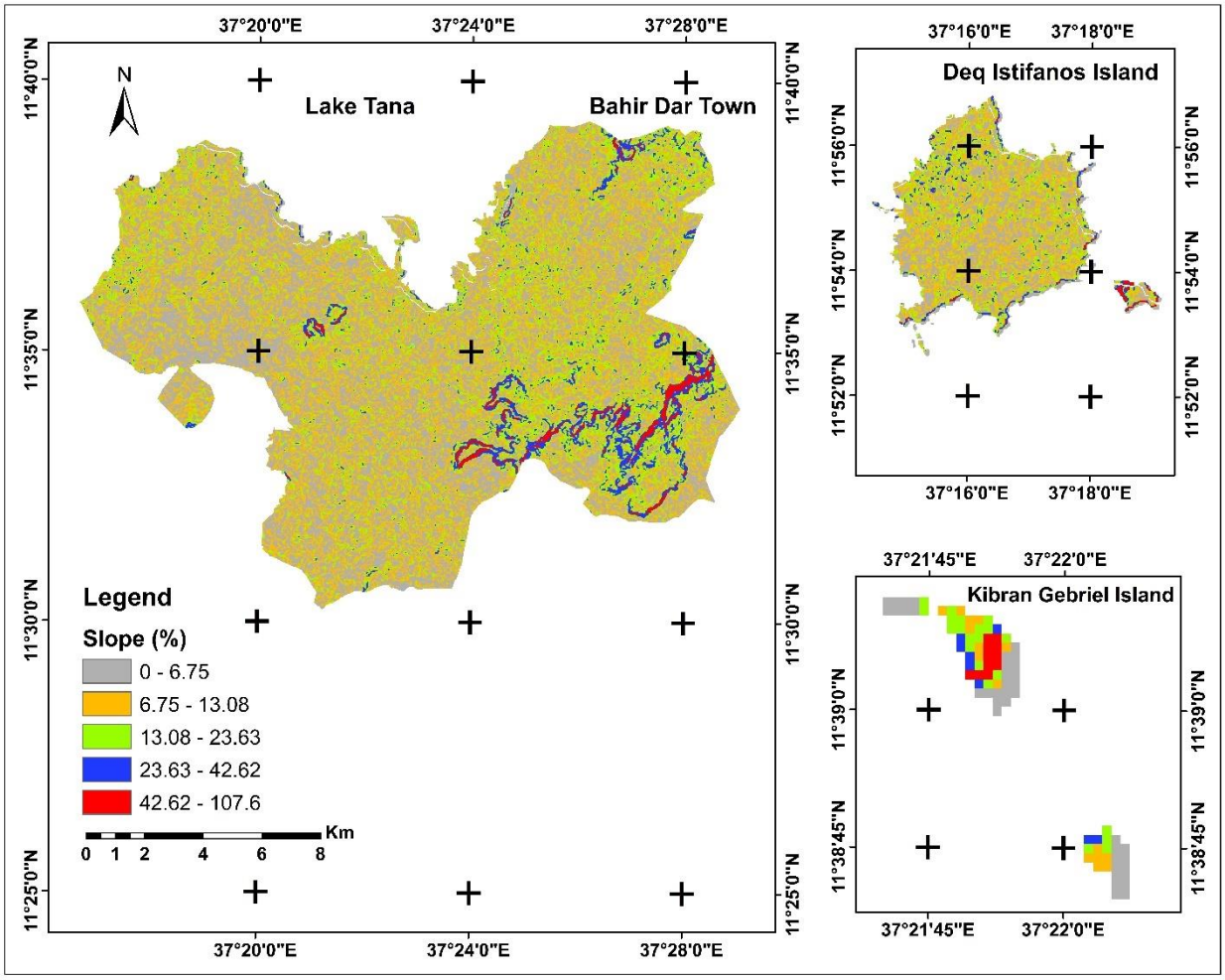

Figure 3.3: Slope map of the study area

3.1.3 Population

Based on the 1984 population and housing census of Ethiopia, the population of Bahir Dar town was about 54,773 (CSA, 1991). 25,136 male and 29,637 females. Ten years later in 1994 census, this population was 96,140 of which 45,436 and 50,704 were male and female respectively (CSA, 1998). Whereas in the third national population and housing census which has taken in 2007, the population of the town was 221,991, from this male was 108,456 while the female was about 113,535 (CSA, 2008). Besides, as estimated by CSA the population of the town could be 362,297 in 2017 (CSA, 2013). The detail of the population is presented in Figure 3.4.

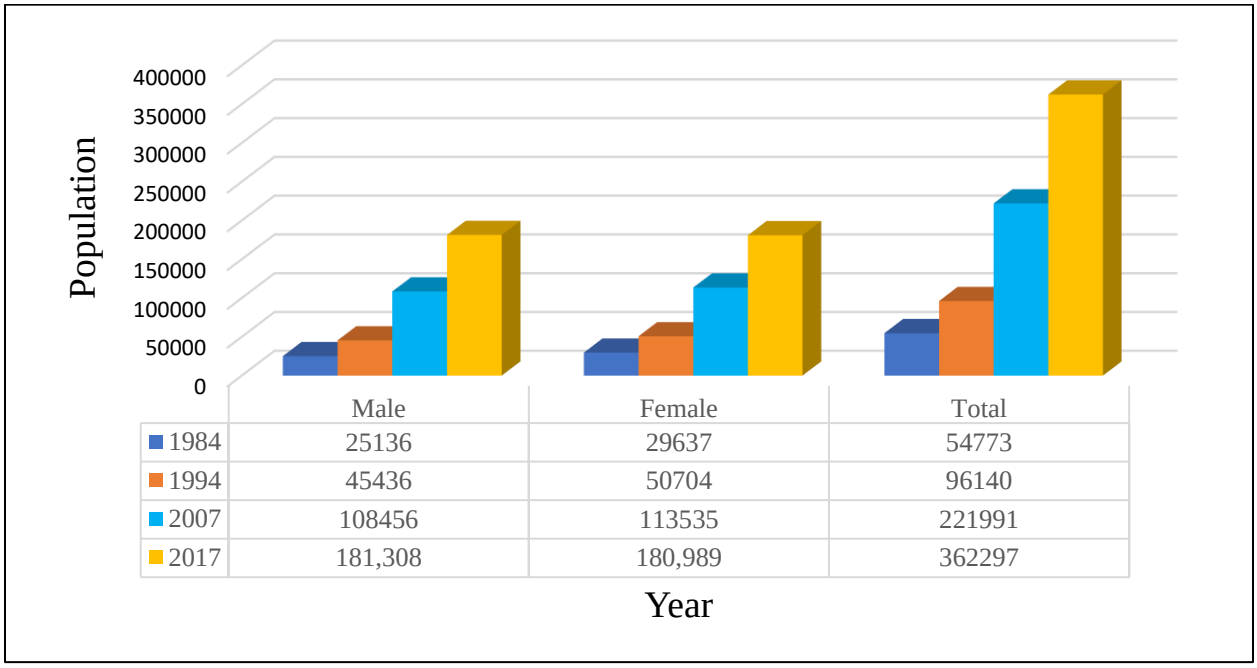

	Male	Female	Total
1984	25136	29637	54773
1994	45436	50704	96140
2007	108456	113535	221991
2017	181,308	180,989	362297

Figure 3.4: Population distribution of Bahir Dar town and its surrounding (1987-2017)

3.1.4 Climate

3.1.4.1 Temperature

As temperature recorded at Bahir Dar town meteorology station from the year 1987-2017, the maximum mean monthly temperature was very high in Belge season, that is, from February-May (NMA, 1996). Nevertheless, of the Belge season months, the maximum mean monthly temperature was very high during April which was 30.2 ℃. Whereas the lowest maximum mean monthly temperature recorded during Kiremt season (from June-September), mainly in July which was 24.3 ℃. Moreover, highest minimum mean monthly temperature of the place was 15.5 ℃ which was occurred in the month of May while the lowest was in January which was about 8.4 ℃. Therefore, April and January are warmest and the coldest month respectively (Figure 3.5).

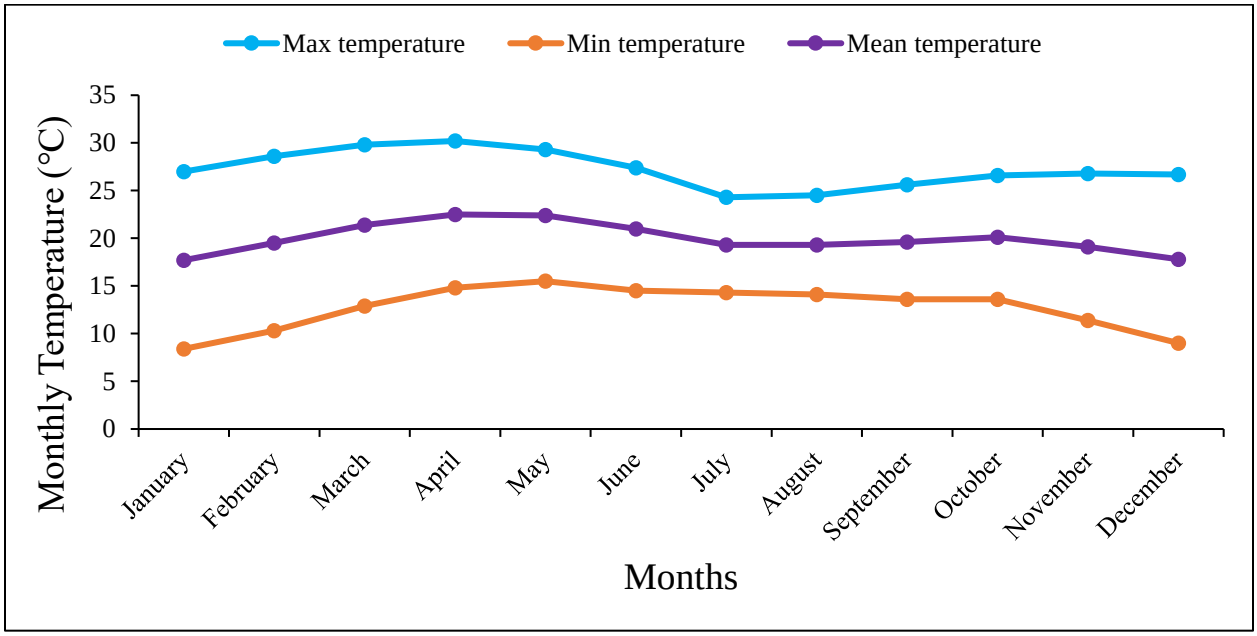

Figure 3.5: Maximum, minimum and mean monthly temperature distribution (1987-2017)

Even though there were variations in temperature from month to month in a year due to the variations in climate parameters, on average the temperature was increased from year 1987 to 2017, particularly, the temperature has been sharply increasing since 2008 (Figure 3.6).

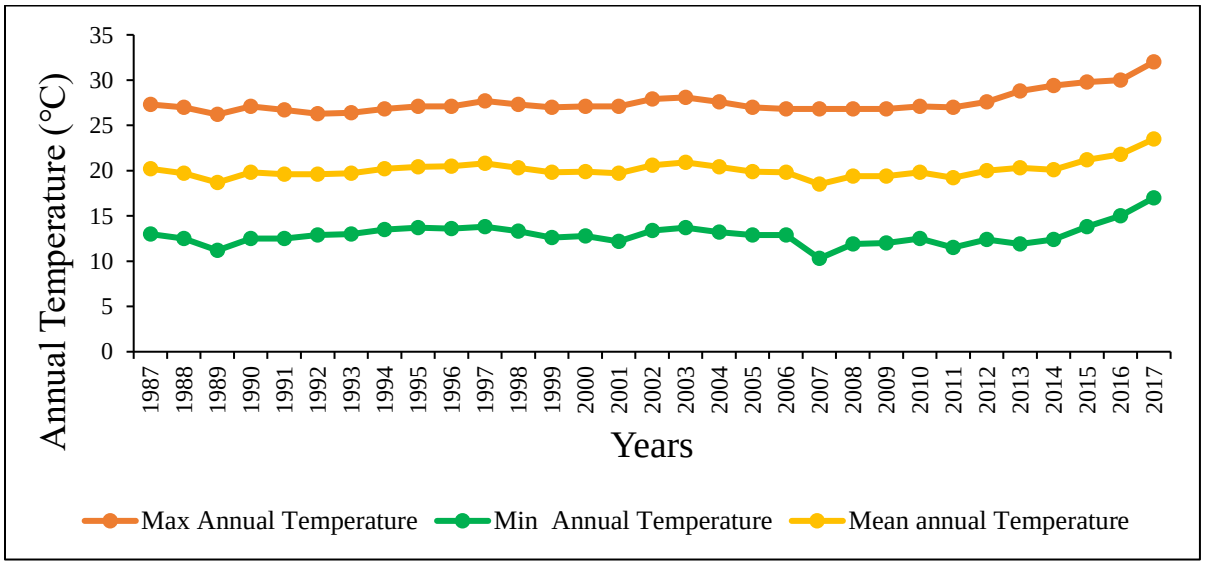

Figure 3.6: Maximum, minimum and mean annual temperature distribution (1987-2017)

3.1.4.2 Rainfall

As data recorded from 1987-2017 at Bahir Dar town meteorological station, monthly average rainfall of the town was 1416.62 mm and the maximum monthly average rainfall was 419.5 mm recorded in the month of July. On average, rainfall was very high in the months of June, July, August and September since these are rainy months in most parts of Ethiopia (NMA, 1996). Whereas January, February, March, April, November and December are the dry months (Figure 3.7**)**.

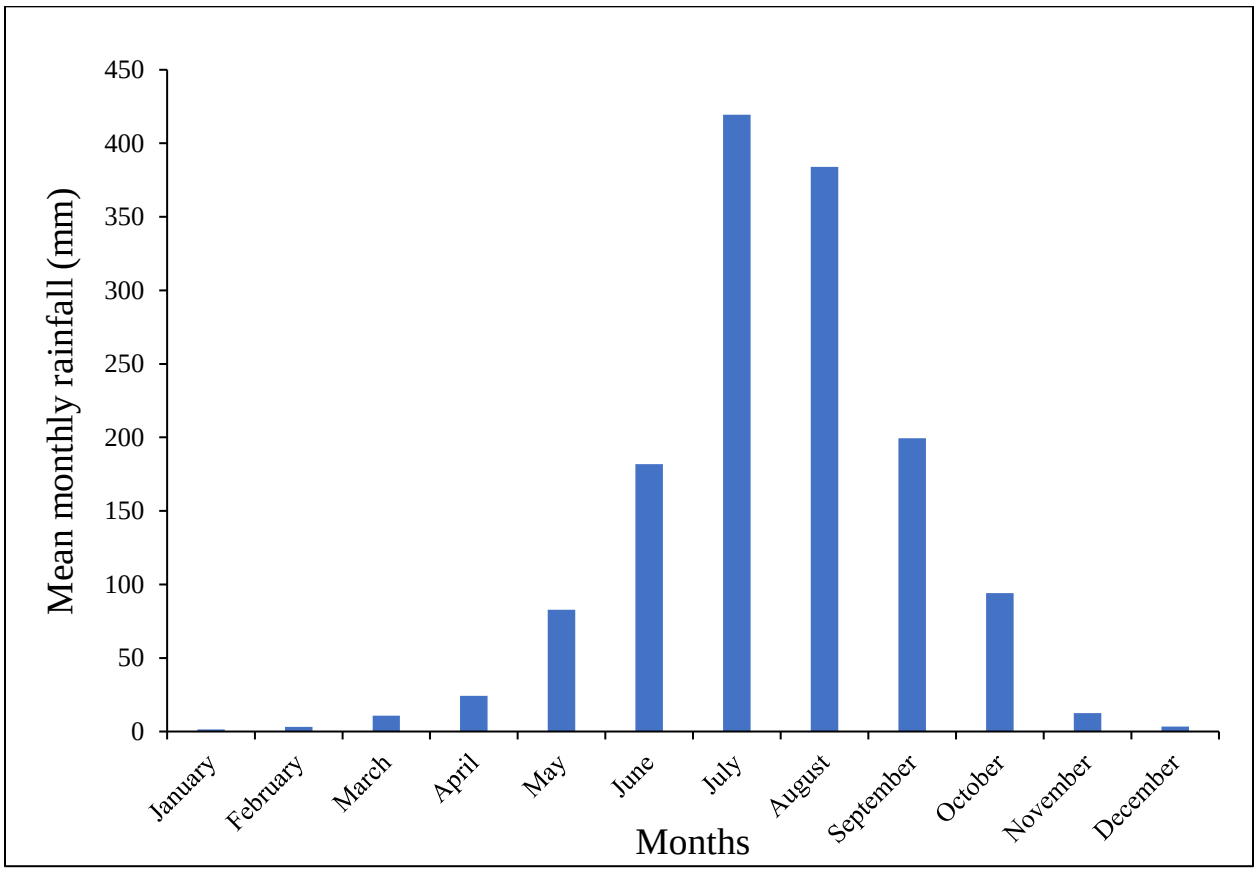

Figure 3.7: Mean monthly rainfall distribution (1987-2017)

The mean annual rainfall of Bahir Dar town from 1987 to 2017 ranges from 89.7 mm to 142.6 mm. As indicated in Figure 3.8, during 31 years of the study periods, the mean annual rainfall was varying from year to year, mostly due to the variations of climate and weather parameters (Figure 3.8).

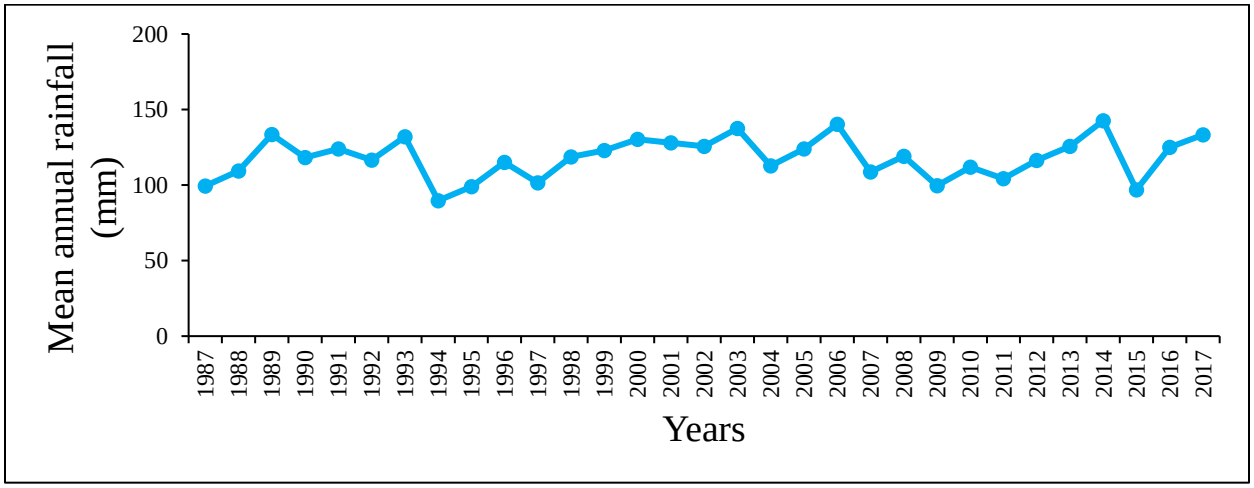

Figure 3.8: Mean annual rainfall distribution (1987-2017)

During 1987 to 2017, the maximum recorded annual rainfall in Bahir Dar town and its surrounding was 1711.6 mm, and this was recorded in 2014 and the minimum annual rainfall was 1076.5 mm in 1994. From 1987 to 2017, the average annual rainfall recorded was 1416.62 mm while it was 1397.4 mm and 1442.8 mm from 1987 to 2002 and 2002 to 2017, respectively. The distribution of annual rainfall of Bahir Dar town and its surrounding from 1987 to 2017 is presented in Figure 3.9.

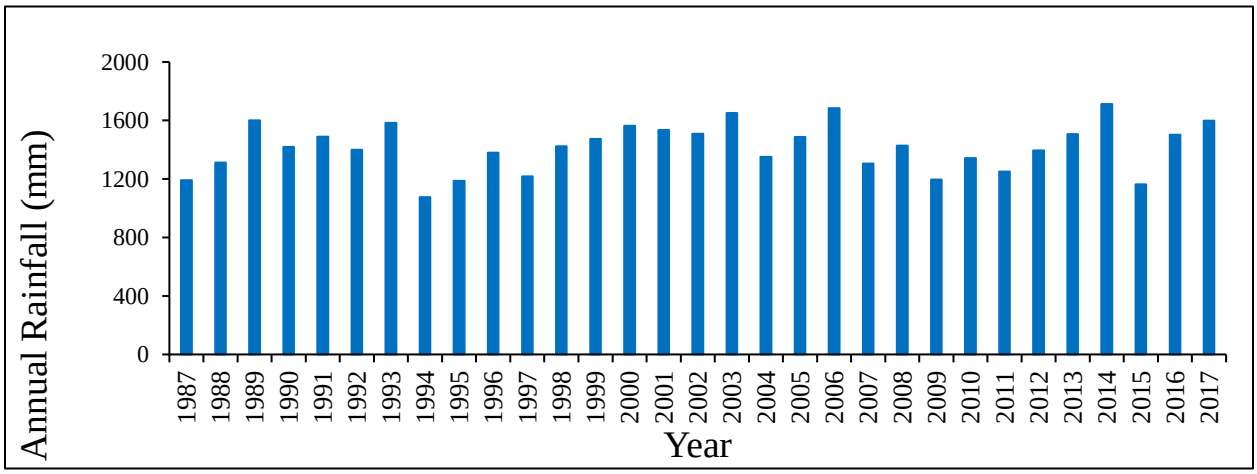

Figure 3.9: Annual rainfall distribution (1987-2017)

3.1.4.3 Humidity

From 1987 to 2017, the maximum mean monthly relative humidity of Bahir Dar town and its surrounding was 81.2 Octa which was recorded in the month of August while the minimum was

42.2 Octa which was in March. Generally, as Figure 3.10 below illustrates relative humidity was continuously increasing from April to August and declining from September to March.

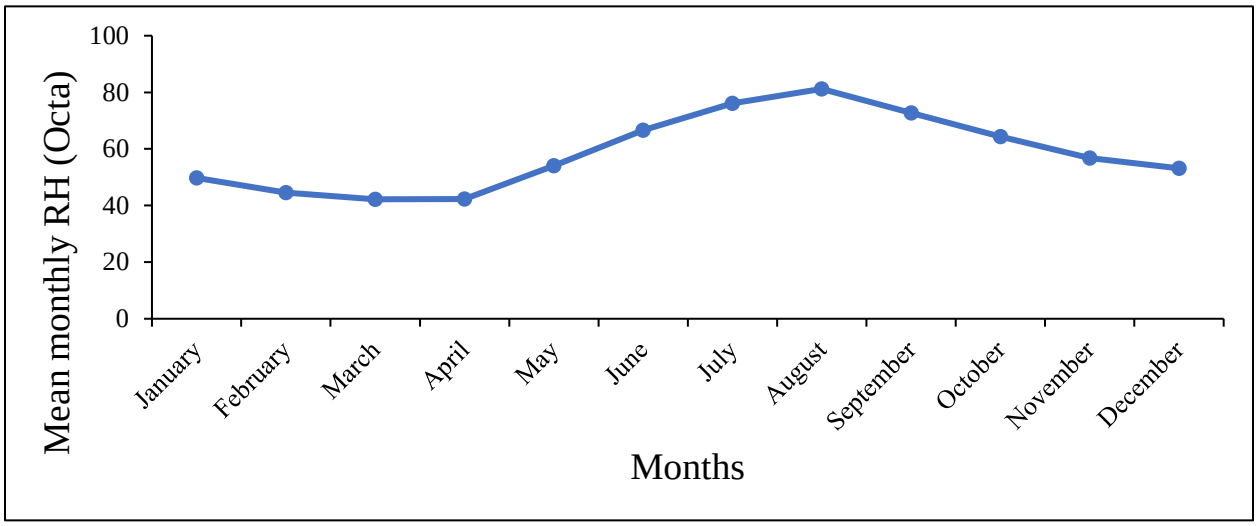

Figure 3.10: Mean monthly relative humidity distribution (1987-2017)

For 31 years relative humidity data which recorded at Bahir Dar town meteorology station indicates that the maximum mean annual relative humidity of the study area was 64 Octa, which was in 2009 and minimum was 54.9 Octa in 2012. The relative humidity of Bahir Dar and its surrounding was continuously declining from 2014-2017 (Figure 3.11).

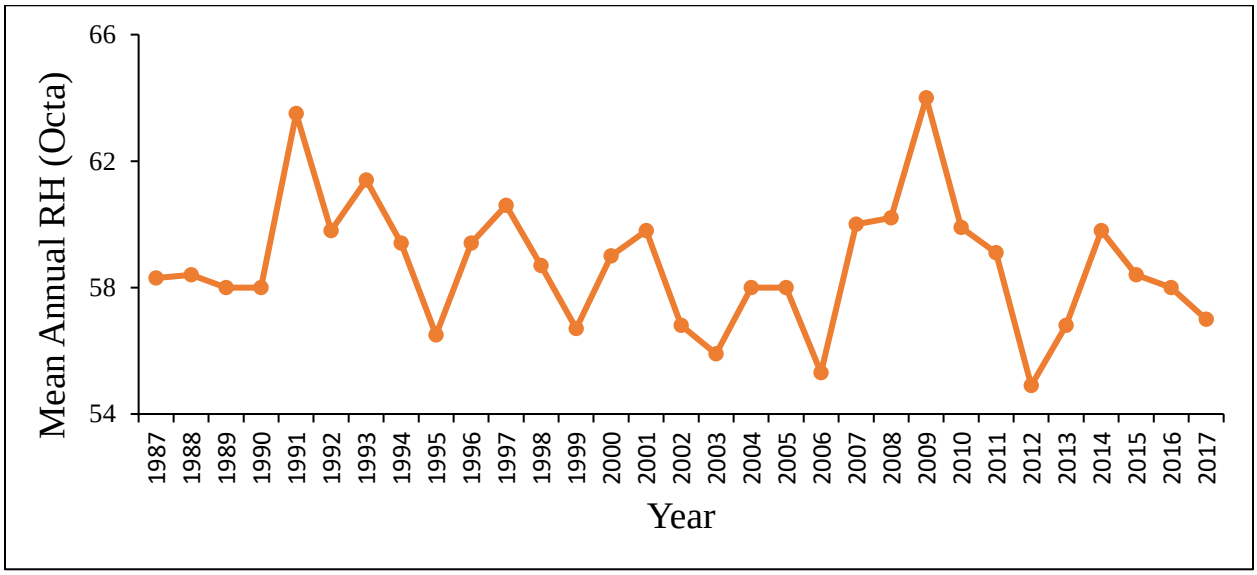

Figure 3.11: Mean annual relative humidity distribution (1987-2017)

3.1.4.4 Wind Direction

Based on meteorological data of 2016, it was observed that the wind direction was to south, southeast, east and northeastwards throughout the year during the daytime. Whereas in the year 2017, the persistent wind direction was towards southeast and south. In both years it was observed that the wind was blowing from Lake Tana and River Abay towards Bahir Dar town during the daytime (Figure 3.12). This is because at daytime the lake is cooler than the town and its surrounding and there is high pressure on the surface of the lake. As a result, the wind blows from high to low-pressure body.

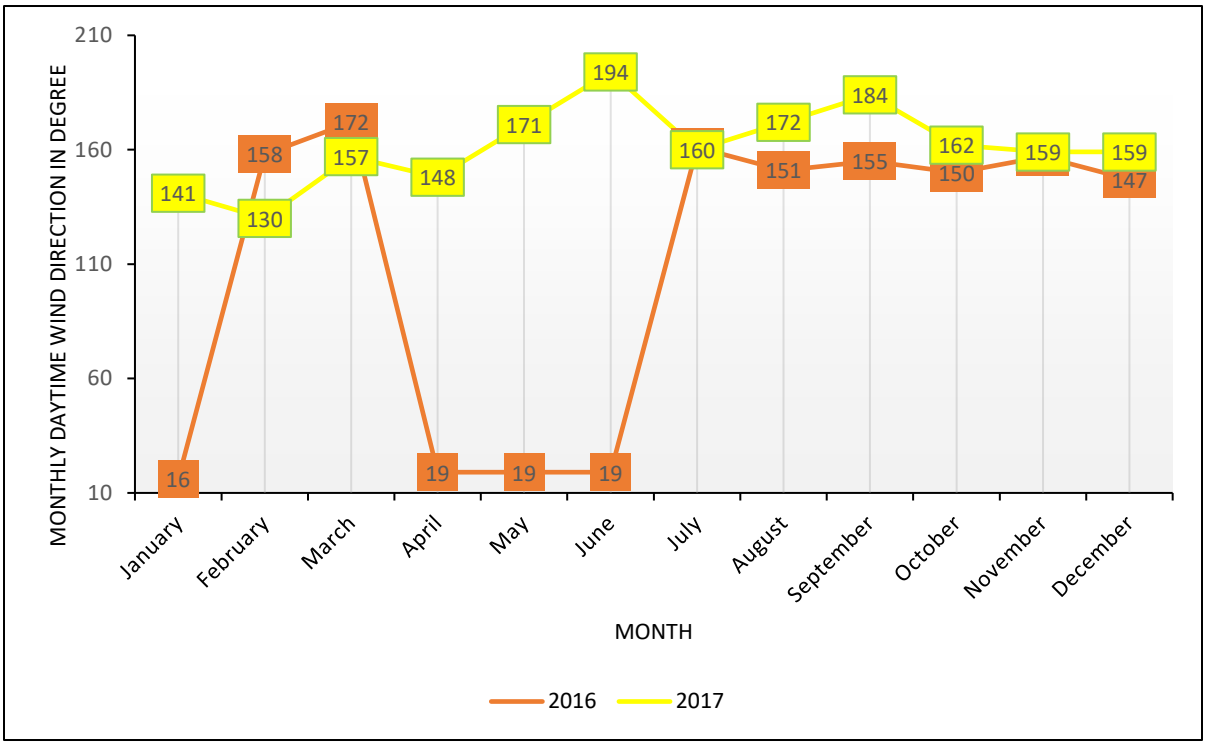

Figure 3.12: Monthly daytime wind direction distribution (2016-2017)

In contrary, at night the town is cooler than Lake Tana and River Abay, therefore, the wind blows towards these water bodies. Due to this, both in 2016 and 2017, the wind blows in the direction of north, northwest, and west from the town. In August 2016, it was blowing towards the southeastern direction from Bahir Dar town (Figure 3.13).

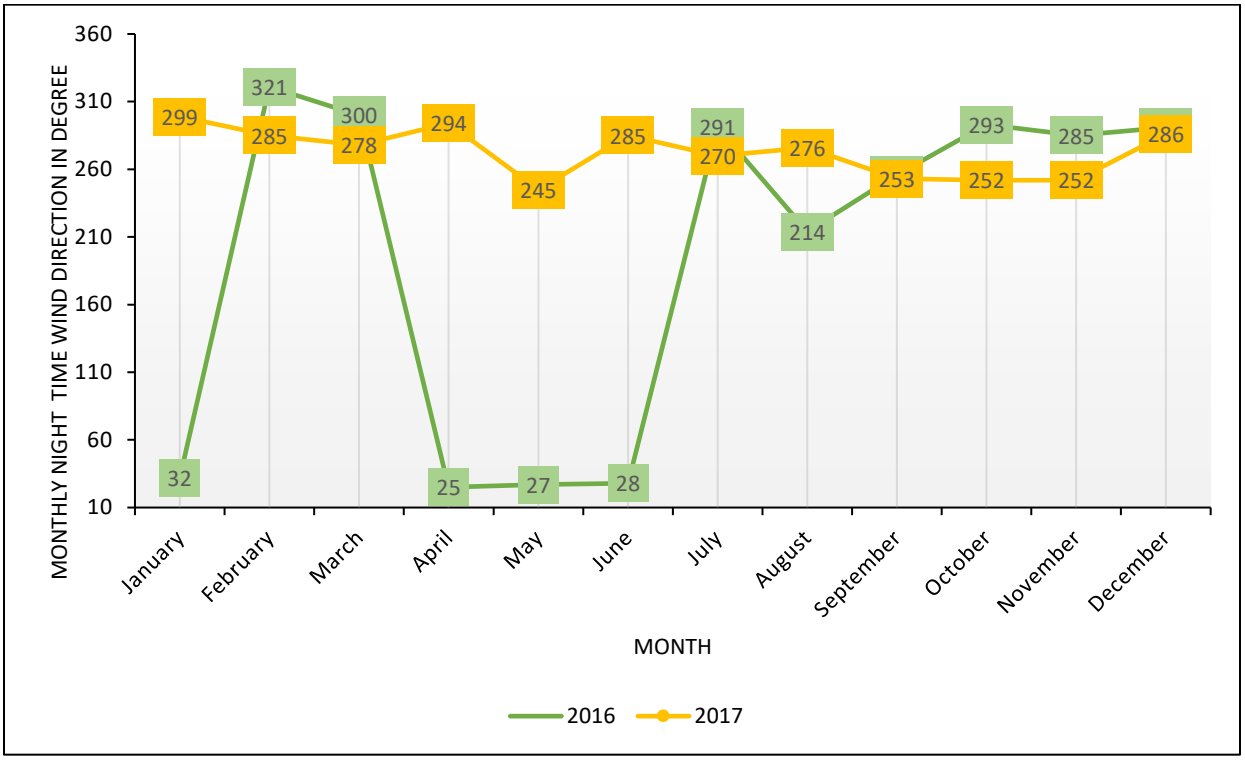

Figure 3.13: Monthly night time wind direction distribution (2016-2017)

3.2 Datasets and Source

3.2.1 Remote Sensing Data

The study area is covered by one scene with the path of 170 and row of 52 of the Landsat satellite series. Due to the problem of poor resolution of MSS sensor and data availability, the study period covered only from year 1987 to 2017. Thus, years 1987, 2002 and 2017 were selected for analysis with 15 years interval. Imageries which were acquired during the month of March were used, because, cloud and haze free imageries can easily be obtained during dry seasons where there is no cloud cover and rain. To analyze the impacts of LULC changes on the distribution and changes on LST in the study area, images acquired by Landsat 5 TM, Landsat 7 ETM+ and Landsat 8 OLI/TIRS were used. These imageries were downloaded from the United States Geological Survey website (http://earthexplorer.usgs.gov) which is free of charge. Detail descriptions of Landsat datasets which was used for Landsat image sharpening, analyzing of LULC change, NDVI and LST distribution of Bahir Dar town and its surroundings are given in Table 3.1.

Table 3.1: Remote sensing datasets used for the study and their source

Path & row	Acquisition date	Satellite	Sensors	Resolution (PAN/MS/TIRS)	Source
170-052	27 March 1987	Landsat	TM	15/30/120 m	USGS
	12 March 2002		ETM+	15/30/60 m	
	13 March 2017		OLI	15/30/100 m	
275/125,127,130,132 300/125,127,130,132 325/125,127,130,132	2005	SPOT 5	HRG	5 m	EMA
	14 March 2017	Terra	MODIS	1k m	LP DAAC
		SRTM DEM		30 m	USGS

A. Landsat Thematic Mapper (TM)

Landsat Thematic Mapper (TM) sensor was carried on Landsat 4 and Landsat 5 from July 1982 to May 2012. It consists of seven spectral bands; three in the visible, three in infrared and one in the thermal region of the spectrum. Thematic Mapper image has a spatial resolution of 30m MS (band 1 to 5 and 7) and 120 m in thermal (band 6). Therefore, TM Band 6 is specifically sensitive to thermal infrared radiation to measure the surface temperature of the earth surface. Moreover, TM has a temporal resolution or repeat the cycle of 16 days. Scene size of TM images is approximately 170 km north-south and 183 km east-west. Detail about thematic mapper sensor bands and other descriptions are provided in Table 3.2.

Table 3.2: Landsat 4 and 5 TM sensor description

Landsat 4 & 5	Bands with description	Wavelength (µm)	Temporal resolution (days)	Spatial Resolution (meters)
Thematic Mapper (TM)	Band 1-Blue	0.45-0.52	16	30
	Band 2-Green	0.52-0.60	16	30
	Band 3-Red	0.63-0.69	16	30
	Band 4-NIR	0.76-0.90	16	30
	Band 5-Shortwave IR (SWIR) 1	1.55-1.75	16	30
	Band 6-Thermal	10.40-12.50	16	120
	Band 7-Shortwave IR (SWIR) 2	2.08-2.35	16	30

B. Landsat Enhanced Thematic Mapper Plus (ETM+)

Landsat Enhanced Thematic Mapper Plus sensor (ETM+) was carried on Landsat 7 since July 1999. Landsat 7 ETM+ images consist of eight spectral bands with a spatial resolution of 30 m for bands 1-5 and 7 which are Multi-spectral (MS) images. While band 8 is panchromatic with 15 m resolution and band 6 is thermal with a resolution of 60 m. 16 days is a revisit period of the ETM+ sensor. All ETM+ sensor bands can collect one of two gain settings (high or low) for increased radiometric sensitivity and dynamic range whereas ETM+ Band 6 collects both high and low gain for all scenes. The approximate size of the scene is 170 km north-south by 183 km east-west. Detail descriptions about Landsat 7 ETM+ are given in Table 3.3.

Table 3.3: Landsat 7 ETM+ sensor description

Landsat 7	Bands with description	Wavelength (µm)	Temporal resolution (days)	Spatial Resolution (meters)
Enhanced Thematic Mapper (ETM+)	Band 1-Blue	0.45-0.52	16	30
	Band 2-Green	0.52-0.60	16	30
	Band 3-Red	0.63-0.69	16	30
	Band 4-NIR	0.77-0.90	16	30
	Band 5-Shortwave IR (SWIR) 1	1.55-1.75	16	30
	Band 6-Thermal	10.40-12.50	16	60
	Band 7-Shortwave IR (SWIR) 2	2.09-2.35	16	30
	Band 8-Panchromatic	0.52-0.90	16	15

C. Landsat Operational Land Imager (OLI) and Thermal Infrared Sensor (TIRS)

Landsat 8 was launched on February 11, 2013, with Landsat Operational Land Imager (OLI) and Thermal Infrared Sensor (TIRS). It has 11 bands; from bands 1 to 7 and 9 are MS, and band 8 is panchromatic while band 10 and 11 are thermal. The spatial resolution of Landsat 8 is 30 m, 15 m and 100 m for MS, PAN and TIRS. Ultra-blue Band 1 is useful for coastal and aerosols studies while Band 9 is useful for cirrus cloud detection. The approximate scene size of Landsat 8 images is 170 km north-south by 183 km east-west. Detail descriptions about OLI and TIRS are presented in Table 3.4.

Table 3.4: Landsat 8 OLI and TIRS description

Landsat 8	Bands with description	Wavelength (µm)	Temporal resolution (days)	Spatial Resolution (meters)
Operational Land Imager (OLI) and Thermal Infrared Sensor (TIRS)	Band 1-Ultra Blue (coastal/aerosol)	0.43-0.45	16	30
	Band 2-Blue	0.45-0.51	16	30
	Band 3-Green	0.53-0.59	16	30
	Band 4-Red	0.64-0.67	16	30
	Band 5-NIR	0.85-0.88	16	30
	Band 6-Shortwave IR (SWIR) 1	1.57-1.65	16	30
	Band 7-Shortwave IR (SWIR) 2	2.11-2.29	16	30
	Band 8-Panchromatic	0.50-0.68	16	15
	Band 9-Cirrus	1.36-1.38	16	30
	Band 10-TIRS 1	10.60-11.19	16	100
	Band 11-TIRS 2	11.50-12.51	16	100

3.2.2 Meteorology Data

Meteorological data such as wind direction, humidity, temperature and rainfall data were gathered from National Meteorological Agency (NMA) of Ethiopia. Wind direction was used to evaluate the influence of Lake Tana on LST distribution of Bahir Dar town and its surrounding while temperature, relative humidity and rainfall data were used to describe the climate of the study area during the study periods (Table 3.5).

Table 3.5: Meteorology data description

Data type	Year	Source
Rainfall	1987-2017	NMA
Temperature		
Humidity		
Wind direction	2016-2017	

3.2.3 Aerial Photograph and Master Plan

Google Earth images for the year 1987 and 2002 are not visible and clear to develop LULC thematic layers. Therefore, to aid image classification for these two study years, aerial photographs acquired in 2003 and Bahir Dar town master plan prepared in the same year were used.

3.2.4 Ground Truth Data

Ground truth data were collected from the field using GPS after stratified sample points generated from the image of 2017 and their coordinates from Google Earth. Field data is therefore used for validating the LULC classified image into different classes by observing the real LULC of the study area. Besides, ground truth data was used for accuracy assessment for an image acquired in 2017. In order to minimize errors in classification, pictures showing different LULC classes in the study area were captured.

3.2.5 Google Earth Data

Google Earth map was used as a base map for 2017 Landsat 8 OLI image classification. Google Earth was also used to extract coordinates for sample points, which were selected based on stratified sampling technique to verify LULC classes of 2017 image. It was also used to extract reference points for inaccessible areas.

3.3 Software

To process satellite imageries and analyze land-use and land-cover changes, normalized difference vegetation index and land surface temperature, the following software packages were used (Table 3.6).

Table 3.6: Software packages used for this study

Software Type	Application
ENVI 5.1	Image preprocessing and TM and ETM+ atmospheric correction, and computation of NDVI, PV, LSE, and LST
ERDAS IMAGINE 2015	OLI atmospheric correction, and change detection analysis
ArcGIS 10.5	Image digitizing, split and merge polygons, zonal statistics, reclassification, LST zonation and mapping, and mapping NDVI
Google Earth Pro 2017	Use as a base map in visual image interpretation, and generate coordinate points for the image of 2017
EasyGPS 5.7	Transfer field data from GPS to computer (for 2017)
MS Excel 2016	To develop correlation statistics of LST and NDVI
6S 2.1	To process near air surface temperature, and atmospheric transmittance

3.4 Methods

This study had three main methods. The first was land-use and land-cover analysis from Landsat 5, 7 and 8. Estimation of land surface temperature from Landsat imageries was the second step. Finally, zonal and correlation statistics were done for NDVI and LST. Relationship analysis were done for LULC and NDVI, and LULC and LST. The overall methods are presented in the following schematic flow chart (Figure 3.14).

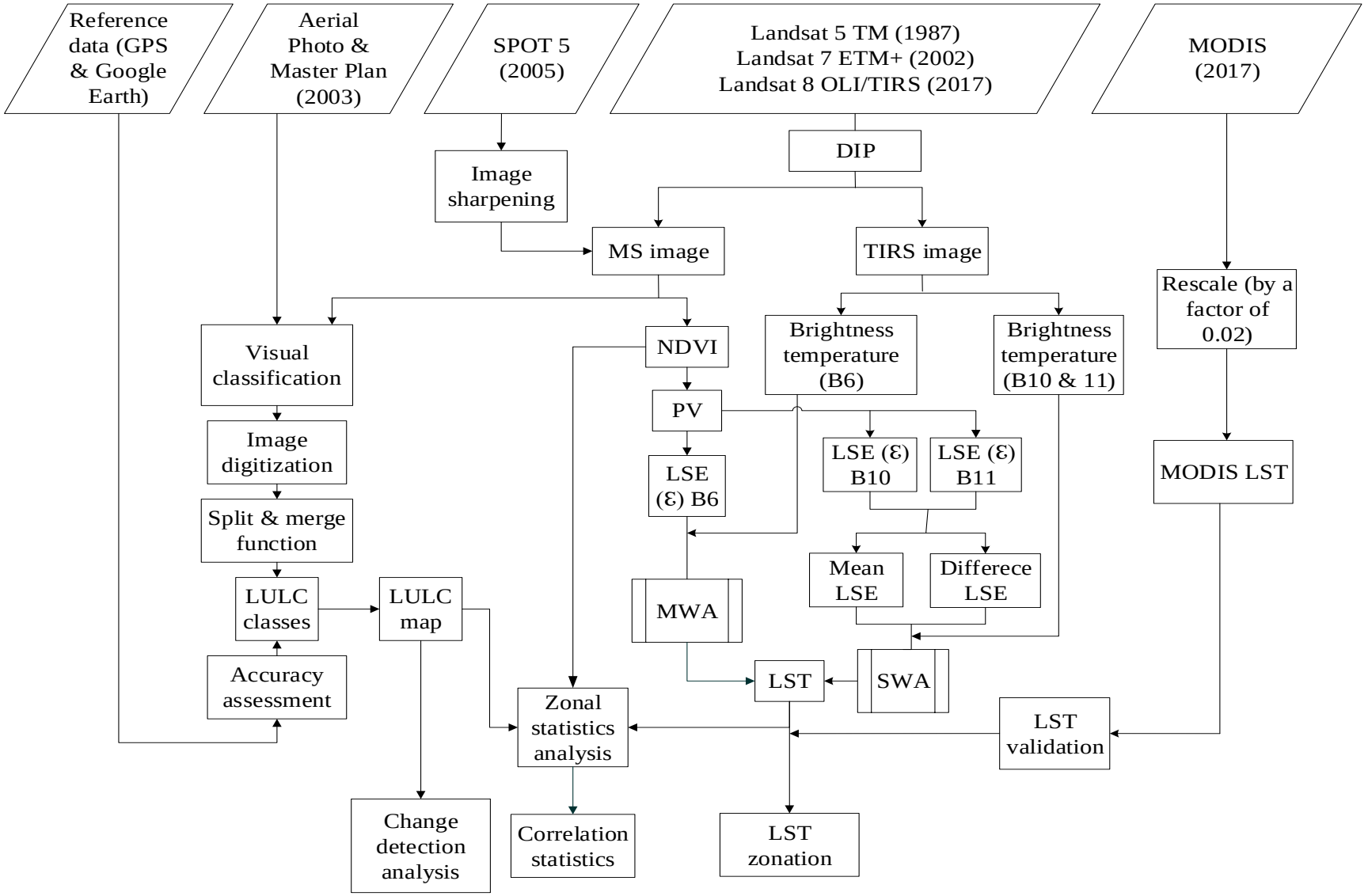

Figure 3.14: Schematic methodology flowchart of the present study

3.4.1 Digital Image Preprocessing

In remote sensing, digital numbers are very important since they represent reflectance of surface materials when they are detected by a sensor and tells about the properties of an object. The objects are represented in the form of a pictorial element called pixels. Therefore, to obtain meaningful information from those pixels, they should be processed and corrected digitally before using them for further analysis. Digital image processing involves manipulation and interpretation of digital image through the help of computer application software. It is helpful to increase the quality of an image and maintain the quality image for the purpose of interpretation and classification; therefore, it is possible to minimize interpretation errors since the image can easily be manageable in a computer. Digital image processing starts from image layer stacking to image enhancement and prepares them for classification.

Image sub-setting: image sub-setting is a process by which image is extracted from a particular image based on the boundary of the area of the interest. Therefore, the images which lay in between 11° 30' 11"-11° 58' 11"N and 37° 2' 2"-37° 29' 4"E were processed from the stacked images.

Image sharpening: To improve the resolution of the images and enhance image interpretation, resolution merge or image sharpening technique can be used. For instance, using high-resolution images like SPOT, QuickBird, and IKONOS the quality of low-resolution images such as Landsat can be improved. Among many image sharpening techniques, Gram-Schmidt spectral sharpening algorithm was used. Because Gram-Schmidt method is typically more accurate because it uses the spectral response function of a given sensor to estimate what the panchromatic data look. SPOT 5 image was used to sharpening Landsat images since it has a 30 m resolution, therefore, the refined Landsat images were visible and better than the original images.

3.4.2 Multispectral Radiometric Correction

Atmospheric image correction or preprocessing is very significant in order to get an accurate image because radiation which comes from the source always interacts with the atmosphere. The energy which is reflected back to the sensor after its contacts with the target objects is useful for remote sensing. Therefore, in atmospheric preprocessing, DN should be converted into spectral radiance. To do so, Quick Atmospheric Correction (QUAC) algorithm was carried out in the ENVI image processing program version 5.1 for Landsat 5 TM and Landsat 7 ETM+ images. Quick

Atmospheric Correction is a visible-near infrared through shortwave infrared (VNIR-SWIR) relative atmospheric correction method for multispectral and hyperspectral imagery. It estimates atmospheric compensation parameters directly from the information contained within the scene (observed pixel spectra) without ancillary information (Bernstein et al., 2005)

Like Landsat 5 TM and Landsat 7 ETM+ images, Landsat 8 OLI image was also radiometrically corrected and spectral radiance converted to radiance in ERDAS IMAGINE using the formula given by USGS (2016):

$$L_\lambda = M_\lambda * Q_{\text{cal}} + A_L \quad (1)$$

Where; L_λ = Spectral radiance (W/ (m^2 * sr * μm)); M_λ= Radiance multiplicative scaling factor for the band (RADIANCE_MULT_BAND_N from the metadata); AL = Radiance additive scaling factor for the band (RADIANCE_ADD_BAND_N from the metadata); Qcal = Level 1 pixel value in DN.

Then, level 1 pixel DN values were converted to top of atmosphere (TOA) reflectance using the equation (USGS, 2016):

$$\rho'_\lambda = M_\rho * Q_{\text{cal}} + A_\rho \quad (2)$$

Where; ρ_λ' = Top-of-Atmosphere Planetary Spectral Reflectance, without correction for solar angle; M_ρ= Reflectance multiplicative scaling factor for the band; (REFLECTANCEW_MULT_BAND_N from the metadata); A_ρ = Reflectance additive scaling factor for the band (REFLECTANCE_ADD_BAND_N from the metadata); Qcal = Level 1 pixel value in DN.

Once a solar elevation angle is chosen, then conversion to true TOA reflectance is given by:

$$\rho_\lambda = \frac{\rho_\lambda'}{\cos \theta_{SZ}} \quad (3)$$

where: ρ_λ = Top-of-Atmosphere Planetary Reflectance; θ_{SZ} = Local solar zenith angle.

3.4.3 Image Classification

Image classification is a technique of extracting information from the image based on the reflectance value of an object (Gao, 2009, Lillesand et al., 2004; Richards and Jia, 2006). The information class can be grouped into a thematic layer of having similar LULC in the image. Though there are automated image classification techniques, manual or visual image interpretation procedure was used. This is because there is a problem of pixel mixing especially in low-resolution imageries such as Landsat and this has seriously affected the land-use and land-cover classification accuracy of the study. To aid visual image interpretation and maintain classification accuracy, Google Earth map, Bahir Dar town master plan and aerial photo were used. Thus, to generate land-use and land-cover thematic layers image digitizing and split and merge functions were employed.

3.4.3.1 Accuracy Assessment

Accuracy assessment is a comparison of image interpretation by a computer with the aid of ground truth data (Gao, 2009; Richards and Jia, 2006). For this comparison, training sites which used for accuracy assessment were identified based on the stratified method of sampling because the classified image has virtually been thematically stratified. Stratified sampling technique guarantees that a specified number of evaluation pixels that can be selected from a given land cover, that is all LULC classes can be adequately represented in the evaluation samples. No matter how small a land cover is in size or limited in its spatial distribution, this specified number of evaluation pixels can always be selected, although not in a single pass (Gao, 2009). Therefore, stratified training pixels for validation were selected based on the number of bands and LULC classes, i.e., $N(N + 1)$ is the formula which used for taking the total samples for validation and for each LULC class $(N+1)$ training pixels is required (Lillesand et al., 2004; Richards and Jia, 2006).

Based on the aforementioned formula, eight samples were taken for each thematic layer and 112 for all LULC classes for each study images (1987, 2002 and 2017). Using these training sites, each LULC classes of the study area checked and classification accuracy was assessed. The overall accuracy, producer's and user's accuracy were calculated based on the error matrix derived from each classification result.

3.4.3.2 Land-use and Land-cover Thematic Layer

After classification accuracy was conducted, final land-use and land-cover thematic layers were identified and mapped for three study periods (that is, 1987, 2002 and 2017). So, Bahir Dar town and its surrounding has the following land-use and land-cover classes (Table 3.7).

Table 3.7: Land-use and land-cover classes and description of the study area.

LULC Classes	Description
Cropland	Areas used for annual crop cultivation.
Forest	Areas covered with large trees with woodland and dense shrubland.
Grassland	The area which used for grazing and spare trees and bushes.
High density settlement	The area occupied by dense house buildings including mixed and pure residence.
Industrial area	Areas used for factories and their Wearhouse.
Low density settlement	The area occupied by low density house buildings.
Open space	Areas used for recreation, and sport field, and land covered with green areas, and bare land (Areas covered with dry soil, sand/rocks and, dry salt flats, beaches, sand dunes, exposed rocks and gravel pits/non-vegetated area dominated by rock, eroded and degraded lands).
Paved surface	The area covered with road networks, vehicle parking areas, bus station.
Plantation	Area cover with perennial agriculture like chat, Banana, Mango, and tree plantations such as eucalyptus tree.
Riparian vegetation	Vegetation which grows along the seasonal river banks.
Service area	The area covered with offices, churches, schools, mosques, hospitals, hotels, garage and open marketplaces.
Shrubland	Areas covered with shrubs, bushes and small trees, mixed with some grasses and less dense than forests.
Water body	Areas covered with rivers and ponds.
Wetland vegetation	The area covered with aquatic vegetation, bushes, shrubs, woodland and wetlands or marshland.

3.4.4 Change Detection Analysis

Change detection is a process of detecting differences with the objects or phenomena which are observed in the different time intervals. DeltaCue is an application designed to help to identify changes of interest in remotely sensed imagery acquired on two dates. The DeltaCue change detection process operates on co-registered image data and performs a differencing operation as its core change detection process. In order to analyze the total area of LULC changed from 1987 to the 2017 year, the following formula was used.

$$LULC\ change\ \ (\%) = \big(Area\ of\ recent\ year(\%) - Area\ of\ former\ year(\%)\big) \quad (4)$$

3.4.5 Thermal Atmospheric Correction

During 1G product, rendering image pixels were converted to units of absolute radiance using 32-bit floating point calculations. Pixel values were then scaled to byte values prior to media output. Hence, spectral radiance of TM, ETM+ and OLI images were converted into radiance using the equation (Markham and Barker, 1986):

$$L_\lambda = \big((LMAX_\lambda - LMIN_\lambda)\ /(QCALMAX - QCALMIN)) * (QCAL - QCALMIN\big) + LMIN_\lambda \quad (5)$$

Where: L_λ = Spectral radiance received by the sensor (W/ (m^2 * sr * μm))

QCAL = the quantized calibrated pixel value in DN

$LMIN_\lambda$ = the spectral radiance that is scaled to QCALMIN (W/ (m^2 * sr * μm))

$LMAX_\lambda$ = the spectral radiance that is scaled to QCALMAX (W/ (m^2 * sr * μm))

QCALMIN = the minimum quantized calibrated pixel value (corresponding to $LMIN_\lambda$ in DN which is 1

QCALMAX = the maximum quantized calibrated pixel value (corresponding to $LMAX_\lambda$ in DN which is 255

3.4.6 Land Surface Temperature Computation

Land surface temperature can be computed in different ways based on the parameters (for instance, normalized difference vegetation index, emissivity, water vapor, air temperature and mean effective temperature) and resources (data and software) used.

3.4.6.1 Normalized Difference Vegetation Index

Normalized Difference Vegetation Index (NDVI) is very important to discriminate vegetation from no-vegetation and indicates the amount of vegetation present on the surface. Normalized difference vegetation index also used to infer general vegetation condition and to determine the LST. Besides, NDVI computation is important because it used to calculate the proportion of the vegetation (PV) and emissivity (ε) since these parameters are highly related with the NDVI (Weng et al., 2004). Normalized difference vegetation index is obtained by using red band (high absorption of radiation or low reflection) and infrared band (low absorption of radiation or high reflection). Accordingly, NDVI can be computed as

$$NDVI = \frac{\rho_{NIR} - \rho_{Red}}{\rho_{NIR} + \rho_{Red}} \quad (6)$$

Where; ρ_{NIR} reflectance in near infrared band; ρ_{Red} reflectance in red band

3.4.6.2 Land Surface Emissivity

Emissivity is the ratio of the radiance which is emitted by the real surface materials at their temperature and the radiance emitted by the black body at the same temperature (Becker and Li, 1995). Emissivity is the efficiency of transmitting thermal energy across the surface into the atmosphere. In contrast to that of the ocean, the emissivity of land is significantly different and varies with the heterogeneity of vegetation, surface moisture, roughness, and viewing angle (Rozenstein et al., 2014) and wavelength. Since LSE can change substantially over short distances, it is important to estimate its value for every pixel through applying LST algorithms. Therefore, in order to estimate LST the land surface emissivity (LSE (ε)) must be known, because LSE is a proportional factor that scales blackbody radiance (Planck's law) to predict emitted radiance.

In satellite images, pixels representing the land surface which are usually mixed pixels, that is, they are a combination of surfaces-types such as water, vegetation and soil. Therefore, the effective emissivity of a pixel can be calculated by summing up the contributions from those surface types because the emissivity value change from surface to surface. Though to estimate the emissivity from satellite thermal band data quite a lot of methods have been suggested, NDVI threshold method was used in this study. According to Van De Griend and Owe (1993), there is a high

correlation between measured Ɛ and NDVI. Emissivity value can be considered in four NDVI cases (Sobrino et al., 2001; Wang et al., 2015).

a) **NDVI < 0-** Water pixels with negative NDVI values were set to LSE values of 0.67,0.63 0.99 and 0.986 for TM, ETM+, OLI band10 and band11, respectively.

b) **NDVI < 0.2 -** Pixel with NDVI values smaller than 0.2 is considered as soil and the emissivity is obtained from reflectivity values in the red region. It is possible to extract the mean value for the emissivity of soils from ASTER spectral library (http://asterweb.jpl.nasa.gov) and will be filtered according to band TM, ETM+ and OLI 10 and 11 filter functions. Accordingly, soil emissivity in TM, ETM+, OLI 10 and 11 is 0.974, 0.973, 0.964 and 0.970, respectively.

c) **NDVI>0.5 -** Pixel with NDVI values higher than 0.5 is considered as vegetation, and the emissivity value is assumed to be 0.98, 0.99, 0.984 and 0.980 for TM, ETM+, OLI 10 and 11 respectively.

d) **0.2≤ NDVI ≥ 0.5** - Pixel with NDVI values between 0.2 and 0.5 is considered as a mixture of soil and vegetation (Barsi et al., 2014), and the emissivity is calculated according to the equation suggested by (Price, 1984, 1983).

$$\mathcal{E}_\lambda = \mathcal{E}_V \mathrm{P}_V + \mathcal{E}_s(1 - \mathrm{P}_V) + (1 - \mathcal{E}_s)(1 - \mathcal{E}_v)\mathrm{F}\mathcal{E}_v \quad (7)$$

where $\mathcal{E}_V$ and $\mathcal{E}_s$are the vegetation and soil emissivity, respectively, F = 0.55 shape factor considering different geometrical distributions, P_V proportion of vegetation which is given by equation (8).

According to (Meijun et al., 2015) proportion of vegetation (P_V) can be calculated using the NDVI values for vegetation and soil which presented as follows

$$\mathrm{P}_V = \left(\frac{NDVI - \mathrm{NDVI}_{min}}{\mathrm{NDVI}_{max} - \mathrm{NDVI}_{min}}\right)^2 \quad (8)$$

Where; $\mathrm{P}_V$is proportion of vegetation or the scaled *NDVI* value, whereas $\mathrm{NDVI}_{max}$and $\mathrm{NDVI}_{min}$are the *NDVI* values for fully vegetated and non-vegetated land covers.

3.4.6.3 Land Surface Temperature Algorithms

After spectral radiance is converted to radiance, the raw digital numbers of the thermal bands are converted to Top of Atmosphere (TOA) brightness temperatures, which are the effective temperature viewed by the satellite under an assumption of emissivity (Chander et al., 2009) using Planck's equation as stated below:

$$BT = \frac{K2}{\ln(\frac{K1}{L_\lambda} + 1)} \quad (9)$$

Where; BT is effective at-sensor brightness temperature (K); $K2$ is calibration constant 2 (K); $K1$ is calibration constant 1 (W/ (m^2 * sr * μm)); L_λ is spectral radiance at the sensor's aperture (W/ (m^2 * sr * μm)); ln is natural logarithm

Table 3.8: Thermal constants of Landsat images

Satellite	sensors	Categories	Band 6	Band 10	Band 11
Landsat 5	TM	K1	607.76		
		K2	1260.56		
Landsat 7	ETM+	K1	666.09		
		K2	1282.71		
Landsat 8	OLI/TIRS	K1		774.8853	480.8883
		K2		1321.0789	1201.1442

3.4.6.3.1 Mono Window Algorithm

Mono-window algorism (MWA) also called single-channel algorithm use radiance measurements in a single thermal infrared channel and correct the atmospheric effects to determine land surface temperature. This algorithm requires that the vertical and horizontal distribution of temperature and water vapor in the atmosphere is accurately known (Dash et al., 2002). Thus, the single-channel algorithm was used to compute land surface temperature for 1987 and 2002 images which are acquired by TM and ETM+ sensors. The mono-window algorithm for Landsat TM and ETM+ requires three critical parameters to estimate LST: ground emissivity, atmospheric transmittance and effective mean atmospheric temperature. The mono-window algorithm used by Jiménez-Muñoz and Sobrino (2003), Qin et al. (2001a), and Sobrino et al. (2004a, and 2004b) to retrieve LST from satellite data. Land surface temperature computes from TM and ETM+ using single channel algorithm developed by (Qin et al., 2001a).

$$T_s = \frac{1}{C}[a\,(1 - C - D) + (b(\,1 - C - D)\; + C + D)\,BT - DT_a\,] \quad (10)$$

Where ε is LSE, τ is the total atmospheric transmissivity, $BT$is brightness temperature at-sensor, T_a is the mean atmospheric temperature, and $C = \varepsilon\tau,\ D = (1-\tau)[1 + (1-\varepsilon)],\ \varepsilon = 0.99, \tau = 0.9$

$a = -67.355351, b = 0.458606$ *constants adopted from* Qin et al. (2001a)

$$T_a = 17.9769 + 0.91715T_0 \quad (11)$$

T_0 being the near-surface air temperature (376.46 K which was processed from 6S software).

3.4.6.3.2 Split Window Algorithm

Split window algorithm (SWA) also called multi-channel algorithm uses different absorption between two thermal infrared channels within one atmospheric window in order to eliminate the atmospheric influence and calculates surface temperature as a linear combination of two brightness temperatures (Dash et al., 2002). The algorithm assumes that the land surface emissivity (LSE) values in both thermal infrared channels are known (Meijun et al., 2015). This algorithm is functional for sensor where there are two TIR channel, for instance, OLI in Landsat-8 (TIRS band 10 and 11), which was used by Du et al. (2014), Jimenez-Munoz et al. (2014), Meijun et al. (2015), Qin et al. (2001b) and Rozenstein et al. (2014).

The general algorithm of the split window is given by

$$T_s = TB_{10} + C_1(TB_{10} - TB_{11}) + C_2(TB_{10} - TB_{11})^2 + C_0 + (C_3 + C_4W)(1-\varepsilon) + (C_5 + C_6W)\,\Delta\varepsilon \quad (12)$$

Where: T_s =Land Surface Temperature

C_0 up C_6 =Split Window Coefficient Value

TB_{10}=Brightness Temperature of band 10

TB_{11}=Brightness Temperature of band 11

ε =Mean Land Surface Emissivity of thermal infrared bands (mean of band 10 and band 11)

$$\varepsilon = \frac{LSE10 + LSE11}{2}$$

W =Atmospheric water vapor content (0.005) from Earth science reference table (ESRT) Relative humidity table.

$\Delta\varepsilon$ =Difference in Land Surface Emissivity (LSE); $\Delta\varepsilon = LSE10 - LSE11$

Table 3.9: Split window algorithm constant value

Constant	Value
C0	-0.268
C1	1.378
C2	0.138
C3	54.3
C4	-2.238
C5	-129.2
C6	16.4

Land surface temperature computed from Landsat TM, ETM+ and OLI/TIRS was converted into degree Celsius, by subtracting 273.15. Therefore, to convert temperature in degree Kelvin to degree Celsius equation 14 was used.

$$℃ = \mathrm{K} - 273.15 \quad (13)$$

Where: ℃: LST result in degree Celsius; K: LST result in degree Kelvin

3.4.7 Land Surface Temperature Zonation

Besides, land surface temperature was divided into three temperature zones that are low, average and high temperature zones based on minimum, maximum, mean and standard deviation. Each zone was identified using a pair of temperature thresholds that was determined based on the lowest, highest and mean temperatures of the study area (including all land-use and land-cover types) and its standard deviation. The range of the average zone was determined by subtracting the standard deviation from the mean and adding the standard deviation to the mean. Therefore, the lower limit of the average zone was obtained by subtracting the standard deviation from the mean and its upper limit is calculated by adding the standard deviation to the mean. The lowest temperature and lower limit of the average zone were used to determine the range of low zone, while the range of high zone was determined by the upper limit of the average zone and the highest temperature of the study area (Wei et al., 2015). Finally, the distribution of the three temperature zones were mapped in comparison to LULC maps.

3.4.8 Zonal Statistics

A zone is all the cells in a raster that have the same value. Zonal statistics is used to calculates statistics for each zone of a zone dataset based on values from another dataset, a value raster. It divides the raster data based on the zone and calculates statistics for the raster data in the same zone, the cells in the same zone will be assigned the same value and output to a new raster dataset. A single output value is computed for each cell in each zone defined by the input zone dataset. To analyze NDVI and LST and to understand their spatial distribution in each LULC type and their variation, zonal statistics (Zonal statistics as table) was applied in ArcGIS 10.5 environment. Land-use and land-cover, NDVI and LST maps were prepared for the year 1987, 2002 and 2017 and statistics were generated. Therefore, to analyze the spatial distribution and temporal variation of LST in each LULC and analyze the impacts of LULC change on LST data were summarized using MS Excel 2016.

3.4.9 Land Surface Temperature Validation

Land surface temperature results extracted from Landsat 5 TM, Landsat 7 ETM+ and Landsat 8 OLI/TIRS was verified using MODIS data. The MODIS land surface temperature and emissivity product at 1km spatial resolution and 8-day temporal resolution retrieved in the Hierarchical Data Format (HDF-EOS), which accessed from the NASA Land Processes Distributed Active Archive Center (NASA LP DAAC) website (https://earthdata.nasa.gov/about/daacs/daac-lpdaac).

.

CHAPTER FOUR

4. RESULTS AND ANALYSIS

4.1 Land-use and Land-cover of Bahir Dar Town and its Surrounding

As indicated in the land-use and land-cover classification result of 1987 image (Figure 15), cropland was the main land-use class in the study area. From the total study area, cropland accounted for 143.49 km^2 (59.03%). Whereas wetland vegetation, grassland, and shrubland accounted for 21.27 km^2 (8.75%), 19.17 km^2 (7.89%) and 18.06 km^2 (7.43%), respectively. Furthermore, out of the total area, service area, low density settlement, forest, open space, water body, and plantation accounted for 9.21 km^2 (3.79%), 7.7 km^2 (3.17%), 7.53 km^2 (3.1%), 6.72 km^2 (2.76%), 4.04 km^2 (1.66%), and 3.85 km^2 (1.58%), respectively (Table 4.1). Riparian vegetation, paved surfaces, industrial area and high-density settlement area together accounted for 2.03 km^2 (0.84%). From the total LULC classes of 1987 high-density settlement covered the smallest area. Details of each LULC class of the study area for 1987 are illustrated in Table 4.1 and Figures 4.1 and 4.4.

Table 4.1: LULC classes and their area coverage in 1987, 2002 and 2017

LULC Classes	1987		2002		2017	
	Area (km^2)	Area (%)	Area (km^2)	Area (%)	Area (km^2)	Area (%)
Cropland	143.49	59.03	146.58	60.3	122.63	50.45
Forest	7.53	3.1	4.62	1.9	4.43	1.82
Grassland	19.17	7.89	16.97	6.98	13.22	5.44
High density settlement	0.31	0.13	1.47	0.6	3.74	1.54
Industrial area	0.44	0.18	0.59	0.24	2.12	0.87
Low density settlement	7.70	3.17	11.14	4.58	18.44	7.59
Open space	6.72	2.76	8.13	3.34	13.27	5.46
Paved surface	0.61	0.25	0.71	0.29	1.45	0.6
Plantation	3.85	1.58	7.5	3.09	15.52	6.38
Riparian vegetation	0.67	0.28	0.66	0.27	0.67	0.28
Service area	9.21	3.79	12.42	5.11	17.23	7.09
Shrubland	18.06	7.43	10.58	4.35	9.39	3.86
Water body	4.04	1.66	4	1.65	3.91	1.61
Wetland vegetation	21.27	8.75	17.7	7.28	17.05	7.01
Total	**243.07**	**100**	**243.07**	**100**	**243.07**	**100**

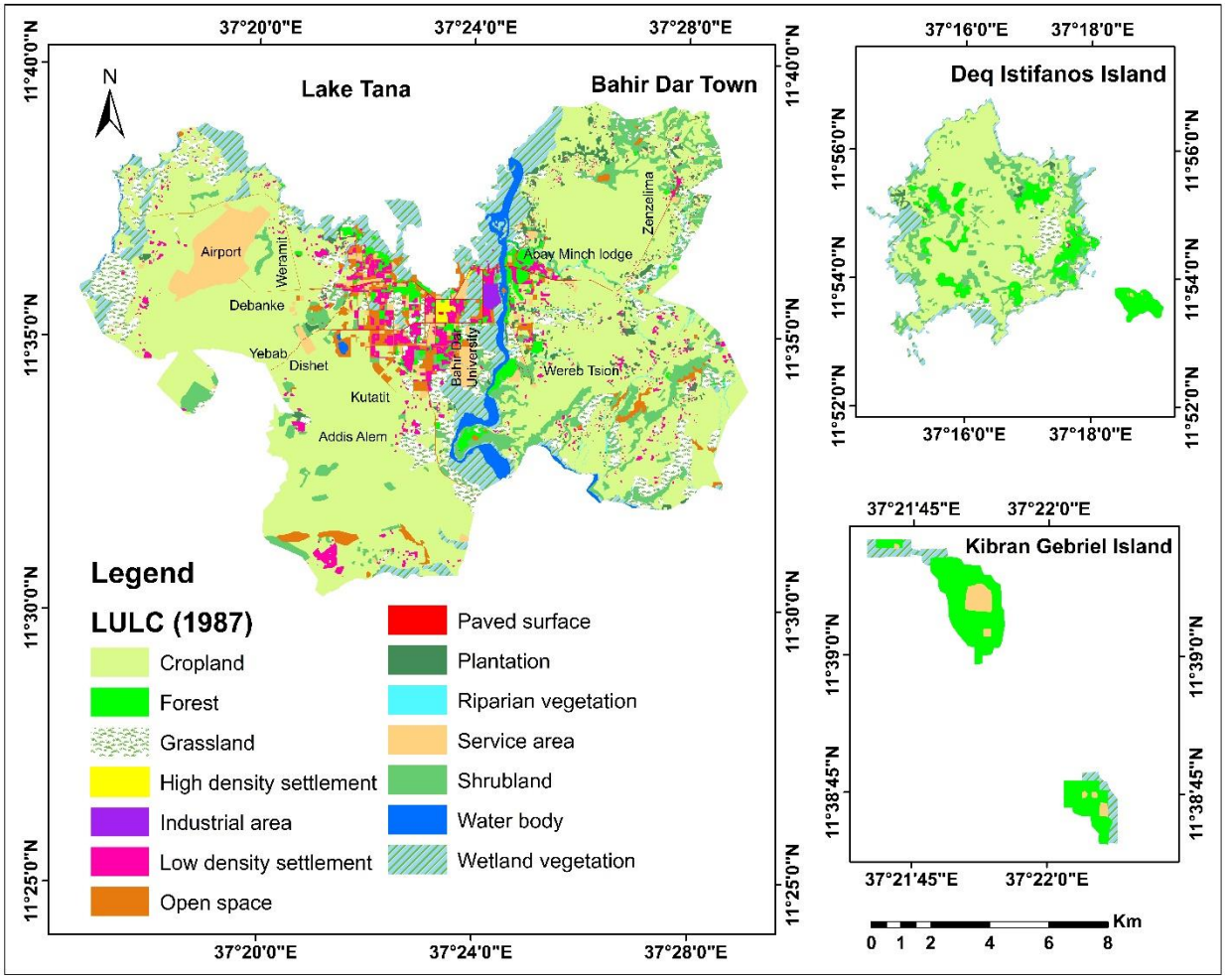

Figure 4.1: LULC map of Bahir Dar town and its surrounding in 1987

The LULC classification results of 2002 image (Figure 4.2) showed that cropland covered the largest surface in the study area again. It accounted for 146.58 km^2 (60.3%) followed by wetland vegetation, grassland, service area, low density settlement, shrubland, open space, plantation, forest and water body accounted for 17.7 km^2 (7.28%), 16.97 km^2 (6.98%), 12.42 km^2 (5.11%), 11.14 km^2 (4.58%), 10.58 km^2 (4.35%), 8.13 km^2 (3.34%), 7.5 km^2 (3.09%), 4.62 km^2 (1.9%) and 4 km^2 (1.65%), respectively (Table 4.1). Riparian vegetation, paved surfaces, industrial area and high-density settlement were other LULC classes together accounted for 3.43 km^2 (1.4%). Unlike in 1987, from the total LULC classes of 2002, the smallest area was covered by industry. Details about each LULC class of the study area for 2002 are presented in Table 4.1 and Figures 4.2 and 4.4.

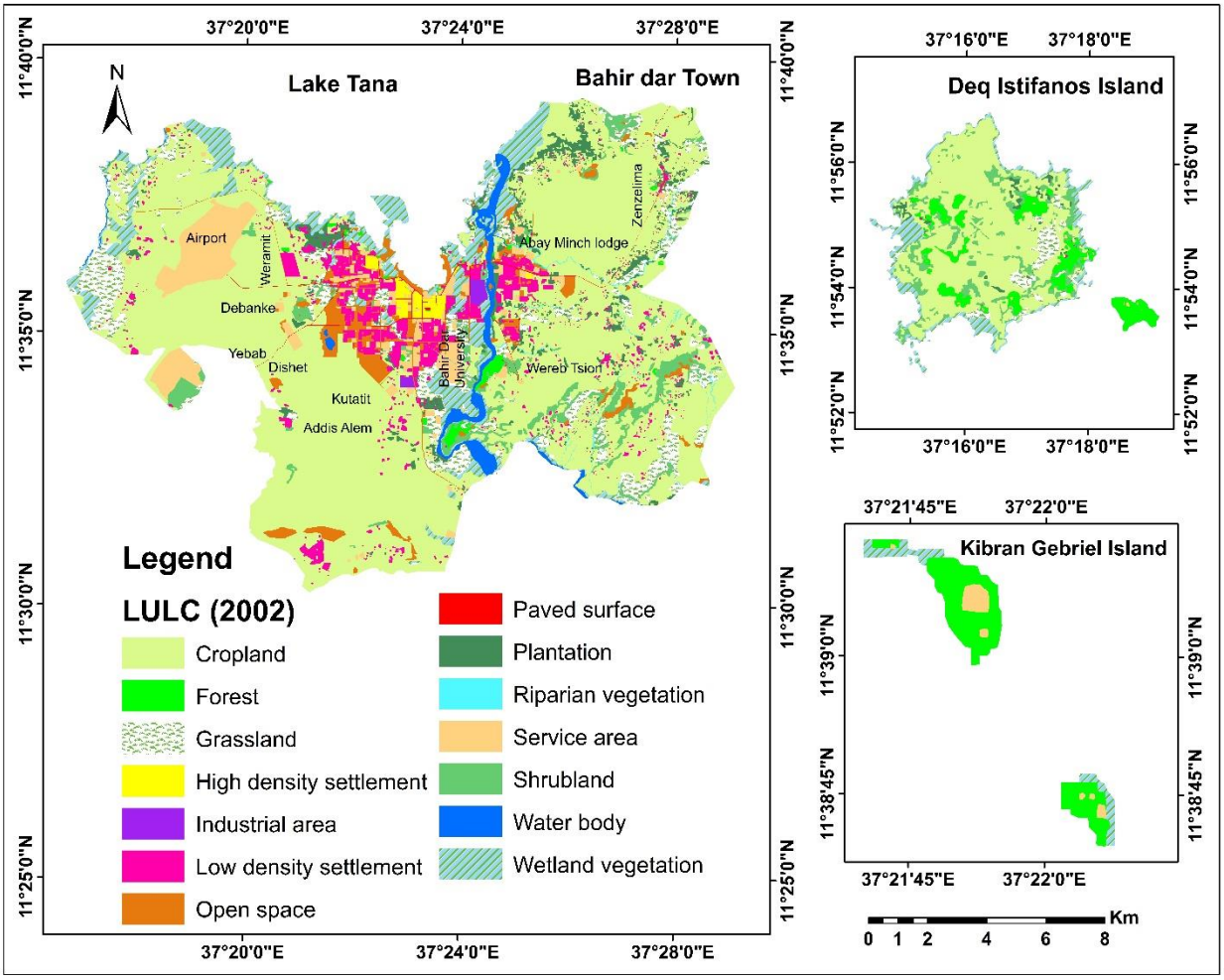

Figure 4.2: LULC map of Bahir Dar town and its surrounding in 2002

As observed in 1987 and 2002 classification map, cropland was again the leading land-use and land-cover class in 2017 having an area of 122.63 km^2 (50.45%) though it has decreased by 23.95 (9.85%) from 2002. Further, 2017 investigation indicated that from the total area of the study, 18.44 km^2 (7.59%), 17.23 km^2 (7.09%), 17.05 km^2 (7.01%), 15.52 km^2 (6.38%), 13.27 km^2 (5.46%), 13.22 km^2 (5.44%), 9.39 km^2 (3.86%), 4.43 km^2 (1.82%), 3.91 km^2 (1.61%) and 3.74 km^2 (1.54%), respectively covered by low density settlement, service area, wetland vegetation, plantation, open space, grassland, shrubland, forest, water body and high-density settlement (Table 4.1). Riparian vegetation, paved surface, and industrial area were also other LULC classes together covered 4.24 km^2 (1.75%). Details about LULC classes of the study area for 2017 are presented in Table 4.1 and Figures 4.3-4.4.

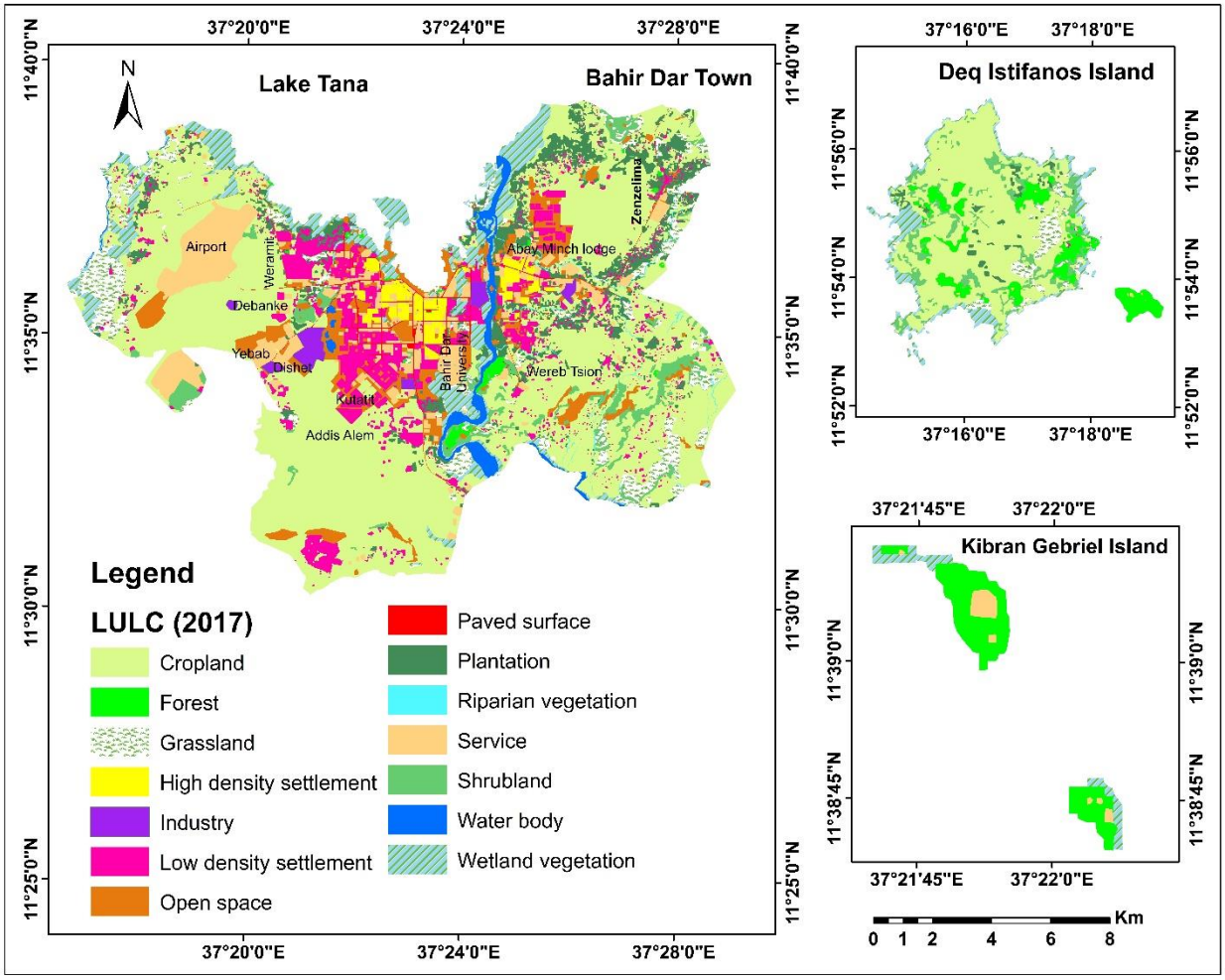

Figure 4.3: LULC map of Bahir Dar town and its surrounding in 2017

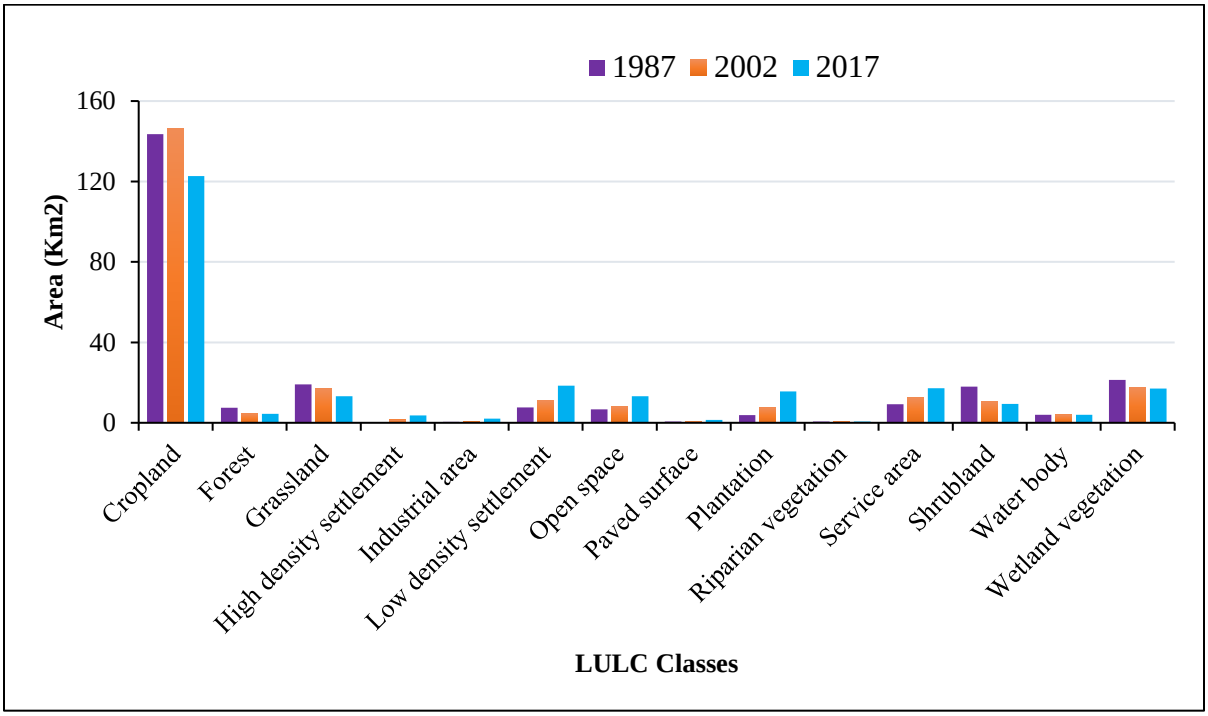

Figure 4.4: Temporal LULC changes in 1987, 2002 and 2017

4.2 Spatio-temporal Land-use and Land-cover Changes

The results of the study indicated that there was a significant change in the pattern of LULC in Bahir Dar town and its surrounding from 1987 to 2017. From the total LULC classes, half of the study area was cropland though it has reduced from 143.49 km^2 (59.03%) in 1987 to 122.63 (50.45%) in 2017. Shrubland has also declined from 18.06 km^2 (7.43%) by 1987 to 10.58 km^2 (4.35%) in 2002 and reached to 9.39 km^2 (3.86%) in 2017. Grassland diminished from 19.17 km^2 (7.89%) in the year 1987 to 16.97 km^2 (6.98%) in 2002 and 13.22 km^2 (5.44%) in 2017. Besides, the area extent of wetland vegetation has reduced since 1987 which was 21.27 km^2 (8.75%), then reduced to 17.7 km^2 (7.28%) in 2002 and 17.05 km^2 (7.01%) in 2017. Similarly, the spatial extent of forest cover has been decreasing from 7.53 km^2 (3.1%) in 1987 to 4.62 km^2 (1.9%) in 2002 and 4.43 km^2 (1.82%) in 2017. Further, the cover of water body reduced from 1987 to 2017. It was 4.04 km^2 (1.66%), 4 km^2 (1.65%) and 3.91 km^2 (1.61%) in 1987, 2002 and 2017 respectively.

However, landscape covered with plantation has increased from 1987-2017. It increased from 3.85 km^2 (1.58%,) in 1987 to 7.5 km^2 (3.09%) in 2002 and 15.52 km^2 (6.38%), in 2017. Moreover, low-density settlement changed from 7.7 km^2 (3.17%) in 1987, 11.14 km^2 (4.58%) in 2002 to 18.44

km^2 (7.59%) in the year 2017. The service area was another land-use class that showed continuous increment from 1987 to 2017. It was 9.21 km^2 (3.79%) in 1987 and this has increased to 12.42 km^2 (5.11%) in 2002 and 17.23 km^2 (7.09%) in 2017. Open space type of urban land use and land-cover has also increased from 6.72 km^2 (2.76%) by 1987 to 8.13 km^2 (3.34%) in 2002 and 13.27 km^2 (5.46%) in 2017. High-density settlement has increased from 0.31 km^2 (0.13%) by 1987 to 1.47 km^2 (0.6%) in 2002 and 3.74 km^2 (1.54%) by 2017. Furthermore, industrial area has increased from 1987 to 2002 and 2017 with 0.44 km^2 (0.18%), 0.59 km^2 (0.24%) to 2.12 km^2 (0.87%) respectively. The paved surface has expanded in 2017 which was 1.45 (0.6%) while it was 0.61 km^2 (0.25%) and 0.71 km^2 (0.29%) in 1987 and 2002, respectively. However, riparian vegetation has not changed during the study periods. Details of spatial and temporal land-use and land-cover change of Bahir Dar town and its surroundings are presented in Table 4.2 and Figures 4.5-4.8.

Table 4.2: LULC change in Bahir Dar town and its surrounding in 1987, 2002 and 2017

LULC Classes	1987		2002		2017		Net-Change 1987-2002 (km^2)	Net-Change (1987-2002) %	Net-change 2002-2017 (km^2)	Net-change 2002-2017 %	Net-change 1987-2017 (km^2)	Net-change 1987-2017 %
	Area km^2)	Area (%)	Area (km^2)	Area (%)	Area (km^2)	Area (%)						
CL	143.49	59.03	146.58	60.30	122.63	50.45	3.09	1.27	-23.95	-9.85	-20.86	-8.58
FO	7.53	3.10	4.62	1.90	4.43	1.82	-2.91	-1.20	-0.19	-0.08	-3.1	-1.28
GL	19.17	7.89	16.97	6.98	13.22	5.44	-2.2	-0.91	-3.75	-1.54	-5.95	-2.45
HDS	0.31	0.13	1.47	0.60	3.74	1.54	1.16	0.48	2.27	0.93	3.43	1.41
IN	0.44	0.18	0.59	0.24	2.12	0.87	0.15	0.06	1.53	0.63	1.68	0.69
LDS	7.7	3.17	11.14	4.58	18.44	7.59	3.44	1.42	7.3	3.00	10.74	4.42
OP	6.72	2.76	8.13	3.34	13.27	5.46	1.41	0.58	5.14	2.11	6.55	2.69
PS	0.61	0.25	0.71	0.29	1.45	0.60	0.1	0.04	0.74	0.30	0.84	0.35
PL	3.85	1.58	7.5	3.09	15.52	6.38	3.65	1.50	8.02	3.30	11.67	4.80
RV	0.67	0.28	0.66	0.27	0.67	0.28	-0.01	0.00	0.01	0.00	0	0.00
SA	9.21	3.79	12.42	5.11	17.23	7.09	3.21	1.32	4.81	1.98	8.02	3.30
SH	18.06	7.43	10.58	4.35	9.39	3.86	-7.48	-3.08	-1.19	-0.49	-8.67	-3.57
WB	4.04	1.66	4	1.65	3.91	1.61	-0.04	-0.02	-0.09	-0.04	-0.13	-0.05
WV	21.27	8.75	17.7	7.28	17.05	7.01	-3.57	-1.47	-0.65	-0.27	-4.22	-1.74
Total	243.07		243.07		243.07							

Where: CL=cropland, FO= forest, GL=grassland, HDS=high density settlement, IN=industrial area, OP=open space, PL=plantation, PS=paved surface, RV=riparian vegetation, SA=service area, SH=shrubland, LDS=low density settlement, WB=water body, WV=wetland vegetation

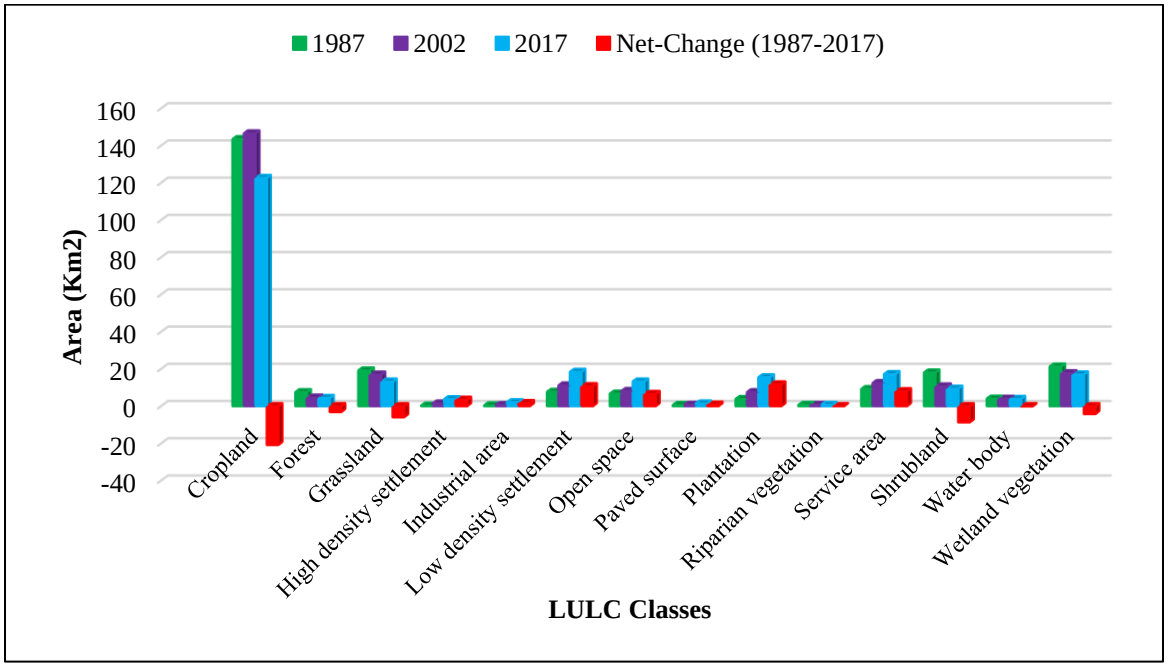

Figure 4.5: Temporal LULC distribution and changes in 1987, 2002 and 2017

Land-use and land-cover transformation matrix presented in Table 4.3 shows that cropland in 1987 converted into service area, low-density settlement, plantation, open space, and grassland in 2002. The major cropland transformation made by the expansion of service area (2.03 km^2) and low-density settlement (1.79 km^2). In contrary to this, 5.35 km^2 cropland area was gained from shrubland in 2002. Shrubland also changed to grassland, open space, plantation, service, and low-density settlement. Furthermore, 3.33 km^2 grassland were converted to cropland in 2002. Grassland in 1987 was also changed to high and low-density settlement, open space, plantation, service area, and cropland. Wetland vegetation was converted to cropland, service area, open space and low-density settlement particularly places along the shore of Lake Tana and Abay River, places found in the side of Bahir Dar University, and some place in the west of Bahir Dar general market. Wetland vegetation also transformed to grassland, plantation, and shrubland. In the year 1987, from the total forest cover change, 1.28 km^2 and 0.34 km^2 were converted to low and high-density settlement respectively. In the same year, forest cover also changed into plantation, service area, cropland, open space, shrubland, and grassland. In addition, water body receded and the area was covered with wetland vegetations (bushland and grassland) in 2002. Details about land-use and land-cover transformation matrix from 1987-2002 are illustrated in Table 4.3 and Figures 4.6.

Table 4.3: LULC changes matrix of Bahir Dar town and its Surrounding during 1987-2002 (in km^2)

LULC 1987	LULC Class	LULC 2002														
		CL	FO	GL	HDS	IN	OP	PL	PS	RV	SA	SH	LDS	WB	WV	Class Total
	CL	**136.32**	0.03	0.02			1.39	1.94			2.03		1.79			143.49
	FO	0.25	**4.59**	0.07	0.34		0.22	0.33			0.30	0.15	1.28			7.53
	GL	3.33		**14.72**	0.06		0.26	0.39			0.22		0.14		0.05	19.17
	HDS				**0.31**											0.31
	IN					**0.44**										0.44
	OP	0.01			0.10	0.15	**5.38**	0.02	0.12		0.40		0.53			6.72
	PL	0.02						**3.82**								3.85
	PS						0.04		**0.57**							0.61
	RV									**0.66**						0.67
	SA				0.08						**9.13**					9.21
	SH	5.35		1.02			0.37	0.61			0.13	**10.34**	0.24			18.06
	LDS				0.57						0.07		**7.04**			7.7
	WB													**3.98**	0.05	4.04
	WV	1.30		1.14			0.49	0.39			0.14	0.10	0.11		**17.62**	21.27
	Class Total	146.58	4.62	16.97	1.47	0.59	8.13	7.50	0.71	0.66	12.42	10.58	11.14	4	17.7	**243.07**

Where: CL=cropland, FO= forest, GL=grassland, HDS=high density settlement, IN=industrial area, OP=open space, PL=plantation, PS=paved surface, RV=riparian vegetation, SA=service area, SH=shrubland, LDS=low density settlement, WB=water body, WV=wetland vegetation

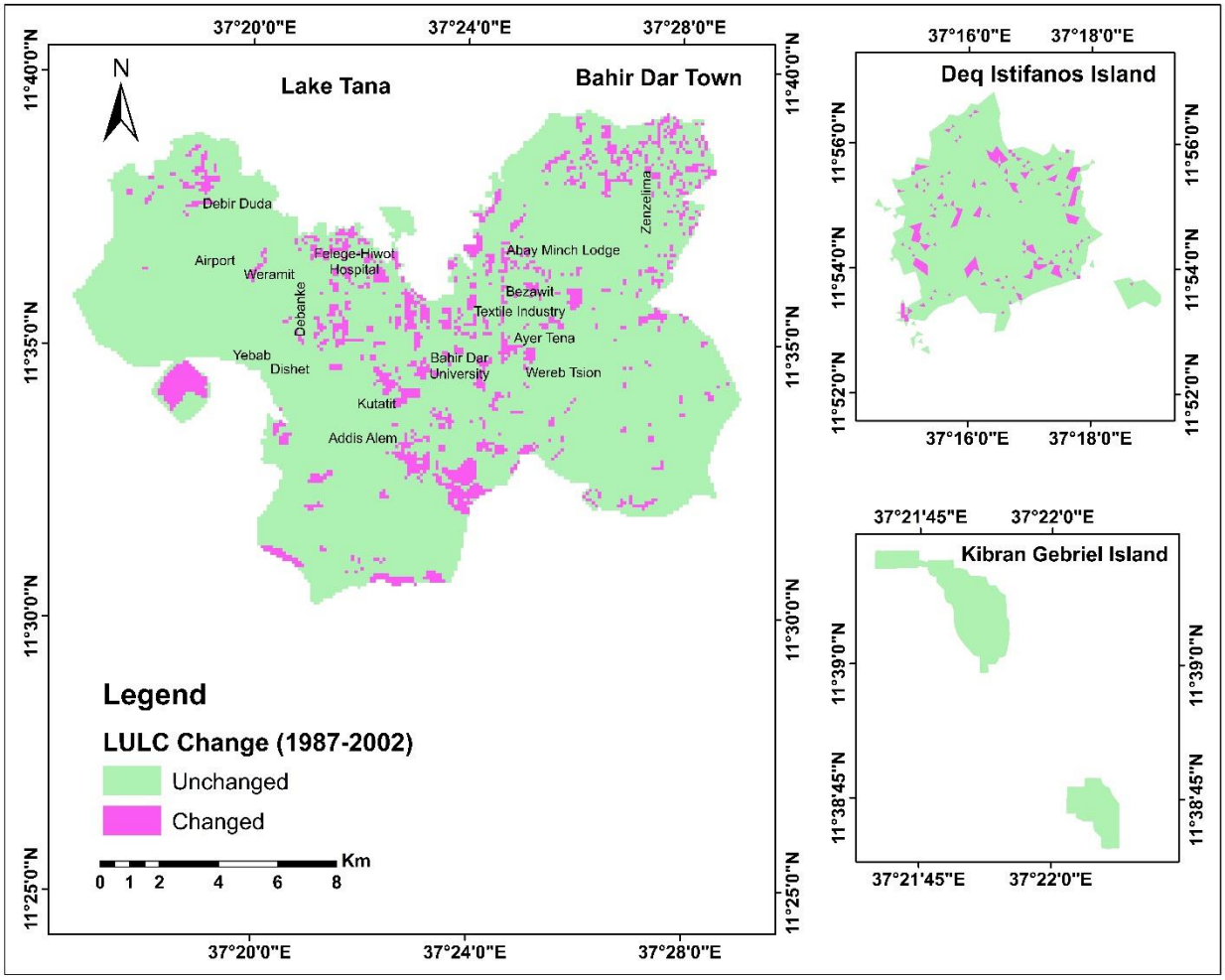

Figure 4.6: LULC changes of Bahir Dar town and its surrounding from 1987-2002

As Table 4.4 shows that, from the total area of cropland in 2002, 7.88 km^2, 7.59 km^2, 5.43 km^2 were respectively converted to low-density settlement, plantation, open space in 2017. During 2002-2017, cropland also converted into service and industrial areas, grassland, high-density settlement, wetland vegetation, and paved surface. Further, place covered with grassland in the year 2002 transformed to open space (1.58 km^2) and cropland (0.82 km^2) after fifteen years. In 2017, service area, plantation, low-density settlement, shrubland, high-density settlement, and wetland vegetation were expanded at the expense of grassland. Shrubland also changed into open space, plantation, cropland, service area, grassland, low-density settlement, forest and wetland vegetation. Table 4.4 and Figure 4.7 present the detail information of land-use and land-cover transformation/change from 2002 to 2017.

Table 4.4: LULC changes matrix of Bahir Dar town and its Surrounding during 2002-2017 (in km^2)

LULC 2002	LULC Classes	LULC 2017														
		CL	FO	GL	HDS	IN	OP	PL	PS	RV	SA	SH	LDS	WB	WV	Class Total
	CL	**121.10**		0.19	0.04	1.33	5.43	7.59	0.01		2.95	0.03	7.88		0.03	146.58
	FO		**4.41**				0.04	0.06			0.04	0.03	0.04			4.62
	GL	0.82		**12.65**	0.14		1.58	0.54			0.54	0.22	0.45		0.04	16.97
	HDS				**1.47**											1.47
	IN					**0.59**										0.59
	OP	0.09		0.03	0.15	0.20	**4.99**	0.04	0.74		0.76		1.04	0.10	0.01	8.13
	PL	0.06		0.01			0.09	**6.66**			0.11	0.02	0.54			7.50
	PS								**0.69**							0.71
	RV									**0.66**						0.66
	SA							0.01			**12.40**		0.01			12.42
	SH	0.31	0.02	0.07			0.51	0.43			0.12	**9.04**	0.07		0.01	10.58
	LDS	0.25			2.00		0.36	0.05	0.01		0.22	0.05	**8.19**			11.14
	WB							0.02		0.01				**3.78**	0.17	4
	WV	0.12		0.26	0.01		0.28	0.12			0.09		0.02		**16.81**	17.7
	Class Total	122.63	4.43	13.22	3.74	2.12	13.27	15.52	1.45	0.67	17.23	9.39	18.44	3.91	17.05	**243.07**

Where: CL=cropland, FO= forest, GL=Grassland, HDS=high density settlement, IN=industrial area, OP=open space, PL=plantation, PS=paved surface, RV=riparian vegetation, SA=service area, SH=shrubland, LDS=low density settlement, WB=water body, WV=wetland vegetation

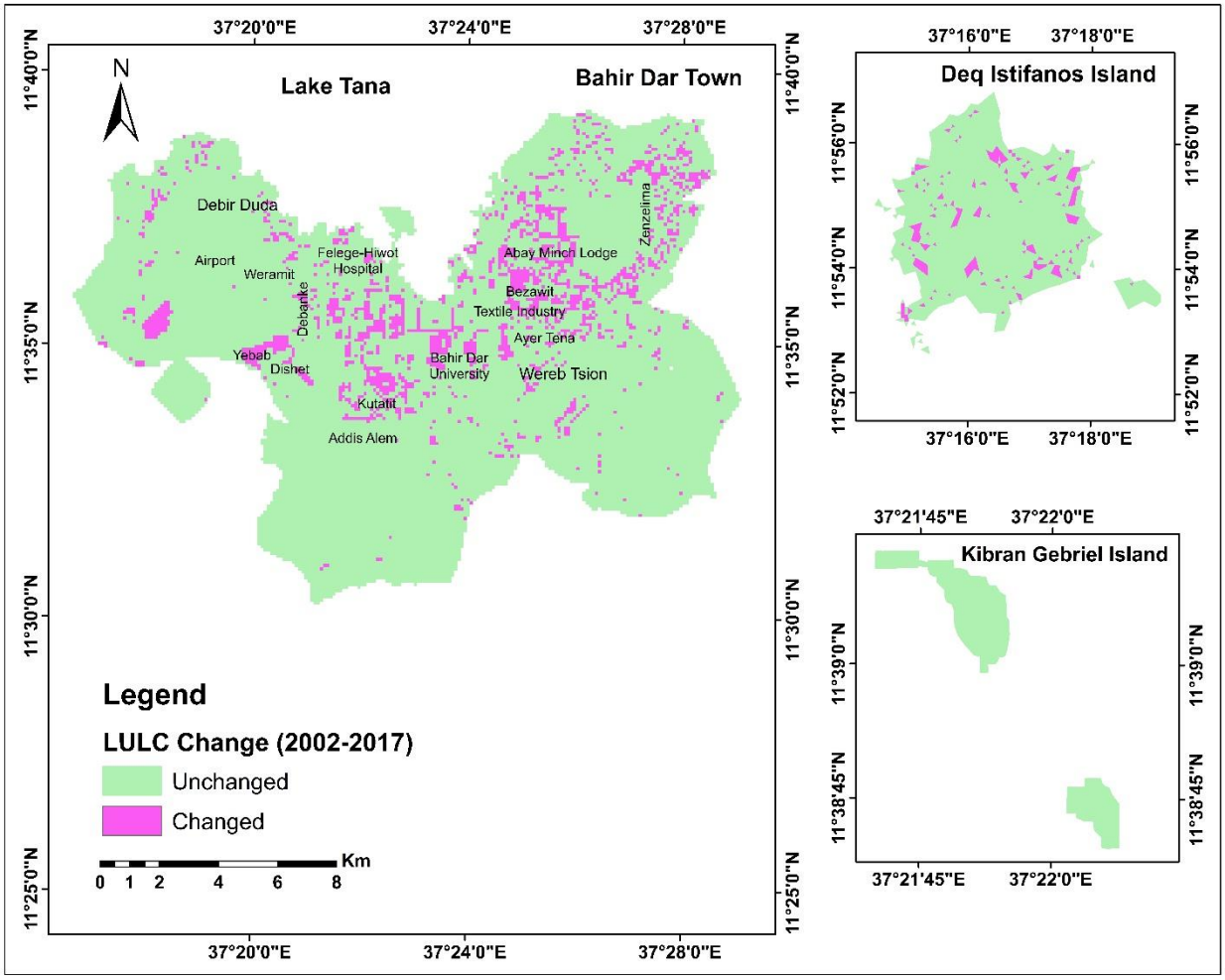

Figure 4.7: LULC changes of Bahir Dar town and its surrounding from 2002-2017

Moreover, wetland vegetation areas in 2017 were reduced due to the expansion of open space, grassland, cropland, plantation, service area, low and high-density settlement particularly place along the shore of Lake Tana and Abay River, and place found in the adjacent of Bahir Dar University. During 2002-2017, forest cover was converted to plantation, service area, open space, low-density settlement, and shrubland. In the same year, areas covered with water body were converted to wetland vegetation, plantation and riparian vegetation. During 1987-2017, cropland, grassland, shrubland, forest, wetland vegetation, water body was converted into other land-use types. Land-use and land-cover change matrix of Bahir Dar town and its surrounding from 1987-2017 is illustrated in Table 4.5 and Figure 4.8.

Table 4.5: LULC changes matrix of Bahir Dar town and its Surrounding during 1987-2017 (in km^2)

		LULC 2017														
	LULC Class	CL	FO	GL	HDS	IN	OP	PL	PS	RV	SA	SH	LDS	WB	WV	Class Total
LULC 1987	CL	**113.45**	0.01	0.19	0.32	1.47	5.77	7.70	0.02		5.05	0.03	9.52			143.49
	FO	0.02	**4.40**	0.02	1.17		0.31	0.37			0.42	0.15	0.64			7.53
	GL	3.23		**11.04**	0.22		1.73	1.25	0.03		0.78	0.06	0.81		0.01	19.17
	HDS				**0.31**											0.31
	IN					**0.44**										0.44
	OP				0.24	0.16	**3.61**	0.02	0.75		0.84		0.99	0.10	0.01	6.72
	PL	0.05					0.04	**3.54**			0.05		0.17			3.85
	PS								**0.61**							0.61
	RV									**0.67**						0.67
	SA				0.08						**9.12**					9.21
	SH	4.64	0.02	0.82	0.08	0.06	0.71	1.78			0.38	**9.09**	0.49		0.01	18.06
	LDS	0.24			1.34		0.26	0.05	0.01		0.27	0.05	**5.47**			7.69
	WB							0.02						**3.78**	0.21	4.04
	WV	1.15		1.15	0.04		0.85	0.78	0.02		0.32		0.15		**16.82**	21.27
	Class Total	122.63	4.43	13.22	3.74	2.12	13.27	15.52	1.45	0.67	17.23	9.39	18.44	3.91	17.05	**243.07**

Where: CL=cropland, FO= forest, GL=grassland, HDS=high density settlement, IN=industrial area, OP=open space, PL=plantation, PS=paved surface, RV=riparian vegetation, SA=service area, SH=shrubland, LDS=low density settlement, WB=water body, WV=wetland vegetation

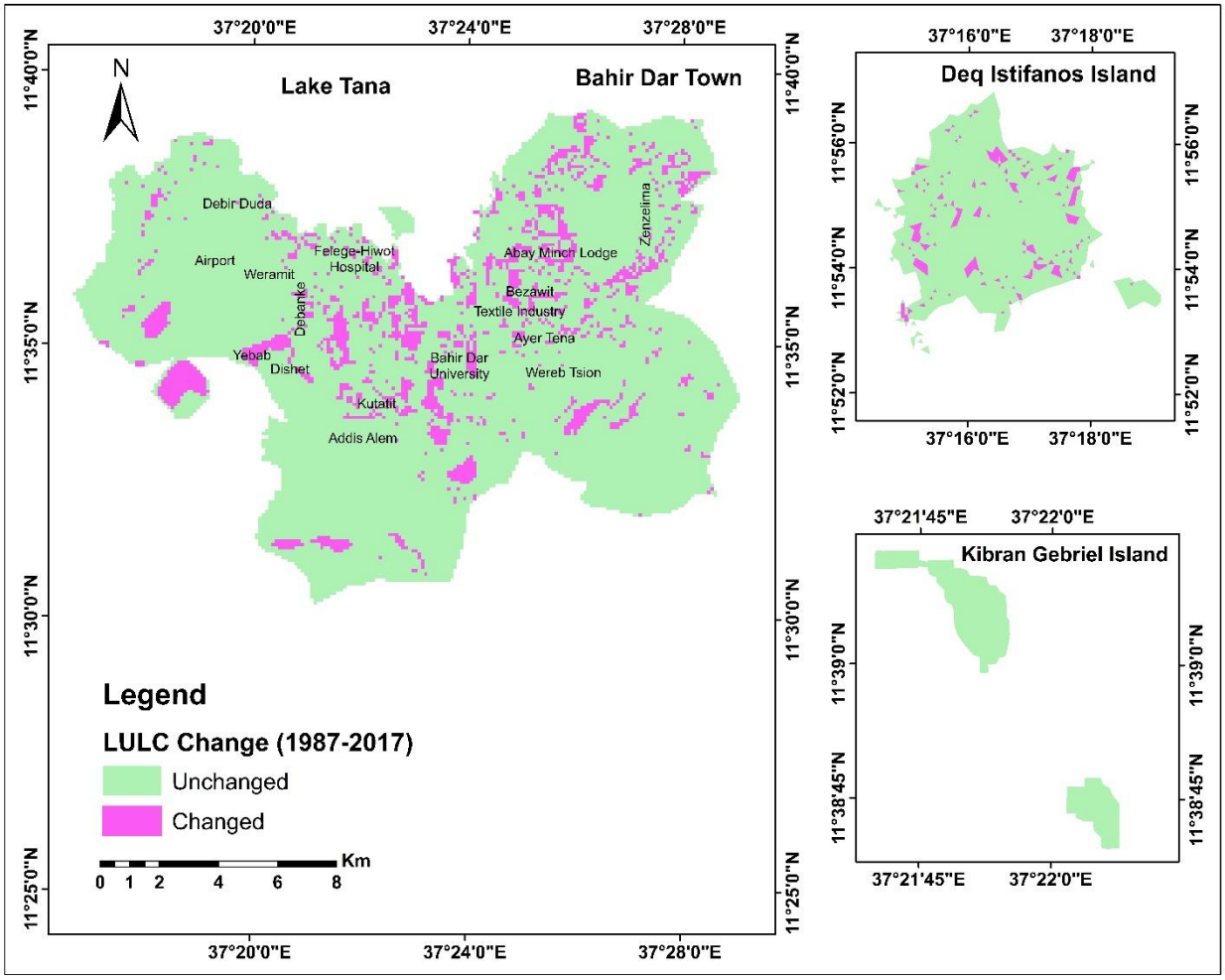

Figure 4.8: LULC changes of Bahir Dar town and its surrounding from 1987-2017

4.3 Accuracy Assessment

Land-use and land-cover accuracy assessment for 1987, 2002 and 2017 years produced the overall classification accuracy of 85.71%, 86.61%, and 92%, respectively. The overall land-use and land-cover classification Kappa statistics for the study periods were 0.854, 0.864 and 0.92, respectively. Table 4.6 presents the details of land-use and land-cover accuracy assessment of the study period.

Table 4.6: Error matrix of land-use and land-cover for 1987, 2002 and 2017

LULC Class	1987		2002		2017	
	Producers Accuracy (%)	Users Accuracy (%)	Producers Accuracy (%)	Users Accuracy (%)	Producers Accuracy (%)	Users Accuracy (%)
CL	66.67	75	75	75	100	87.5
FO	88.89	100	88.89	100	87.5	75
GL	77.78	87.5	83.33	62.5	83.3	62.5
HDS	72.73	100	100	100	100	100
IN	80	100	80	100	89.89	100
LDS	100	75	100	62.5	87.5	87.5
OP	100	87.5	72.73	100	80	100
PL	88.9	100	88.9	100	100	100
PS	100	75	100	75	100	87.5
RV	100	62.5	100	62.5	100	100
SA	100	62.5	88.89	100	88.89	100
SH	70	87.5	70	87.5	87.5	87.5
WB	100	87.5	100	87.5	100	100
WV	88.89	100	88.89	100	88.89	100
Overall Accuracy	85.71		86.61		92	
$\widehat{K}$	0.854		0.864		0.92	

Where: CL=cropland, FO= forest, GL=grassland, HDS=high density settlement, IN=industrial area, OP=open space, PL=plantation, PS=paved surface, RV=riparian vegetation, SA=service area, SH=shrubland, LDS=low density settlement, WB=water body, WV=wetland vegetation, $\widehat{K}$= kappa coefficient

4.4 Spatio-temporal Distribution of Normalized Difference Vegetation Index

The result of this study indicates that the spatial extent of vegetation cover was very high in 1987 than 2002 in the study area. Hence, NDVI values were higher in 1987 with its maximum of 0.61 than 2002 which was 0.45. This indicates that there was high healthy vegetation cover in 1987 than in 2002. In 2017, vegetation cover was slightly increased and this made the NDVI value to increase from 0.45 to 0.48 (Table 4.7).

Table 4.7: Normalized difference vegetation index results in 1987, 2002 and 2017

Year	MIN	MAX	MEAN	STD
1987	-0.48	0.61	0.09	0.09
2002	-0.66	0.45	-0.20	0.10
2017	-0.19	0.48	0.15	0.07

Where: MIN = Minimum, MAX = Maximum, STD = Standard deviation

Figure 4.9-4.11 illustrated that places along the shore of Lake Tana and its neighboring areas and Abay River bank and in some surrounding places, some places in the northeast of Abay waterfall (the place where Abay River leaves from Lake Tana), the western and southern tip of Bahir Dar town have higher NDVI values. Further, in Deq Istifanos Island, some places along Lake Tana shore and southeast part of the Island have higher NDVI. Some parts of central Deq Istifanos which were covered with service areas like Monasteries and churches also have high NDVI values. Kibran Gebriel is another island found in Lake Tana which had higher NDVI values. However, most parts of the south, southeast, west along airport, southeast, east, northeast of the town had low NDVI values. Central parts of Bahir Dar town where there were more settlement areas and most parts of central Deq Istifanos Island also have low NDVI values.

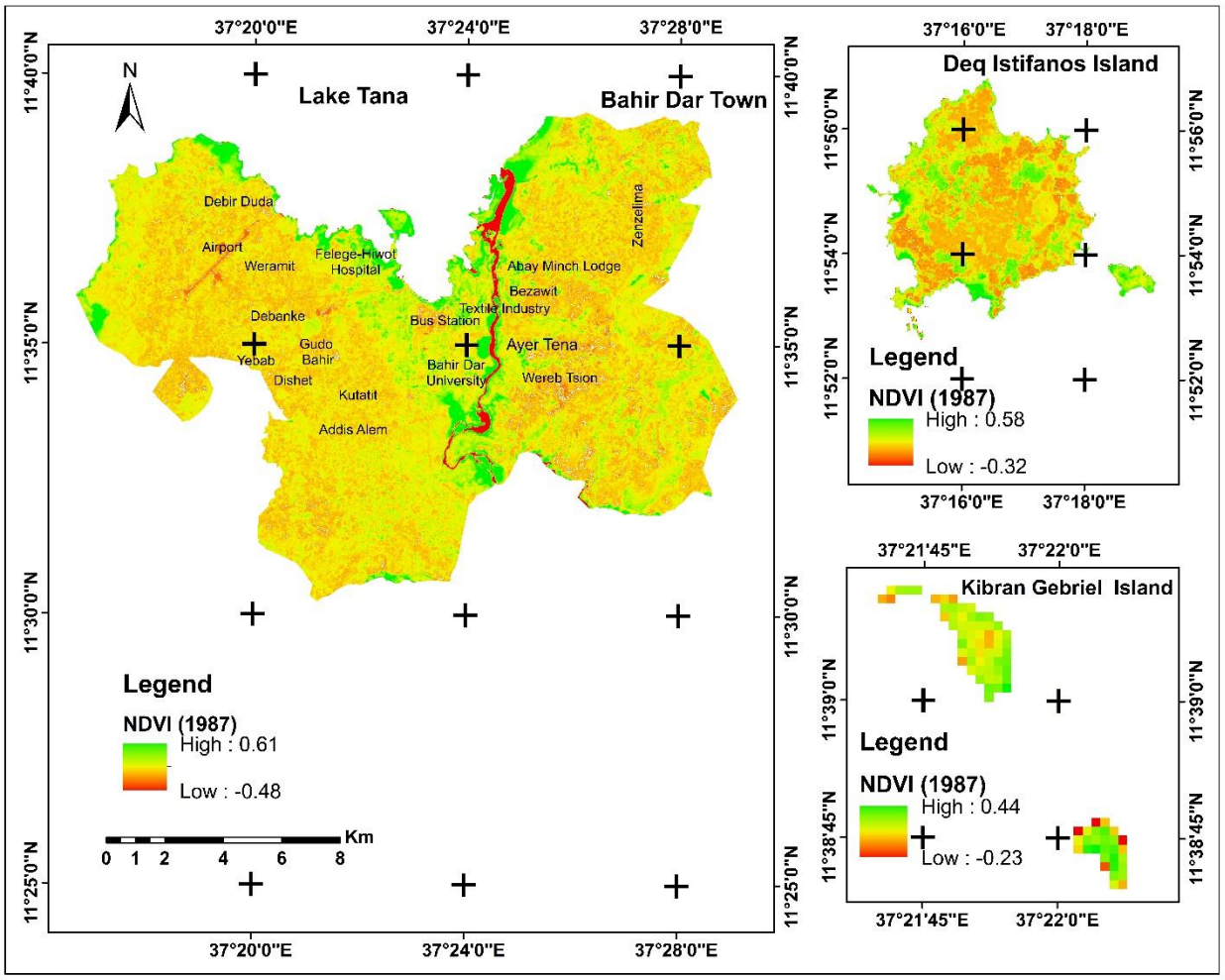

Figure 4.9: NDVI map of Bahir Dar town and its surrounding in 1987

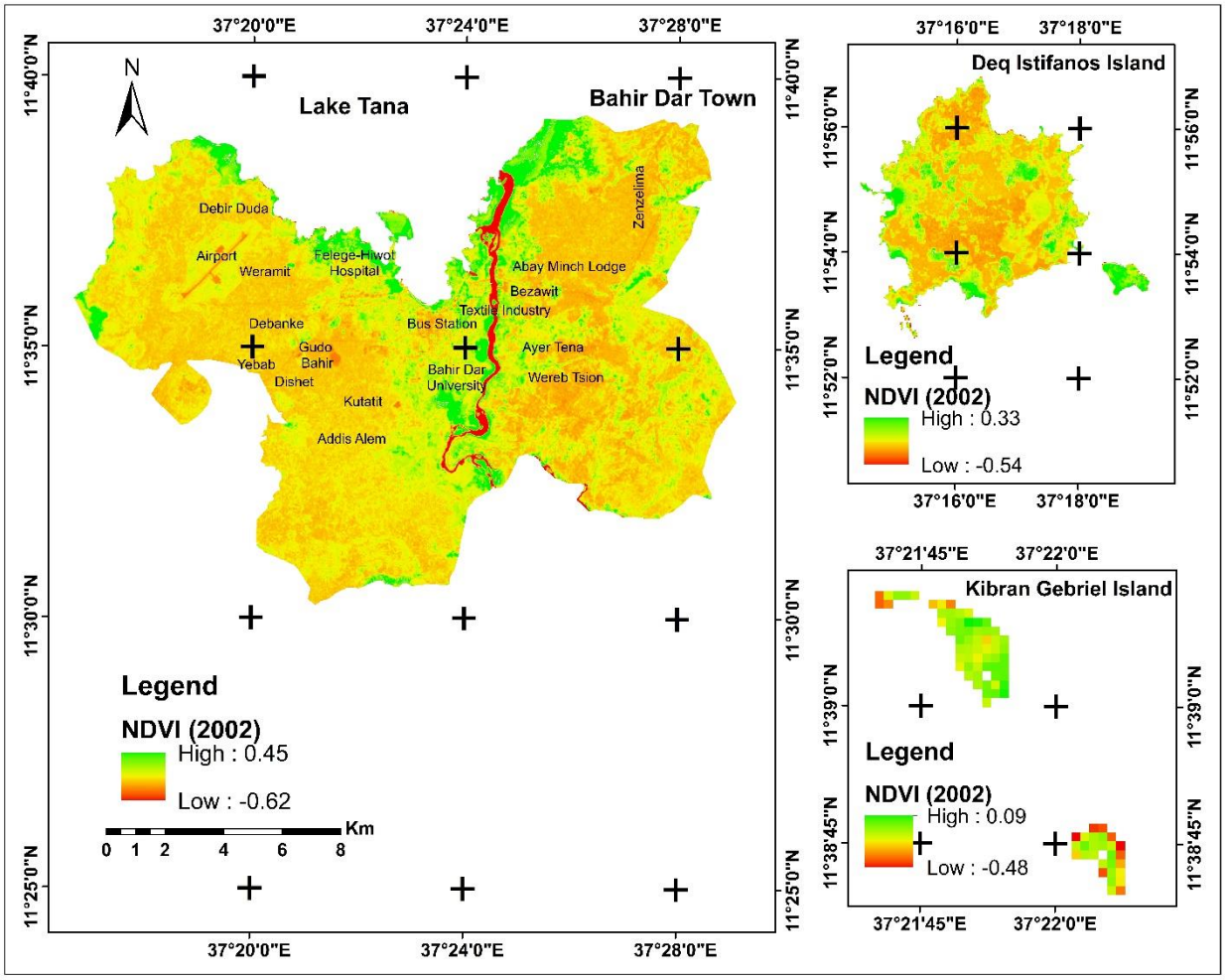

Figure 4.10: NDVI map of Bahir Dar town and its surrounding in 2002

Nevertheless, NDVI value in 2017 has somewhat increased as compared to that of the year 2002 due to the expansion of plantation and green spaces. Therefore, some region in the northeast and northwest of the town that is close to the lake and places on both side of Abay River, and marshland areas located southern and western tip of Bahir Dar town had exceptionally high NDVI values. Besides, central, eastern and southern parts of the town had relatively low NDVI value than in 1987 and 2002 (Figure 4.11).

Contrary to terrestrial bodies, NDVI values of water bodies such as ponds which are located along Addis Ababa Gateway road and Abay River, and marsh area (more water than small grass) in the northwest tip of Bahir Dar and Deq Istifanos and Kibran Gebriel islands were below zero.

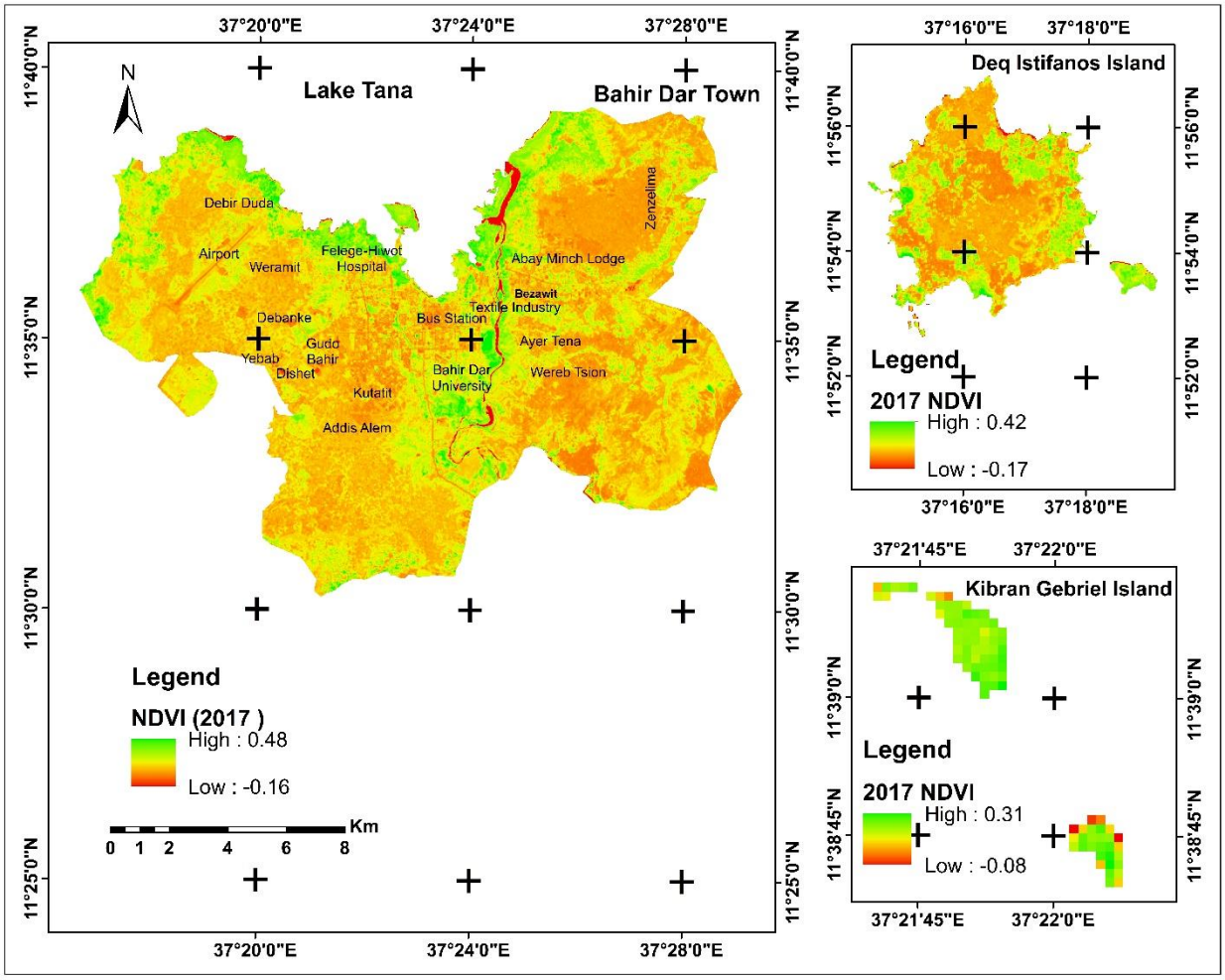

Figure 4.11: NDVI map of Bahir Dar town and its surrounding in 2017

4.5 The Relationship between Land-use and Land-cover Types and Normalize Difference Vegetation Index Values

Figure 4.12 illustrates that forest had high NDVI values because of high chlorophyll concentration and green leaf and dense canopy. Areas covered with wetland vegetation, plantation, shrubland, riparian vegetation and grassland also have higher NDVI values. Open space (a region which was covered with green areas, recreation sites), and service area (covered with tree such as green parks) relatively have high NDVI value. Croplands have low NDVI values (below 0.2). Further, high and low-density settlement, paved surfaces like asphalt, roads, car parking and industrial area also have low NDVI values. The NDVI value for waterbody was below zero.

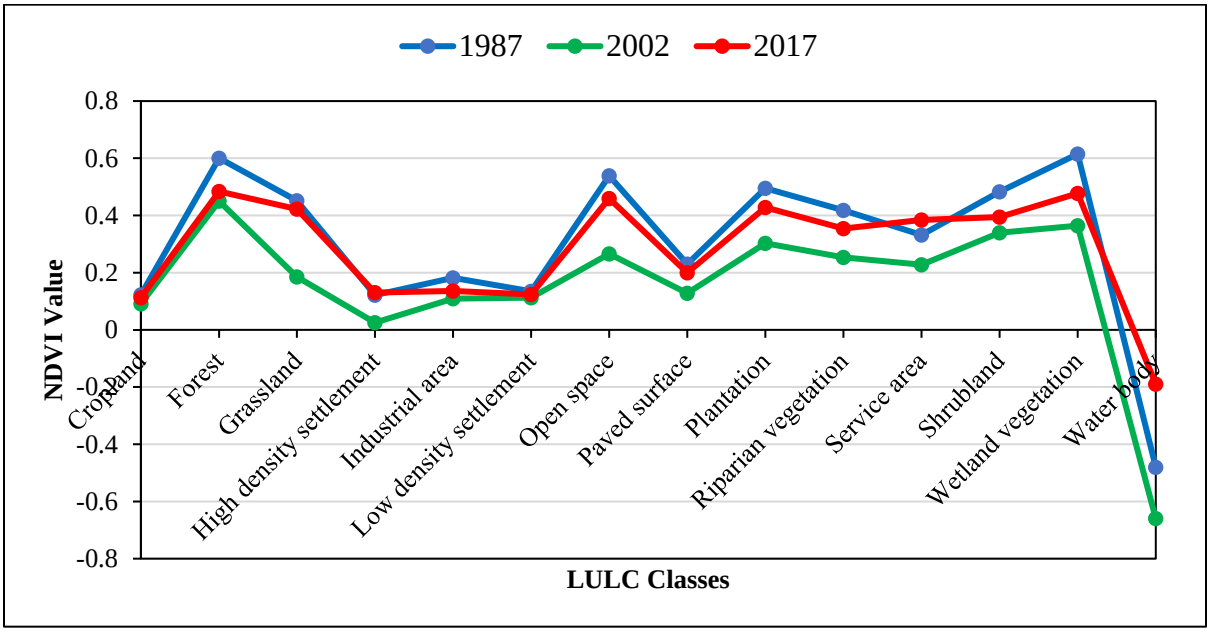

Figure 4.12: NDVI of LULC classes of Bahir Dar town and its surrounding in 2017

4.6 Spatial and Temporal Distribution of Land Surface Temperature in Bahir Dar Town and its Surrounding

The land surface temperature of the study area from 1987 to 2017 ranges from 12.35 ℃ to 43.01 ℃. In 1987, most locations in the southwest, west, east and southeast region of Bahir Dar town had high temperature (Figure 4.13). The majority of those areas were cropland with some barren rock which was exposed directly to incoming radiation during the month of March. The influence of Lake Tana and Abay River on the LST decreases away from this water bodies. The areas that were not included in the influence zone of Abay River and Lake Tana had recorded the highest LST reaching up to 34.93 ℃. In the central part of Bahir Dar town where there was high-density settlement mainly the surrounding areas of bus station have higher LST. In addition, most of the central parts of Deq Istifanos Island which were dominated by cropland have also recorded a higher temperature (i.e. 30.59 ℃) than places covered by plantation, shrubland, forest and wetland vegetations. In contrary, places close to Lake Tana and Abay River, and west and southern tip of the town have a low temperature (i.e. 12.35 ℃). Kibran Gebriel Island also has a low land surface temperature with the range of 12.35 ℃-15.32 ℃. Spatial distribution of LST of Bahir Dar town and its surrounding for the year of 1987 is presented in Figure 4.13.

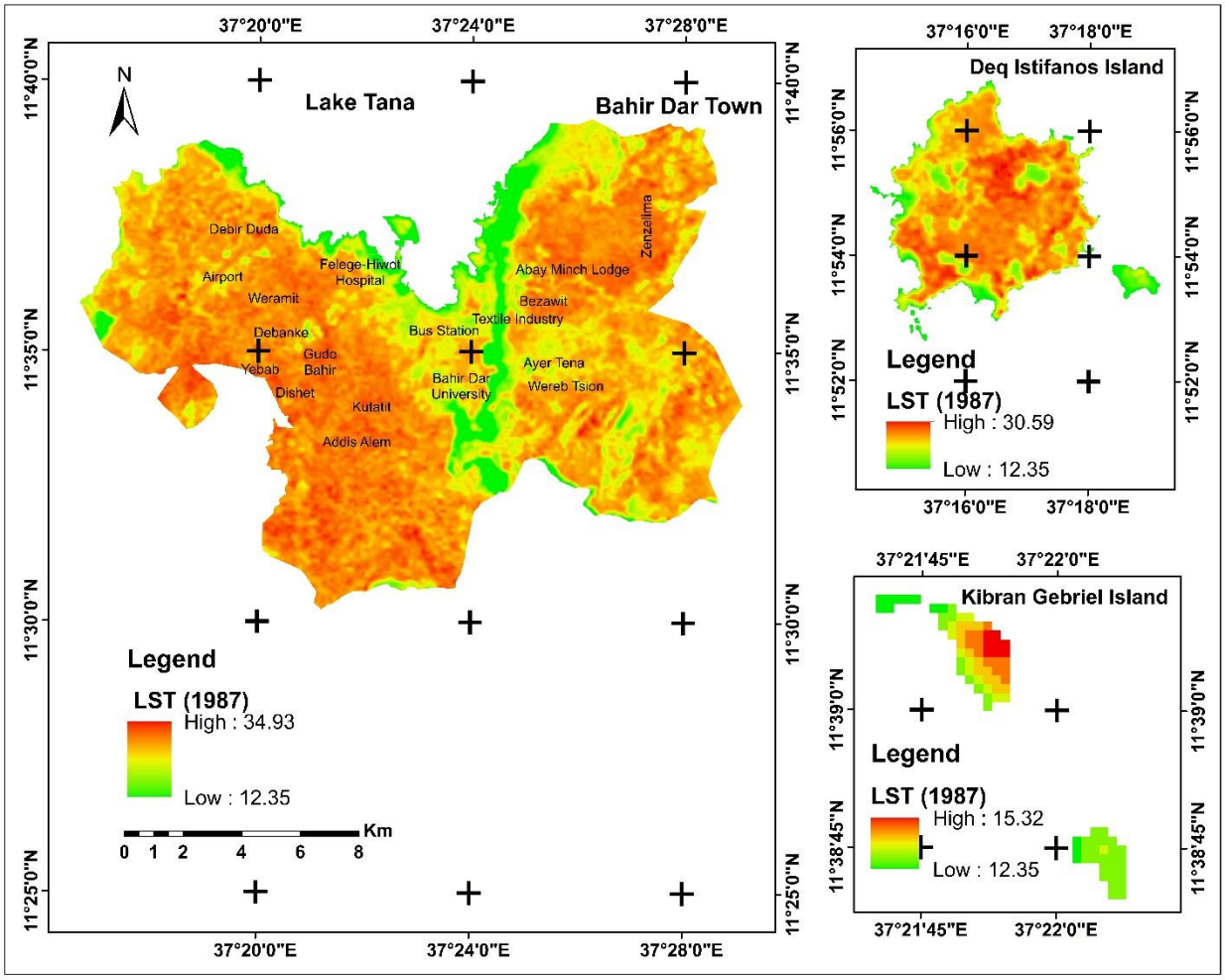

Figure 4.13: LST map of Bahir Dar town and its surrounding in 1987

The spatial extent of LST in 2002 was higher than the year 1987 with its maximum value of 38.87℃, 34℃ and 20.32℃ in Bahir Dar town, and Deq Istifanos and Kibran Gebriel islands respectively. These areas were found in west, south and east of the airport (around Debir Duda, and Weramit), southwestern (area along Yibab, Gudo Bahir and Dishet) and eastern zone (Zenzelima town and its surrounding) of the town as well as central Deq Istifanos Island. However, some places which covered with plantation, green area and shrublands particularly north of Abay waterfall and most of the airport have a low temperature. In the year 2002, the neighboring places of Lake Tana and River Abay such as the low density settlement close to Bahir Dar University and the surrounding areas of Bahir Dar Felege-Hiwot Hospital, recreation areas along the lake and the river, and plantation, shrubland and marshland areas along these places had low temperature even though minimum temperature in 2002 was higher than 1987 (Figure 4.13 and 4.14).

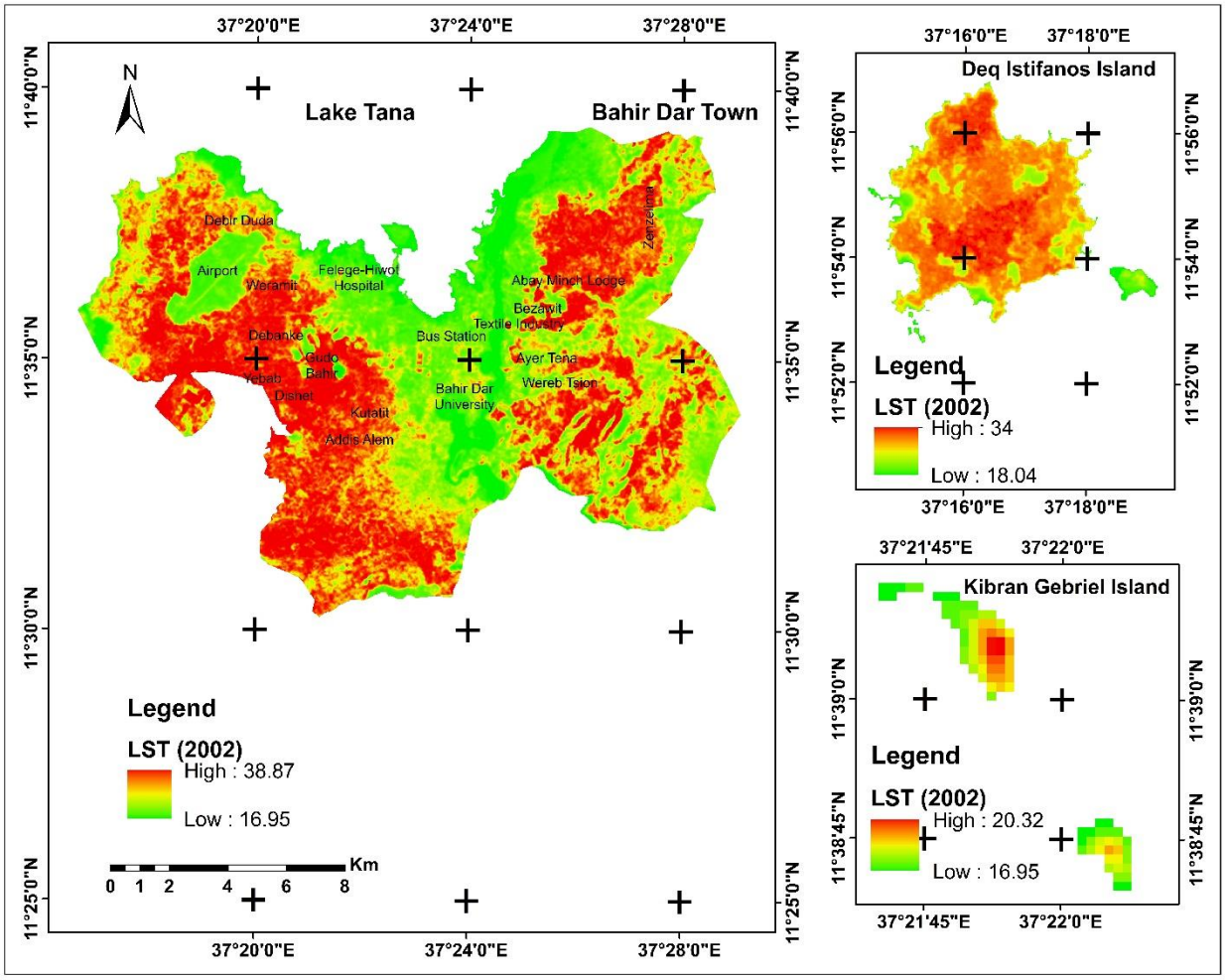

Figure 4.14: LST map of Bahir Dar town and its surrounding in 2002

The land surface temperature analysis in 2017 showed that still east, southeast, southwest and central region of Bahir Dar town and central Deq Istifanos Island were warmer than place located on the side of River Abay and surrounding place of Lake Tana. Besides, high urbanization in south (Addis Alem and Kutatit), southwest (Yibab, Gudo Bahir and Dishet) and eastern region (northeast and east of Abay Minch Lodge) of the town and increase in industrial areas in southwest contribute significantly to the warming of Bahir Dar town in 2017 (Figure 4.15).

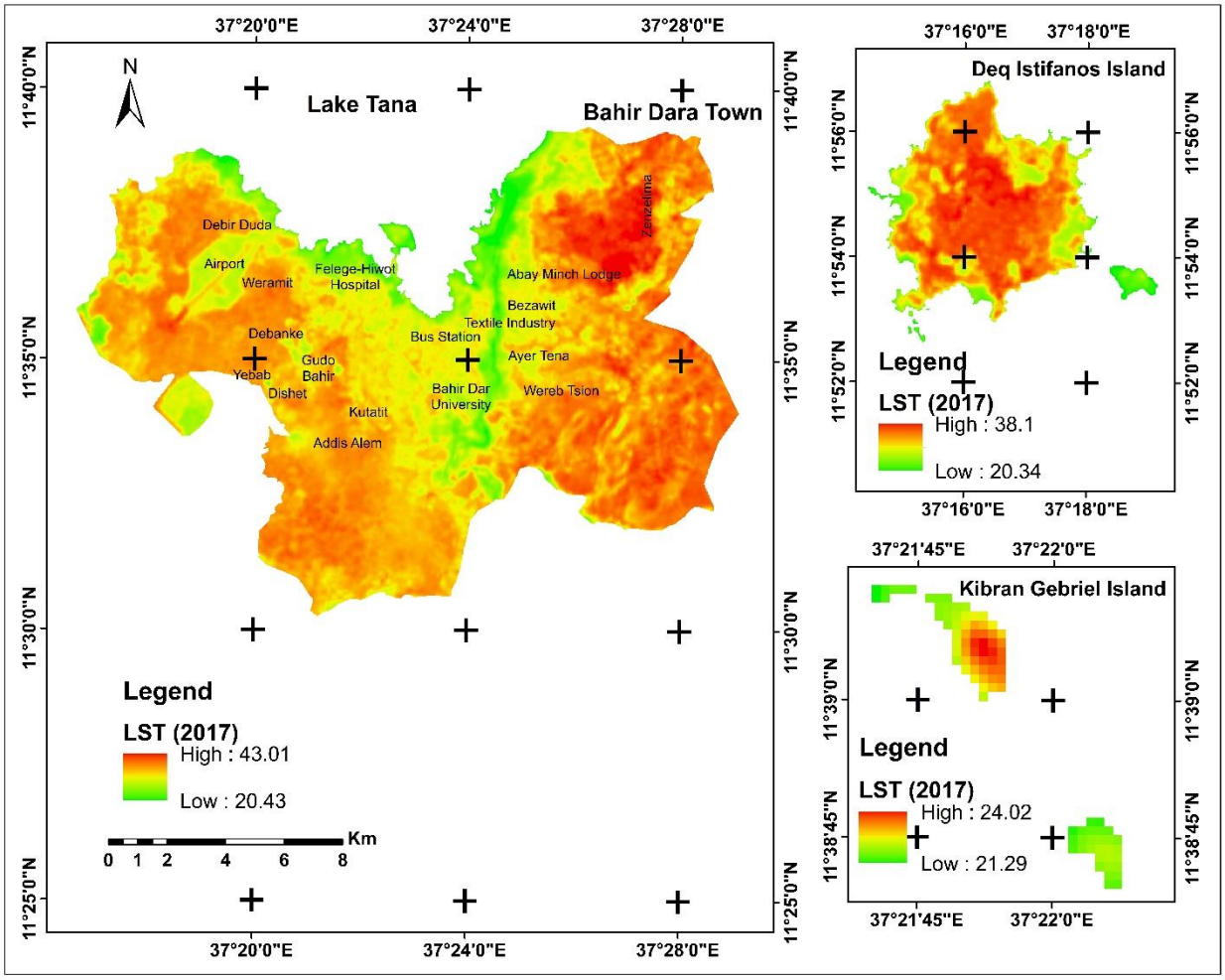

Figure 4.15: LST map of Bahir Dar town and its surrounding in 2017

4.7 Influence of Lake Tana and Abay River for Land Surface Temperature Distribution

Bahir Dar town is situated along the southern shore of Lake Tana. This is valuable for the town since it gets fresh air condition from the lake especially during daytime, and this situation modifies or regulates the surface temperature of the town. During the daytime as the Lake surface is cooler than the town and its surrounding, the prevailing wind blows from the lake towards the town. Thus, such wind brings cooler air and that can refresh the town. Therefore, settlement found along the shore of Lake Tana, for example, places located north of Felege-Hiwot Hospital, and Abay Minch Lodge and major areas in the north and west of the lodge get more moist and cold air from the lake and have low LST. However, distant areas could not get enough cold air from the lake. As the distance increases cold air blowing over the town is gets warm before reaching to those areas. So,

far place such as west of Debanke, Yebab, Weramit, Dishet and its eastern part, Addis Alem and its southern part, Zenzelima and its surrounding, Werb Tsion and its south and eastern parts had high land surface temperature. River Abay also influences the land surface temperature of the surrounding areas. Further, places along Abay River and wetland adjoining areas like Bahir Dar University, textile factory, Abay lodge and neighboring areas had relatively low land surface temperature. In addition, the amount of humidity from Lake Tana and the direction of the wind control the LST of the town. As Figure 4.16 indicates that on 13 March 2017 during the daytime wind blowing towards N130° (southeast), N180° and N190°(south) directions. Details of prevailing wind direction is presented in Figure 4.16.

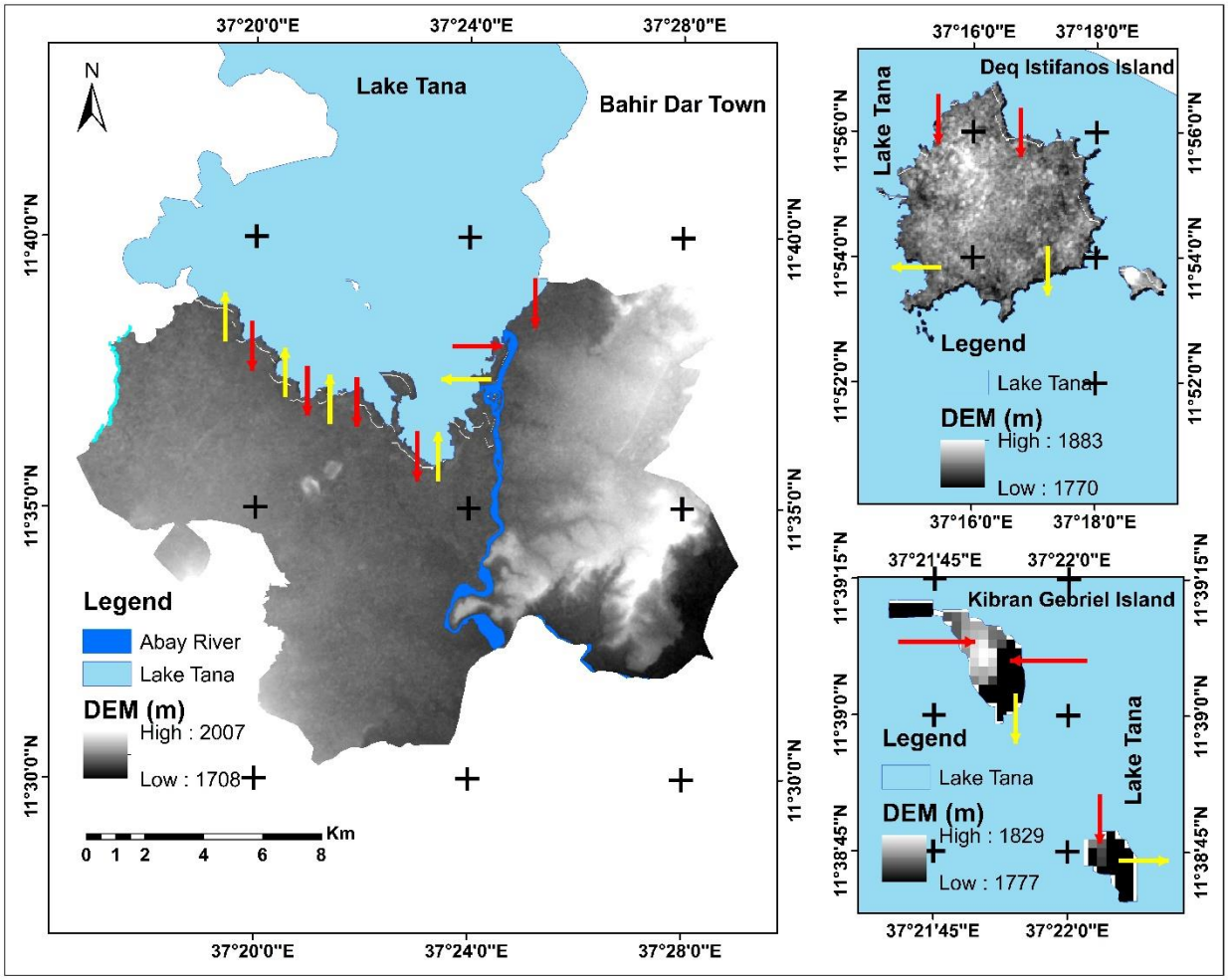

Figure 4.16: Prevailing wind directions and LST distribution (on 13 March 2017)

The red arrow indicates daytime wind direction (sea breeze) and yellow arrow indicates night wind direction (land breeze)

The surrounding and closest areas of the town got moist air and therefore, the temperature of those areas was low. However, during the night time, Bahir Dar town is relatively cooler than the lake and hence, the prevailing wind blows from high pressure and cooler body (town) to low pressure and warmer body (Lake Tana).

The nature of topography and elevation of places also have an effect on the variation of the land surface temperature of Bahir Dar town and its surrounding. For instance, high escarpment areas covered with riparian vegetation, shrubland, and grassland in the northeast, east (west and east of Zenzelima town), southeast parts of the town had high land surface temperature. There is also a ridge in the west and southwest part of the study area that are characterized by higher LST. Moreover, the topography of central part of Bahir Dar town is relatively flat and its elevation ranges from 1755-1826 m, and LST values of the area are relatively high heat island. Places located along Lake Tana and River Abay have similar elevation with central Bahir Dar town, however, LST values were low due to the influence of these water bodies.

4.8 Verification of Land Surface Temperature Result

The land surface temperature extracted from Landsat thermal band of the study area for the study periods were validated based on MODIS data that was acquired during similar period, though, MODIS has a coarser resolution. The LST result extracted from 2017 MODIS ranges from 23.97℃ to 44.55℃. The maximum land surface temperature obtained from 2017 Landsat image varied from 20.43℃ to 43.01℃. The ranges of LST observed using both sensors over the study area were close to each other. As indicated in Figure 4.17, places which are close to Lake Tana shore and Abay River had a low temperature on LST derived from MODIS as well. Most west, southwest, south, southeast, and east parts of Bahir Dar town had a high land surface temperature. The LST result derived from Landsat 8 indicates that central Deq Istifanos Island and the major place in the south and east of the town exhibited high temperature, and places found along the water body and wetland vegetation, and plantation and forest cover had low temperature.

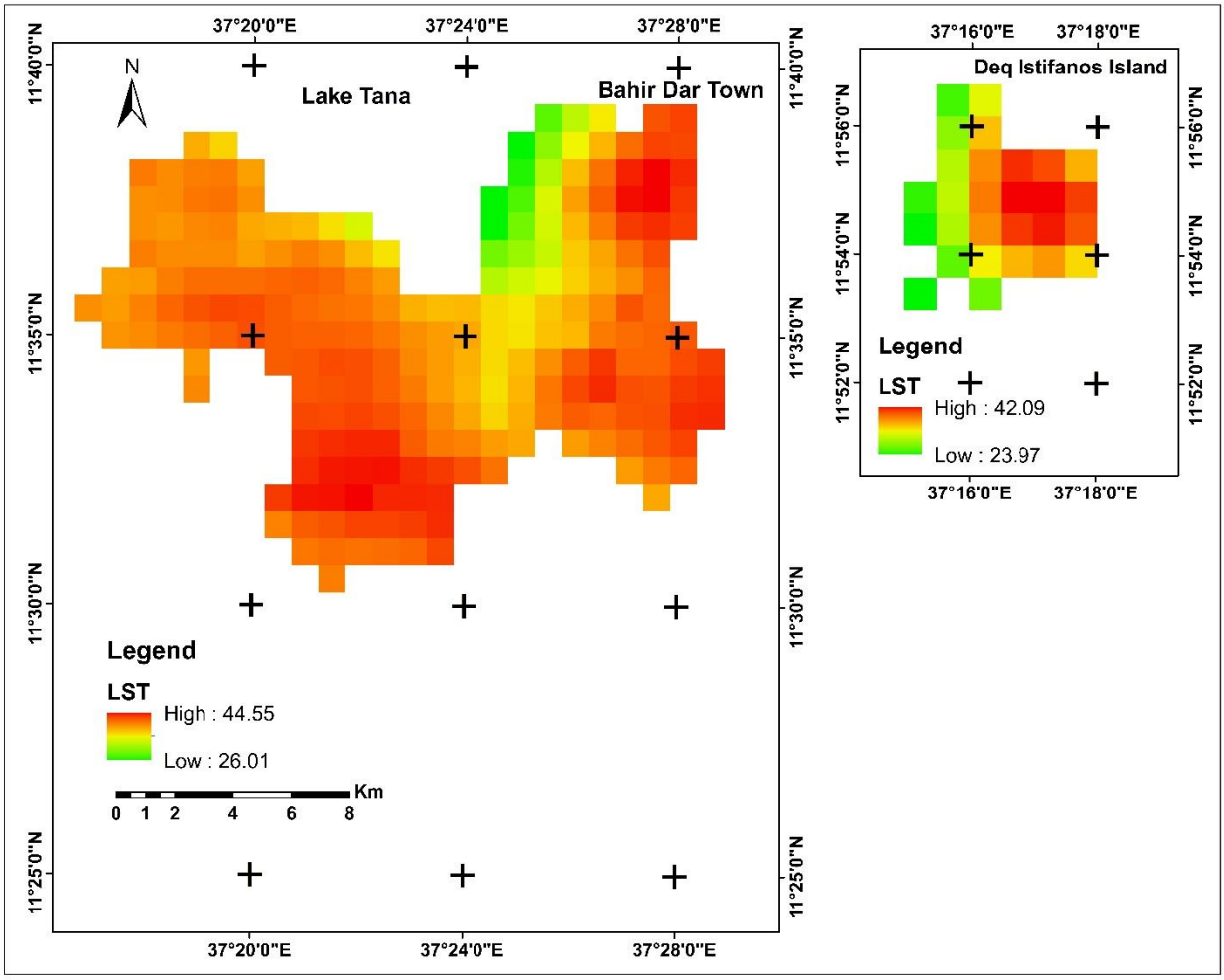

Figure 4.17: MODIS (1km) based LST used to validate the LST derived from Landsat 8

4.9 Land Surface Temperature Distribution and Zonation in 1987, 2002 and 2017

Based on the results obtained from this study, it was observed that the LST has been gradually increasing from 1987 to 2017. Basically, in the study periods, land surface temperature of Bahir Dar town and its surrounding was in the range of 12.35ºC-43.01ºC. The land surface temperature was classified into three zones, namely Low, Average and High zones (Table 4.8 and Figure 4.18-4.20). As Table 4.8 illustrate, in 1987 most of the places of Bahir Dar and its surrounding had an average temperature range from 25.01ºC -32.73 ºC, and it covered an area of 201.65km^2. In the same year, low temperature zone that ranges from 12.35 ºC -25.01 ºC was covered an area of 28.64 km^2. From the total study area, 12.78 km^2 was covered with high temperature zone in 1987. The ranges of temperature for this zone was from 32.73 ºC -34.93 ºC. This temperature was radically changed to 38.78ºC in 2002. As a result, low, high and average temperature zones, respectively

had covered 12.78 km^2, 109.99 km^2 and 103.94 km^2. In 2017, maximum LST was higher than 40℃ and larger parts of the study area were covered by high temperature zone. The details of LST zone and their aerial coverage are presented in Table 4.8.

Table 4.8: LST zones and their aerial coverage in 1987, 2002 and 2017

Year	LST Zone in ℃	Area km^2	Total Area
	12.35-25.01 (Low zone)	28.64	
	25.01-32.73 (Average zone)	201.65	
1987	32.73-34.93 (High zone)	12.78	243.07
	16.96-26.76 (Low zone)	29.14	
	26.76-34.16 (Average zone)	103.94	
2002	34.16-38.78 (High zone)	109.99	243.07
	20.93-30.69 (Low zone)	27.42	
	30.96-38.49 (Average zone)	89.32	
2017	38.49-43.01 (High zone)	126.33	243.07

Figure 4.18 indicates that in 1987 most parts of west, southwest, east and southeast Bahir Dar town was categorized in high temperature zone. Some places in the central Bahir Dar town also have high land surface temperature. Besides, some place in east, southeast and central part of the town and the major area of Deq Istifanos Island, had high temperature and fall under average land surface temperature zone. Besides, places located along Lake Tana shore and Abay River, wetland vegetation in the west, and Kibran Gebriel Island had low LST and were grouped in the low temperature zone.

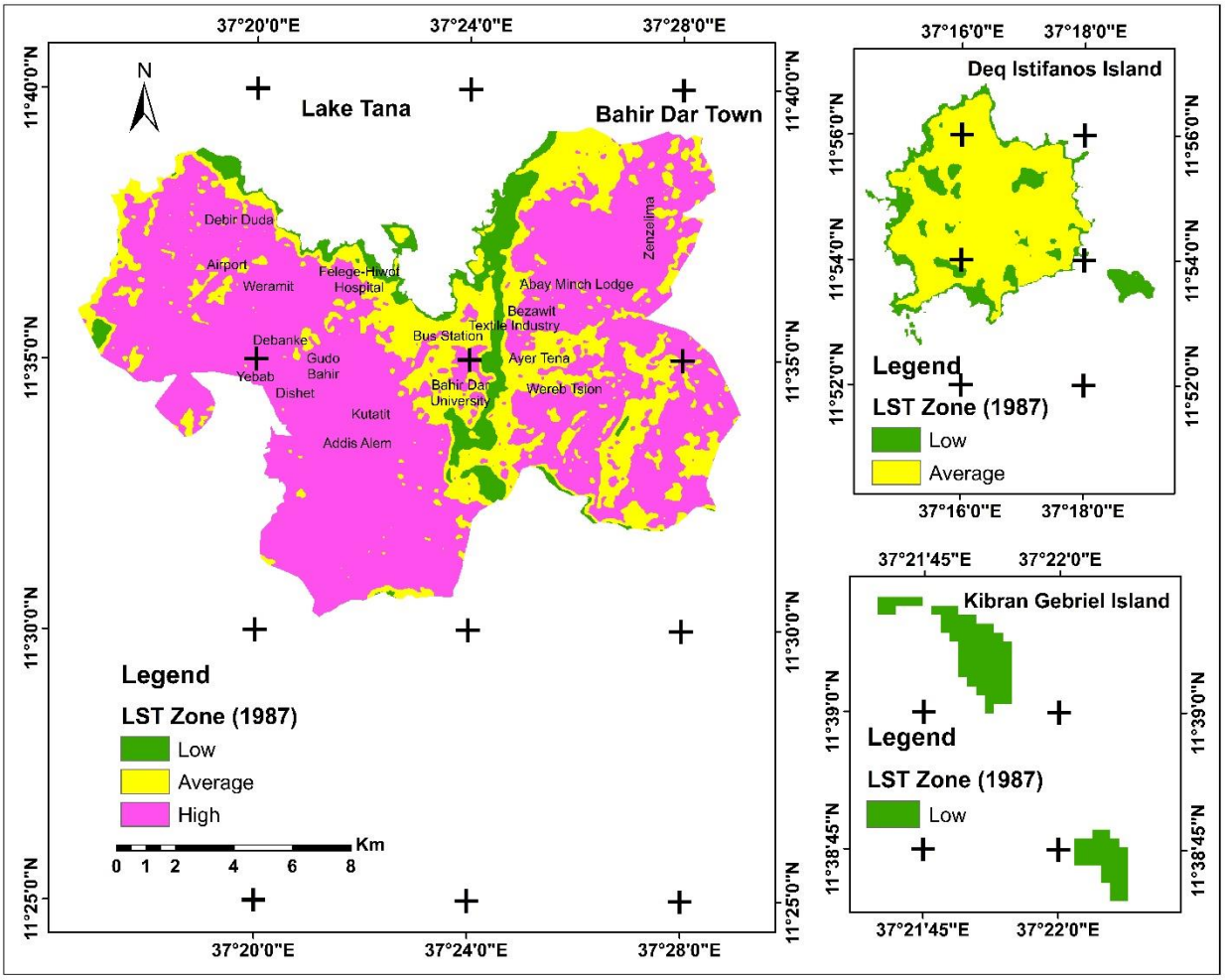

Figure 4.18: LST zone of Bahir Dar town and its surrounding in the year 1987

In 2002, the land surface temperature had increased both in spatial distribution and its amount. However, due to tree plantation in the airport area, it was found that the area was in the highest zone in 1987 was categorized as average land surface temperature zone in 2002. Except in spatial extent and temperature values, the region of low, average and high temperature in 2002 was similar with 1987 (Figure 4.19).

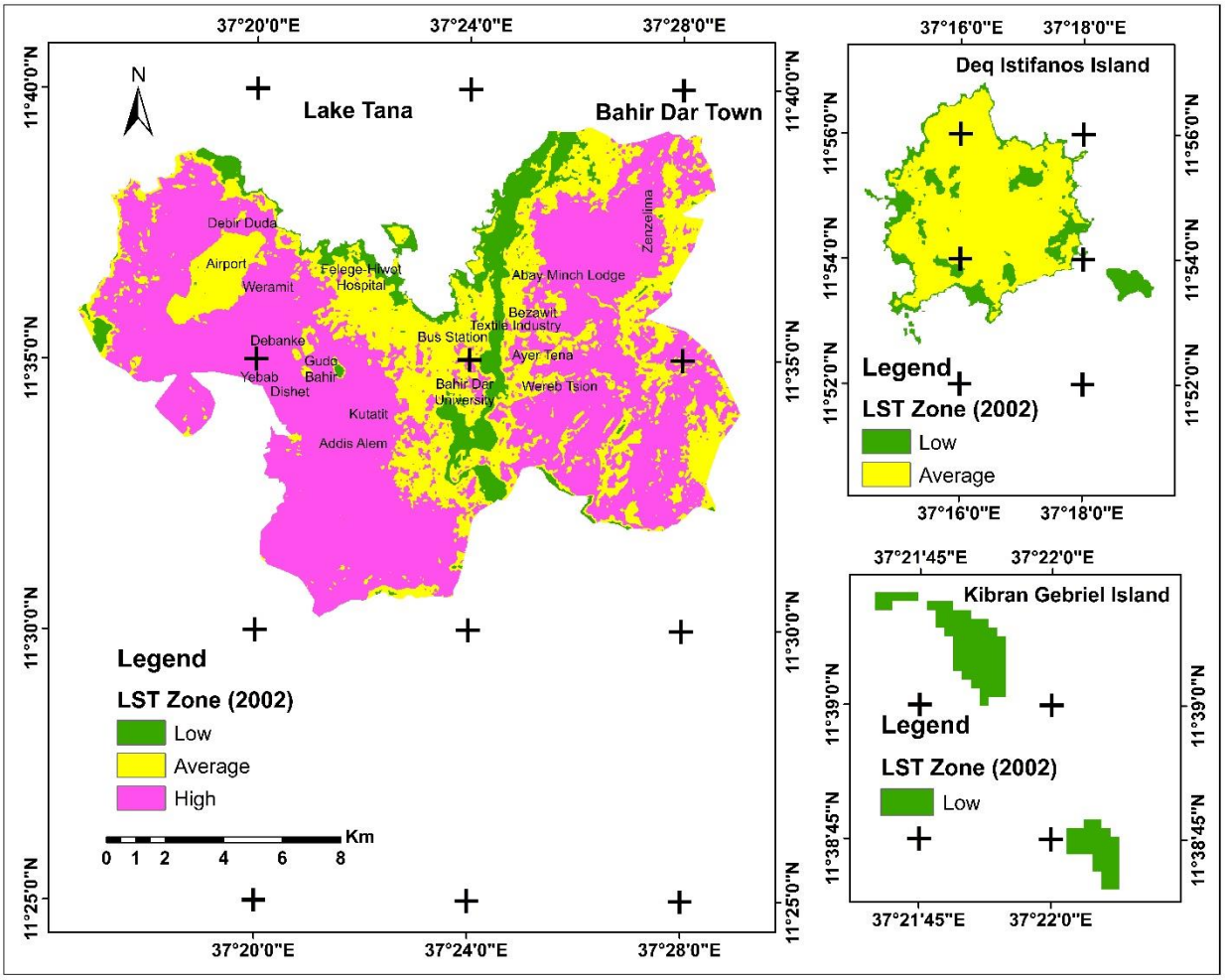

Figure 4.19: LST zone of Bahir Dar town and its surrounding in the year 2002

Further, in 2017 average temperature zone was expanded to the central Bahir Dar and surrounding places of Abay River as well as some place in the west and south (Figure 4.20). Lowest temperature zone also found in wetland vegetation along the water bodies of River Abay and Lake Tana as well as some place in the west and central Bahir Dar town, and Lake Tana shore and Kibran Gebriel Island. Whereas, highest temperature zone was found in southwest, west, east, southeast and northeast Bahir Dar town as well as some settlement areas in the central parts of the town.

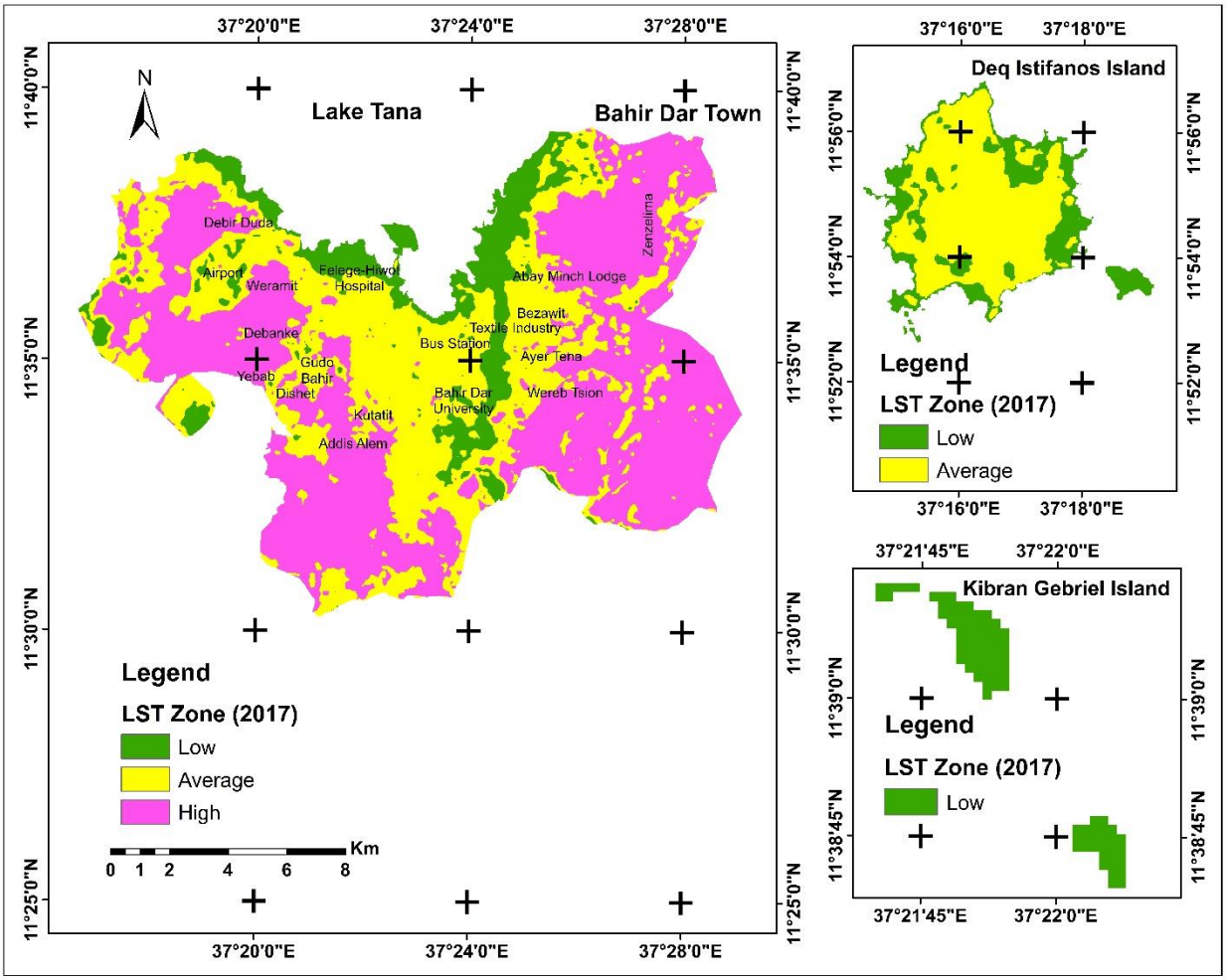

Figure 4.20: LST zone of Bahir Dar town and its surrounding in the year 2017

4.10 The Relationship between Normalized Difference Vegetation Index and Land Surface Temperature

According to the results of this study, it was observed that NDVI and LST have indirect relationships for the year 1987, 2002 and 2017. This shows that the analysis and LST derivation was undertaken correctly. The higher the NDVI, the lower the LST, and the lower the NDVI value the higher the LST. In the case of the water body, however, NDVI and LST have a direct relationship because the reflectance of water body in the infrared region is lower than red spectrum and it emits radiation in thermal region. The correlations between NDVI and LST in 1987, 2002 and 2017 were expressed by the R^2 values of 0.9016, 0.9572 and 0.9804, respectively (Figure 4.21-4.23).

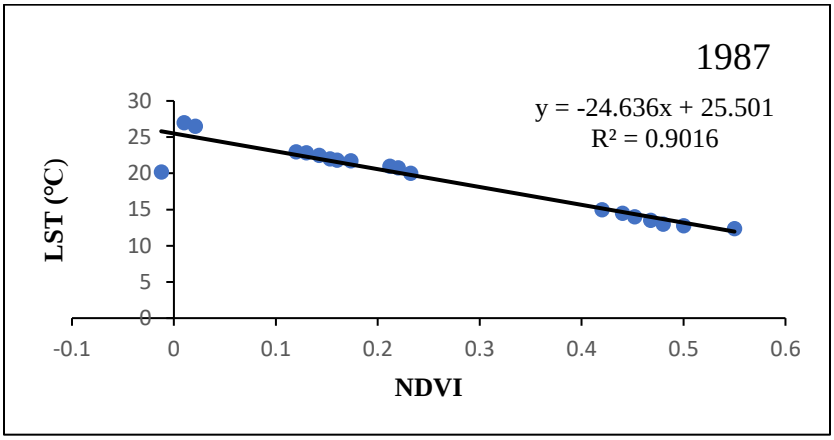

Figure 4.21: NDVI and LST correlation in 1987

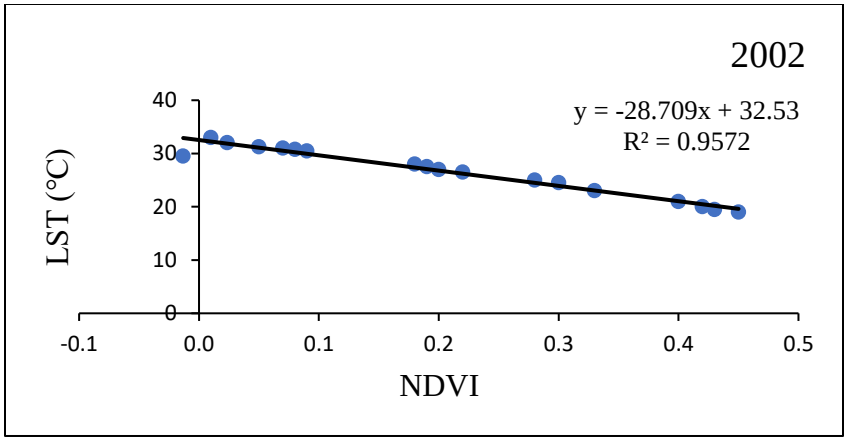

Figure 4.22: NDVI and LST correlation in the year 2002

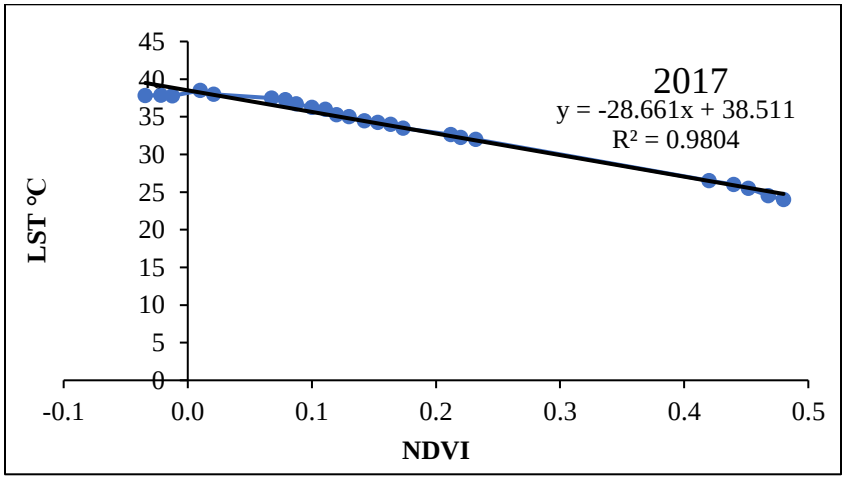

Figure 4.23: NDVI and LST correlation in the year 2017

4.11 Impacts of Land-use and Land-cover Changes on Land Surface Temperature Distribution

This study showed that there was conversion of forest, shrubland, grasslands, and plantations to settlement, industrial and service areas, and agricultural lands (Figure 4.1-4.3). Mainly, expansion of urban areas in the west (around Debanke and Felege-Hiwot Hospital), east (Bezawit, Ayer Tena and Zenzelima town) and south as well as the change of land into industrial area in south (Kutatit) and southwest (Yebab, Dishet and Gudo Bahir) part of the town made the area warmer. Furthermore, huge degradation or conversion of wetlands along Abay River and Lake Tana to other land-use made, western and northwest, south and central parts of the town warmer from 1987 to 2017. Such land-use and land-cover conversion caused the increase of land surface temperature in Bahir Dar town and its surrounding regions. Therefore, the way to use the land and the type of land-cover have an impact on the change and distribution of land surface temperature though LST of the town is also influenced by Lake Tana and Abay river.

As illustrated in Table 4.9, agricultural land recorded higher land surface temperature than other land-use and land-cover. Small barren land accompanied with cropland and the nature of topography also made them warmer even more than urban settlements, paved surface and industrial areas. Land surface temperature of cropland in 1987, 2002 and 2017 was 34.93 ℃, 38.87 ℃ and 43.01 ℃, respectively. Other land-use and land-cover such as plantation, shrubland, open space, riparian vegetation, paved surface, grassland, and service and industrial areas have equally higher LST. Moreover, high-density settlement areas exhibited maximum land surface temperature of 31.15 ℃, 33.04 ℃ and 38.27 ℃ while low-density settlement had LST of around 30.07 ℃, 32.13 ℃ and 36.94 ℃, respectively in 1987, 2002 and 2017.

The land surface temperature of water bodies and marshlands has been increasing relatively fast from 20.21 ℃ to 29.51 ℃ and 21.21 ℃ to 30.50 ℃ in 1987 and 2002 respectively. However, in 2017 the temperature of water bodies and wetlands was 30.88 ℃and 38.33 ℃, respectively. On the other hand, forest cover areas had relatively low land surface temperature. It was 25.34 ℃, 28.02 ℃ and 34.18 ℃ in 1987, 2002 and 2017 respectively. The details information about LULC classes and their land surface temperature are presented in Table 4.9.

Table 4.9: LST statistical information of Bahir Dar town and its surrounding in 1987, 2002 and 2017 (in $°C$)

LULC	1987				2002				2017			
	MIN	MAX	MEAN	STD	MIN	MAX	MEAN	STD	MIN	MAX	MEAN	STD
Cropland	16.77	34.93	30.35	2.07	20.40	38.87	32.58	2.75	23.02	43.01	36.68	2.42
Forest	12.35	25.34	20.58	3.90	16.96	28.02	23.19	4.37	20.34	34.18	29.31	4.33
Grassland	18.69	34.93	29.21	2.06	20.40	38.87	31.54	2.76	23.27	40.98	35.74	2.73
High density settlement	24.30	31.15	28.35	0.94	26.51	33.04	29.31	2.32	28.05	38.27	32.11	0.82
Industrial	18.69	29.26	25.99	1.71	24.87	33.00	28.54	2.08	27.89	37.40	33.63	1.50
Low density settlement	20.11	30.07	29.52	1.96	24.87	32.13	30.15	3.20	23.40	36.94	33.41	2.41
Open space	14.83	34.50	29.48	2.62	19.26	37.43	30.85	4.42	23.39	41.31	34.77	3.33
Paved surface	18.69	33.64	28.78	2.36	21.53	38.87	30.37	3.69	25.38	41.03	32.81	1.91
Plantation	18.69	33.64	28.57	2.34	20.40	36.48	30.03	3.62	22.08	41.84	32.57	3.56
Riparian vegetation	20.59	32.77	29.18	1.62	24.87	37.01	32.02	2.21	27.31	39.99	35.87	2.48
Service area	12.35	34.93	29.59	2.04	16.99	38.87	30.17	3.67	21.93	40.68	32.23	2.12
Shrubland	14.83	34.07	28.36	2.65	18.97	36.43	30.11	3.38	23.81	41.62	34.19	3.22
Water body	12.35	20.21	17.20	4.09	16.95	29.51	20.72	3.51	20.43	30.88	26.29	3.55
Wetland vegetation	12.35	21.21	19.47	4.90	16.95	30.50	21.35	5.49	20.79	38.33	28.15	3.79

(Where: MIN = Minimum, MAX = Maximum, STD = Standard deviation)

4.12 The Relationship between Land-use and Land-cover and Land Surface Temperature

Land-use and land-cover and LST maps of the study area showed how LULC and land surface temperature have changed during the study period. This change was mainly due to the high rate of land transformation. Land surface temperature increased from 1987 to 2017 and varied with the variation of LULC. Among the LULC classes, forest cover regions of the study area had low land surface temperature and high radiation was emitted by cropland. From the year 1987-2017, the mean land surface temperature of Bahir Dar and its surrounding has increased by 5.94 °C (Table 4.10). Details information about LULC classes and their mean LST are presented in Table 4.10 and Figure 4.24.

Table 4.10: Mean land surface temperature and change in 1987, 2002 and 2017 (in *°C*)

LULC	Mean LST			LST Change		
	1987	2002	2017	1987-2002	2002-2017	1987-2017
Cropland	30.35	32.58	36.68	2.23	4.1	6.33
Forest	20.58	23.19	29.31	2.61	6.12	8.73
Grassland	29.21	31.54	35.74	2.33	4.2	6.53
High density settlement	28.35	29.31	32.11	0.96	2.8	3.76
Industrial area	25.99	28.54	33.63	2.55	5.09	7.64
Low density settlement	29.52	30.15	33.41	0.63	3.26	3.89
Open space	29.48	30.85	34.77	1.37	3.92	5.29
Paved surface	28.78	30.37	32.81	1.59	2.44	4.03
Plantation	28.57	30.03	32.57	1.46	2.54	4
Riparian vegetation	29.18	32.02	35.87	2.84	3.85	6.69
Service area	29.59	30.17	32.23	0.58	2.06	2.64
Shrubland	28.36	30.11	34.19	1.75	4.08	5.83
Water body	17.2	20.72	26.29	3.52	5.57	9.09
Wetland vegetation	19.47	21.35	28.15	1.88	6.8	8.68

Figure 4.24 illustrates mean LST of all land-use and land-cover classes has increased during 1987-2017. For example, mean LST of cropland in 1987 was about 30 °C and it raised to 37 °C. During the study periods cropland had high land surface temperature. However, water body had minimum land surface temperature, it was 17 °C in 1987 and increased to 26 °C in 2017.

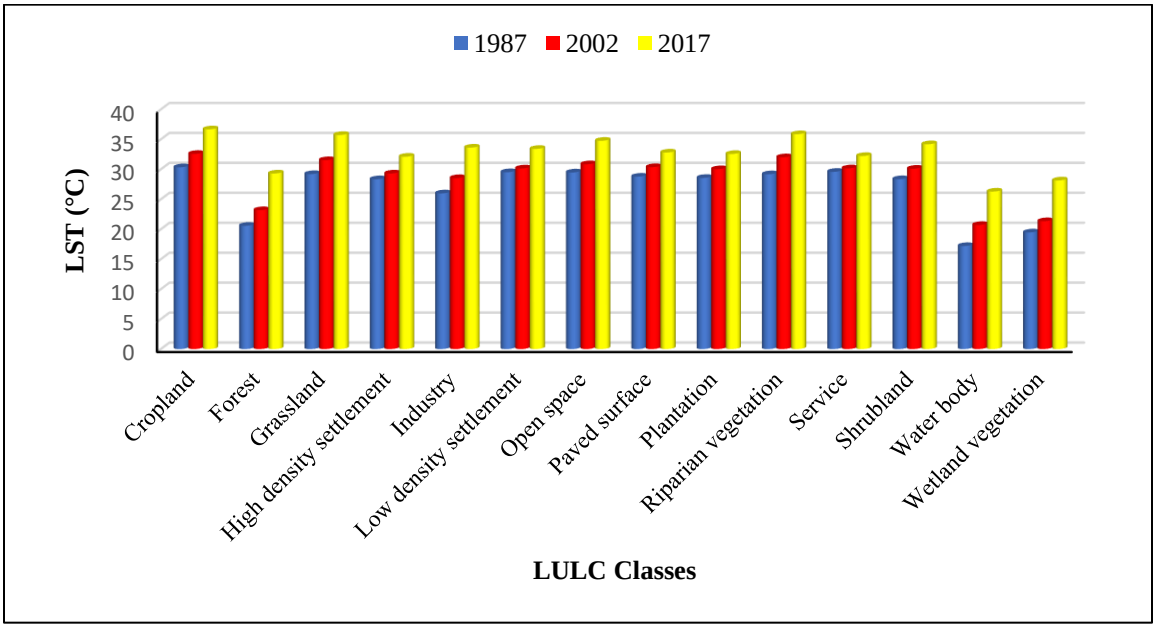

Figure 4.24: Mean LST in each LULC class in 1987, 2002 and 2017

CHAPTER FIVE

5. DISCUSSION

5.1 Land-use and Land-cover Change of Bahir Dar Town and its Surrounding from 1987-2017

Bahir Dar town and its surroundings have experienced major land-use and land-cover changes. These changes were mainly attributed to human population growth and its effect on the environment. Studies conducted by Agarwal et al. (2002), Brink et al. (2014) and Niamir-Fuller et al. (2012) revealed that human activities (anthropogenic effects) seriously affects land-use and land-cover pattern. Jianga and Tiana (2010) and Fenglei et al. (2009) also discovered that urban expansion contributes to the dramatic change of LULC. Population growth and economic development also extremely change LULC (Zhenglei et al., 2009).

The present study revealed that LULC has been changing from 1987 to 2017. In 2017, both high and low-density settlement areas increased to 22.18 km^2 from 8.01km^2 in 1987. This increase was made at the expense of land-cover like forest, grassland, cropland, shrubland, open space and wetland vegetation. Service areas also increased from 9.21km^2 in 1987 to 17.23 km^2 in 2017. Such rapid urban growth brings environmental problems such as pollution. Wu et al. (2013) stated that urbanization causes for air pollution. Zhu et al. (2016) and Jianga and Tiana (2010) stated that expansion of built-up areas due to urbanization cause the destruction of the ecological environment. The study also revealed that change in the pattern and type of LULC increase urban heat island. Qijiao and Zhixiang (2015) and Wu et al. (2013) stated that urban heat island extremely increases because of rapid urban expansion.

The result of this study also shows that other land-cover such grasslands, wetland vegetation, forest, water body were depleted. For example, shrubland reduced from 18.06 km^2 in 1987 to 9.39 km^2 in 2017. Wetland vegetation which was 21.27 km^2 in 1987 but decreased to 17.05 km^2 in 2017. Grasslands also decreased from 19.17 km^2 (7.89%) in 1987 to 13.22 km^2 (5.44%) in 2017. This land-cover depletion resulted from agricultural land expansion (mainly plantation) due to rapid population growth. Increased settlement, service and industrial areas, recreation, and paved surface were also causes for depletion of grasslands, wetlands, and shrublands. Therefore, the study revealed that such land-cover transformation has contribution to climate change and

environmental degradation. The study conducted by Y. Liu et al. (2004), H. Liu et al. (2004), Hussien (2009), Lambin and Meyfroidt (2011) and Donato et al. (2016) indicated that LULC dynamics is a risk for environmental degradation. Further, forest cover has declined from 7.53 km^2 (3.1%) in 1987 to 4.43 km^2 (1.82%) in 2017. Therefore, forest cover degradation/depletion was interrupted as the main cause for the loss of ecosystem and warming of the surrounding environment. The investigation made by Abate (2011) revealed that extreme LULC change harm biodiversity and natural resources. Waterbody also slightly decreased from 4.04 km^2 (1.66%) in 1987 to 3.91 km^2 (1.61%) in 2017. This is due to receding of water and covered with wetland vegetation. Increased plantation agriculture along the water body also has contribution for retreating of water. Qijiao and Zhixiang (2015) and Tang et al. (2014) revealed that urbanization modifies urban surface water content and vegetation cover.

5.2 Influence of Lake Tana and Abay River

This study revealed that Lake Tana and River Abay influence the heat island of Bahir Dar town and its surrounding. Thermal accumulation in the town particularly for places that are very close to the lake and the river is lower because of the influence of moist air. As a result, recreation areas along the lake and on the bank of river exhibits low land surface temperature. In addition, settlement areas located in the central part of the town have relatively high temperature. However, places which are very far from the lake and the river exhibited high land surface temperature. Besides to the distance from the lake, the direction of wind has a significant influence on the distribution of heat island in the study area. Therefore, the central area of Bahir Dar town is mainly dominated by the influence of the lake and river than peripheral places.

5.3 Normalized Difference Vegetation Index

Normalized Difference Vegetation Index is an index that shows the condition of vegetation, and greenness of the earth surface. Therefore, it is used to analyze the urban environment and urban heat island since it indicates the level of dryness and warmness of the area. The result of this study confirmed that places along the shore of Lake Tana and Abay River have high NDVI because areas were dominated by vegetation like green grass, woodland, shrub and forest. Besides, marshland areas in the south and west, plantation, open space, shrubland and forest cover have high NDVI values. Some parts of central Deq Istifanos also have high NDVI values because there was higher vegetation cover with service areas like Monasteries and churches.

However, cropland, settlement, industrial area, and paved surface have low NDVI values. This is because of dry nature of those surface and their high thermal emittance property. Thus, NDVI indicates the land surface temperature of the area though they have an indirect relation between them. Sobrino and Raissouni (2000), Sun et al. (2012) and Yue et al. (2007) revealed that LST has inversely related with NDVI. However, LST values of water bodies increase with the increase of NDVI values because of its large heat emitting capacity in thermal spectrum. The study conducted by Fang et al. (2018) revealed that surface temperature of water bodies raises with increases of NDVI because the heat capacity of water is relatively large.

The result of this study indicated that NDVI was slightly higher in 1987 than in 2002 due to high vegetation cover in 1987. Urban expansion and depletion of vegetation cover in 2002 were responsible for decline NDVI values. In 2017, NDVI values increased due to high expansion of green spaces and recreation areas in urban areas, and tree plantations both in rural and urban places. But in 2017, there was urban expansion in east, southeast and southwest and industrial areas increased in the southeast of the town. This made NDVI value to be lower in the year 2017 than 1987. Moreover, seasonal variations in vegetation condition, in particular, the canopy depth and leaf structure made the NDVI values in 2017 to be higher than that of 2002. Therefore, regions having more vegetation cover have higher normalized difference vegetation index than non-vegetation areas.

The correlations coefficient of NDVI and LST in 1987 was 0.9016, therefore, 90.16% of LST distribution was influenced by NDVI. However, in 2017 the coefficient was $R^2 = 0.9804$ and 98.04% of the change and distribution of LST in the study area was controlled through NDVI (vegetation cover). Thus, there is a strong relationship between NDVI and LST. However, proximity to lake, wind direction, topography and elevation also influence the land surface of the study area. Hence, NDVI is not the only factor for the distribution of LST in the study area.

5.4 Land Surface Temperature of Bahir Dar Town and its surrounding

The study revealed that LST of Bahir Dar town and its surrounding varies in space and time. Landscape dynamics have been contributing to the spatio-temporal variation of land surface temperature, especially, the development of urban settlement with impervious surface material and industries at the expense of other land-use and land-cover types. The influence of Lake Tana and

Abay River, wind direction, elevation, and nature of topography also contribute to land surface temperature variation. Research undertake by Jianga and Tiana (2010) revealed that land-use and land-cover change strongly affect the urban heat island depending on the type of change. This study indicated that NDVI in the study area varies with land-use and land-cover types. Thus, land surface temperature distribution and change vary with the variation in LULC type though it was also controlled through other parameters. Sun et al. (2012), Jianga and Tiana (2010), Weng et al. (2004) and Yue et al. (2007) have indicated that land surface temperature varies with the variation in LULC types. Sobrino and Raissouni (2000), Weng et al. (2004), Wilson et al. (2003) and Yue et al. (2007) also revealed that spatial distribution and temporal change in LST and NDVI vary with the variations of LULC types

This study revealed that cropland exhibited high heat island. Its maximum temperature in 1987 was 34.93 °C and in 2017 it reached 43.01 °C. Grassland, open space, riparian vegetation, shrubland, and plantation exhibited relatively high heat island, though the NDVI of these LULC types was relatively higher. This is partly attributed to their distance from the lake and river, and nature of the surrounding topography and elevation. However, forest, water body and wetland vegetation exhibited low land surface temperature. Buyadi et al. (2014) revealed that green areas and trees have a vital role in regulating urban heat islands.

Because of high thermal emission, paved surfaces, settlement, industrial and service areas relatively have high temperature, and thus classified under average temperature zone. Increased built-up areas, impervious surface, emission from vehicles and industry increased the temperature in 2017. Manea et al. (2013) stated that industrialization and rapid urban expansion increase the level of urban heat island. Jianga and Tiana (2010) and Sun et al. (2012) revealed that land surface temperature increases with the expansion of built-up areas. Jianga and Tiana (2010), Qijiao and Zhixiang (2015) and Tang et al. (2014) also agreed that non-evaporating impervious surfaces like concrete and asphalt contribute to the urban environment heat accumulation. Fenglei et al. (2009) confirmed that the changes in urban biophysical composition increase urban heat island.

The result of this study indicated that Bahir Dar town and its surrounding land surface temperature vary spatially. Therefore, places which are very close to Lake Tana and Abay River have low LST than areas located far from the water bodies. Besides, the wind blowing from Lake Tana during

daytime refreshes the interior parts of the town and made them cooler than peripheral areas. Because the amount of humidity carried by the cold wind reduced away from the lake and as a result, the LST gradually increases. Temporal variation of LST in the Islands was also higher even though they are within the influence of the lake, for instance, Deq Istifanos Island had a maximum temperature of 30.59 ℃, 34 ℃, and 38.1 ℃ in 1987, 2002 and 2017, respectively. This is because most of the area of the Island was covered with cropland. Moreover, Kibran Gebriel Island had a maximum land surface temperature of 15.32 ℃, 20.32 ℃ and 24.02 ℃ in 1987, 2002 and 2017, respectively.

The result of the study revealed that the land surface temperature has been increasing from 1987 to 2017. For example, in 1987 minimum and maximum LST of Bahir Dar town and its surrounding was 12.35 ℃ and 34.93 ℃. However, it was increased to 16.95 ℃-38.87 ℃ in 2002 and 20.43 ℃-43.01 ℃ in 2017. Such continuous increase of heat island affects living condition and elements of climate. The study done by Qijiao and Zhixiang (2015) also confirmed that higher urban temperatures change urban thermal environments and finally lead to thermal discomforts and incidence of heat-related illnesses.

High heat island in the study area also affects ecological and physical cycles. Yanagi (2008) and Zhao and Lai (2007) indicated that high thermal incidence strongly influences hydrological cycles. H. Liu et al. (2004) and Y. Liu et al. (2004) also agreed that higher land surface temperature is the cause of environmental change. As Qijiao and Zhixiang (2015) and Tang et al. (2014) revealed higher urban heat island modifies urban surface water content and vegetation cover. The study revealed that rapid increase in urban heat island cause for the change of urban climate. The study conducted by Du et al. (2007, Luber and McGeehin (2008) and Zheng et al. (2014) confirmed that warming of surface water content and its surrounding contribute to climate change.

CHAPTER SIX

6. CONCLUSIONS AND RECOMMENDATIONS

6.1 Conclusions

Remote sensing data is very essential for analyzing land-use and land-cover change and its dynamics, monitoring and forecasting global climate changes, and landscape analysis and modeling. It has been used effectively in assessing spatio-temporal distribution and changes of land surface temperature and monitoring hydro-climatic circulation and environmental changes.

The study used Landsat 5 TM, Landsat 7 ETM+ and Landsat 8 OLI/TIRS data to analyze the impacts of land-use and land-cover change changes on the spatio-temporal distribution and changes of LST. The study revealed that NDVI, LST and LULC analyzed from those images provide crucial information about the current conditions of land-use and land-cover, landscape dynamics and environmental changes. Furthermore, the study indicated that Landsat imageries are very significant for assessing and mapping LULC, NDVI and LST of Bahir Dar town and its surrounding.

The LULC of Bahir Dar town and its surrounding has been changing in space and time. Rapid population growth associated with exploitation of land-cover and urbanization responsible for the change. Therefore, LULC changes has an impact on land surface temperature. The finding of this study showed that there is a significant spatial variation of LST in the study area. Places found in south, southwest, west, southeast and east Bahir Dar town are characterized by high LST. Low LST areas are located along the shore of Lake Tana and on the bank of River Abay. Central part of Bahir Dar town is characterized by high-density settlement and service areas and have high thermal accumulation. The sub-urban settlements and some areas particularly around general market and bus station have high risk of urban heat island effects. Moreover, croplands located in the southwest, west, east and south Bahir Dar, and central Deq Istifanos Island have high thermal heat island. This is attributed to the barren land (bedrock exposed) effect, and these areas are located relatively far from the Lake Tana and River Abay that major role in refreshing the LST. Industrial areas which are located in the southwestern part of the town also exhibits high heat island. Forest, wetland vegetation and water body areas have low LST.

The finding of this study also revealed that LST has been increasing from 1987 to 2017. This is because of the rapid change of LULC that is driven by human activities, the influence of Lake Tana and Abay River, wind direction, nature of topography and the effect of climate variabilities. Therefore, LST the study area varies with the type of LULC. Normalized difference vegetation index is also a good indicator of the condition of LULC and LST. Hence, using satellite data for analyzing LULC and LST is very effective.

6.2 Recommendations

The study emphasized on the assessment of the impact of land-use and land-cover changes on the distribution and spatio-temporal variations in land surface temperature in Bahir Dar town and its surrounding from Landsat imagery. This study revealed that LULC transformation was one of the major factors that contributed to the increasing of LST from time to time and place to place. Thus, the following recommendations have been forwarded based on the results obtained from this study.

- Land-use and land-cover changes are serious problems, and it result in raise land surface temperature. Therefore, land and urban management, ecology and environmental management experts should focus on strategies and policies that governs proper and environmental use of land and its cover.
- Some place in the center of the town and peripheral settlement areas have higher urban heat islands. Therefore, urban planner should focus on how to expand tree plantation and green parks in those vulnerable areas.
- High heat islands are found on cropland. Hence, tree plantation should be expanded along the agricultural land in order to refresh thermal accumulation effects in the area.
- The effect of industrial areas on thermal emission is increasing. Therefore, there should be thermal refreshing mechanisms such as introducing green areas and continuing tree plantation around the industrial zones.
- Urban areas have been highly expanding towards the south, southwest, east and west parts of the town. However, these areas are already exhibiting high heat island. Therefore, urban expansion should not take place towards those regions. Besides, while expanding urban areas, effective LULC assessment and environmental monitoring should be made.
- The study can be used for further research in the area of land-use and land-cover and its impact.

References

Aadil, M.N., Rafiq, A.H., Aadil, H. and Pervez, A. (2014). Changes in land-use/land-cover dynamics using geospatial techniques: A case study of Vishav drainage basin. *J. Geogr. Reg. Plan*. **7**: 69–77.

Abate, S. (2011). Evaluating the land use and land cover dynamics in Borena Woreda of South Wollo highlands, Ethiopia. *J. Sustain. Dev. Afr*. **13**: 87–105.

Abbas, I., Muazu, M. and Ukoje, J. (2010). Mapping land use-land cover and change detection in Kafur local government, Katsina, Nigeria (1995-2008) using remote sensing and GIS. *J. Environ. Earth Sci*. **2**: 6–12.

Agarwal, C., Green, G.M., Grove, J.M., Evans, T.P. and Schweik, C.M. (2002). A Review and Assessment of Land-Use Change Models: Dynamics of Space, Time, and Human Choice. General Technical Report NE-297. Newtown Square, Pennsylvania: U.S. Department of Agriculture, Forest Service, Northeastern Research Station.

Ahl, D.E., Gower, S.T., Burrows, S.N., Shabanov, N.V., Myneni, R.B. and Knyazikhin, Y. (2006). Monitoring spring canopy phenology of a deciduous broadleaf forest using MODIS. *Remote Sens. Environ*. **104**: 88–95.

Albin, H., Fred, M., Michael, H., Angelika, E. and Georg, L. (2017). Implications of atmospheric conditions for analysis of surface temperature variability derived from landscape-scale thermography. *Int J Biometeorol*. **61**: 575–588.

Alemu, B., Garedew, E., Eshetu, Z. and Kassa, H. (2015). Land use and land cover changes and associated driving forces in north western lowlands of Ethiopia. *Int Res J Agric Sci Soil Sci*. **5**: 28–44.

Amiri, R., Weng, Q.H., Alimohammadi, A. and Alavipanah, S.K. (2009). Spatial–temporal dynamics of land surface temperature in relation to fractional vegetation cover and land use/cover in the Tabriz urban area, Iran. *Remote Sens Env*. **113**: 2606–2617.

Arvor, D., Dubreuil, V., Simões, M. and Bégué, A. (2013). Mapping and spatial analysis of the soybean agricultural frontier in Mato Grosso, Brazil, using remote sensing data. *GeoJournal*. **78**: 833–850.

Badege, B. (2001). Defforestation and land degradation in the ethiopian highlands: strategy for physical recovery. *Northeast Afr Stud*. **8**: 7–26.

Barsi, J.A., Schott, J.R., Hook, S.J., Raqueno, N.G., Markham, B.L. and Radocinski, R.G. (2014). Landsat-8 thermal infrared sensor (TIRS) vicarious radiometric calibration. *Remote Sens*. **6**: 11607–11626.

Becker, F. and Li, Z.-L. (1995). Surface temperature and emissivity at different scales: definition, measurement and related problems. *Remote Sens. Rev*. **12**: 225–253.

Becker, F. and Li, Z.L. (1990). Towards a local split window method over land surface. *Int. J. Remote Sens. **3***: 369–393.

Belay, S., Amsalu, A. and Abebe, E. (2014). Land Use and Land Cover Changes in Awash National Park, Ethiopia: Impact of Decentralization on the Use and Management of Resources. *Open J. Ecol*. **4**: 950–960.

Belay, T. (2002). Land-cover/land-use changes in the Derekolli catchment of the South Welo Zone of Amhara Region, Ethiopia. Mich. State Univ. Press. **18**: 1–20.

Berhan, G. (2010). The role of Geo-information technology for predicting and mapping of forest cover spatio-temporal variability: Dendi district case study, Ethiopia. *J. Sustain. Dev. Afr*. **12**: 9–33.

Bernstein, L.S., Adler-Golden, S.M., Sundberg, R.L., Levine, R.Y., Perkins, T.C., Berk, A. and Hoke, M.L. (2005). Validation of the QUick atmospheric correction (QUAC) algorithm for VNIR–SWIR multi- and hyperspectral imagery. SPIE proceedings, algorithms and technologies for multispectral, hyperspectral, and ultraspectral imager. SPIE Digit. Libr.

Bhattacharjee, P.R. and Nayak, P. (2003). Socio-economic rationale of a regional development council for the Barak Valley of Assam. *J. NEICSSR*. **27**: 13–26.

Biro, K., Pradhan, B., Buchroithner, M.F. and Makeschin, F. (2013). An assessment of land use/land-cover change impacts on soil properties in the northern part of Gadarif region, Sudan. *Land Degrad Dev*. **24**: 90– 102.

Bongers, F. and Tennigkeit, T. (2010). Degraded Forests in Eastern Africa: Management and Restoration. Routledge Lond. UK.

Brink, A.B., Bodart, C., Brodsky, L., Defourney, P., Ernst, C., Donney, F., Lupi, A. and Tuckova, K. (2014). Anthropogenic pressure in East Africa: Monitoring 20 years of land cover changes by means of medium resolution satellite data. *Int J Appl Earth Obs Geoinform*. **28**: 60–69.

Buyadi, S.N.A., Mohd, W.M.N.W. and Misni, A. (2014). Impact of vegetation growth on urban surface temperature distribution. **In**: Preceding of 8th International Symposium of the Digital Earth (ISDE8). Earth and Environmental Science.

Chander, G., Markham, B.L. and Helder, D.L. (2009). Summary of current radiometric calibration coefficients for Landsat MSS, TM, ETM+, and EO-1 ALI sensors. *Remote Sens. Environ*. **113**: 893–903.

Chrysoulakis, N., Kamarianakis, Y., Farsari, Y., Diamandakis, M. and Prastacos, P. (2004). Combining Satellite and Socioeconomic data for Land Use Models estimation. **In**: Preceding of 3rd Workshop of EARSeL Special Interest Group on Remote Sensing for Developing Coutries (in Press), Goossens, R.(Editor).

Claus, R. and Mushtaq, H. (2011). Toronto's Urban Heat Island: Exploring the Relationship between Land Use and Surface Temperature. *Remote Sens*. **3**: 1251–1265.

Cotula, L. (2009). International Institute for Environment and Development; Food and Agriculture Organization of the United Nations; International Fund for Agricultural Development. Land Grab or Development Opportunity? Agric. Invest. Int. Land Deals Afr. Lond. UK FAO Rome Italy IFAD Rome Italy.

Central Statistical Agency (CSA). (2013). Population Projection of Ethiopia for All Regions at Wereda Level from 2014 – 2017 (Population projection). Federal Democratic Republic of Ethiopia Central Statistical Agency, Addis Ababa, Ethiopia.

Central Statistical Agency (CSA). (2008). The 2007 population and housing census of Ethipia: statistical reports for Amhara region (Census report). Federal Democratic Republic of Ethiopia, Office of population and housing census commission, Central Statistical Agency, Addis Ababa, Ethiopia.

Central Statistical Agency (CSA). (1998). The 1994 population and housing census of Ethiopia: results for Amhara region, Volume II analytical report (Census report). Federal Democratic Republic of Ethiopia, Office of population and housing census commission, Central Statistical Agency, Addis Ababa, Ethiopia.

Central Statistical Agency (CSA). (1991). The 1984 population and housing census of Ethiopia: Analytical report at national level (Census report). Transitional government of Ethiopia, Office of the population and housing census commission, Addis Ababa, Ethiopia.

Czajkowski, K.P., Goward, S.N., Mulhern, T., Goetz, S.J., Walz, A., Shirey, D., Stadler, S., Prince, S.D., Dubayah, R.O. (2000). Estimating environmental variables using thermal remote sensing. Quattrochi Luvall JC Eds Therm. Remote Sens. Land Surf. Process. CRC Press LLC Boca Ration Fla. Pp 11–32.

Dash, P., Göttsche, F.M., Olesen, F.S. and Fischer, H. (2002). Land surface temperature and emissivity estimation from passive sensor data: Theory and practice-current trends. *Int. J. Remote Sens*. **23**: 2563–2594.

De Boer, M.E. (2000). Landcover monitoring: an approach towards pan European land covers classification and change detection. Beleids Commissie Remote Sensing (BCRS), Delft.

Defries, R.S., Foley, J.A. and Asner, G.P. (2004). Land-use choices: Balancing human needs and ecosystem function. *Front Ecol Env*. **2**: 249–257.

Desta, L., Menale, K., Benin, S. and Pender, J. (2000). Land degradation and strategies for sustainable development in the Ethiopian high land, Amhara region: socio-economic and policy research working paper 32.

Donato, S.L.M.V., Sebastiano, C., Sebastiano, S. and Federico, G.M. (2016). Anthropogenic Influences in Land Use/Land Cover Changes in Mediterranean Forest Landscapes in Sicily. Land 5.

Du, C., Ren, H.Z., Qin, Q.M., Meng, J.J. and Li, J. (2014). Split-window algorithm for estimating land surface temperature from Landsat 8 TIRs data. **In**: Preceding of 2014 IEEE Int. Geosci. Remote Sens. Symp. IGARSS Quebec City QC Can. 3578–3581.

Du, Y., Xie, Z.Q., Zeng, Y., Shi, Y.F. and Wu, J.G. (2007). Impact of urban expansion on regional temperature change in the Yangtze River Delta. *J. Geogr. Sci*. **17**: 387–398.

Duan, S.B., Li, Z.L., Tang, B.H., Wu, H. and Tang, R.L. (2014). Generation of a timeconsistent land surface temperature product from MODIS data. *Remote Sens Env*. **140**: 339–349.

Ethiopian Forest Action Program (EFAP). (1993). Ethiopia, Ministry of Natnral Resources Deveopment and Environmtal Protection. 1993. The Challenge for Development. Ethiopia Forestry Action Programn Draft Final Report. Addis Ababa.

EPA (Environmental Protection Authority). (1997).

Eyayu, M., Heluf, G., Tekalign, M. and Mohammed, A. (2009). Effects of land-use change on selected soil properties in the tara gedam catchment and adjacent agro-ecosystems, North West Ethiopia. *Ethiop J Nat Res*. **11**: 35–62.

Fang, D., Jian, C. and Fan, Y. (2018). A Study of Land Surface Temperature Retrieval and Thermal Environment Distribution Based on Landsat-8 in Jinan City. **In**: Preceding at the ESMA 2017, Earth and Environmental Science.

Food and Agricultural Organization (FAO). (2000). Global Forest Resources Assessment 2000 (FRA 2000).

Feddema, J.J., Oleson, K.W., Bonan, G.B., Mearns, L.O., Buja, L.E., Meehl, G.A. and Washington, W.M. (2005). The importance of land-cover change in simulating future climates. *Science*. **310**: 1674–1678.

Fei, Z., Tashpolat, T., Hsiangte, K., Verner, C.J., Matthew, M., Mei, Z. and Juan, W. (2016). Dynamics of land surface temperature (LST) in response to land use and land cover (LULC) changes in the Weigan and Kuqa river oasis, Xinjiang, China. *Arab J Geosci*. **9**: 499.

Fenglei, F., Yunpeng, W., Maohui, Q. and Zhishi, W. (2009). Evaluating the Temporal and Spatial Urban Expansion Patterns of Guangzhou from 1979 to 2003 by Remote Sensing and GIS Methods. *Int. J. Geogr. Inf. Sci*. **23**: 1371–1388.

Feyisa, G.L., Meilby, H., Darrel Jenerette, G. and Pauliet, S. (2016). Locally optimized separability enhancement indices for urban land cover mapping: Exploring thermal environmental consequences of rapid urbanization in Addis Ababa, Ethiopia. *Remote Sens. Environ*. **175**: 14–31.

Foly, J.A., Defries, R.S., Asner, G.P., Barford, C., Bonan, G., Carpenter, S.R., Chapin, F.S., Coe, M.T., Daily, G.C. and Gibbs, H.K. (2005). Global Consequences of Land Use. *Science*. **309**: 570–574.

Franca, G.B. and Cracknell, A.P. (1994). Retrieval of land and sea surface temperature using NOAA-11 AVHRR data in north-eastern Brazil. *Int. J. Remote Sens*. **15**: 1695–1712.

Frey, C., M. and Parlow, E. (2012). Flux measurements in Cairo. Part 2: On the determination of the spatial radiation and energy balance using ASTER satellite data. *Remote Sens*. **4**: 2635–2660.

Gao, J. (2009). Digital Analysis of Remotely Sensed Imagery. McGraw-Hill.

Gessesse, D. and Kleman, J. (2007). Pattern and Magnitude of Deforestation in the South Central Rift Valley Region of Ethiopia. *Mt. Res. Dev*. **27**: 162–168.

Getachew, F., Heluf, G., Kibebew, K., Birru, Y. and Bobe, B. (2011). Analysis of land use/land cover changes in the Debre-Mewi watershed at the upper catchment of the Blue Nile Basin, Northwest Ethiopia. *J Biodivers Env. Sci*. **1**: 184–198.

Gete, Z. and Hurni, H. (2001). Implications of land use and land cover dynamics for mountain resource degradation in the Northwestern Ethiopian Highlands. *Mt. Res. Dev*. **21**: 184–191.

Girma, T. (2001). Land degradation: A challenge to Ethiopia.

Gluch, R., Quattrochi, D.A. and Luvall, J.C. (2006). A multiscale approach to urban thermal analysis. *Remote Sens. Environ*. **104**: 123–132.

Goldewijk, K.K. and Ramankutty, N. (2004). Land cover change over the last three centuries due to human activities: the availability of new global data sets. *GeoJournal*. **61**: 335–344.

Gregorio, D.A. (2005). Land Cover Classification System Classification: concepts and user manual. Food and Agriculture Organization of the United Nations, Rome.

Hansen, M.C., Potapov, P.V., Moore, R., Hancher, M., Turubanova, S.A., Tyukavina, A., Thau, D., Stehman, S.V., Goetz, S.J. and Loveland, T.R. (2013). High-Resolution Global Maps of 21st Century Forest Cover Change. *Science*. **342**: 850–853.

Hassen, M.Y., Mohammed, A., Assefa, M. and Tena, A. (2015). Detecting land use/land cover changes in the Lake Hayq (Ethiopia) drainage basin, 1957–2007. *Lakes Reserv*. **20**: 1–18.

Huang, S. and Siegert, F. (2006). Land cover classification optimized to detect areas at risk of desertification in North China based on SPOT VEGETATION imagery. *J. Arid Environ*. **67**: 308–327.

Hurni, H., Kebede, T. and Gete, T. (2005). The Implication of Changes in Population, Land Use and Land Management for Surface Runoff for Upper Nile Basin Area of Ethiopia. *Mt. Res. Dev*. **25**: 147–154.

Hussien, A.O. (2009). Land use and land cover change, drivers and its impact: A comparative study from Kuhar Michael and Lenche Dima of Blue Nile and Awash Basins of Ethiopia (A MScThesis). Cornell University, Ethiopia.

IPCC. (2007). Mitigation of Climate Change: Contribution of Working Group III to the Fourth Assessment Report of the Inter-governmental Panel on Climate Change, Camb. Univ. Press Camb. UK N. Y. NY USA 863.

Jianga, J. and Tiana, G. (2010). Analysis of the impact of Land use/Land cover change on Land Surface Temperature with Remote Sensing. *Procedia Environ. Sci*. **2**: 571–575.

Jiménez-Muñoz, J.C., Sobrino, J.A. (2003). A generalized single-channel method for retrieving land surface temperature from remote sensing data. *J. Geophys. Res*. 108.

Jimenez-Munoz, J.C., Sobrino, J.A., Skokovic, D., Matter, C. and Cristobal, J. (2014). Land surface temperature retrieval methods from Landsat-8 Thermal Infrared Sensor data. *IEEE Geosci Remote Sens*. **11**: 1840–1843.

Kalma, J., McVicar, T. and McCabe, M. (2008). Estimating land surface evaporation: a review of methods using remotely sensed surface temperature data. *Surv Geophys*. **29**: 421–469.

Karnieli, A., Agam, N., Pinker, R.T., Anderson, M., Imhoff, M.L. and Gutman, G.G. (2010). Use of NDVI and land surface temperature for drought assessment: merits and limitations. *J Clim*. **23**: 618–633.

Kueppers, L.M. and Snyder, M.A. (2012). Influence of irrigated agriculture on diurnal surface energy and water fluxes, surface climate, and atmospheric circulation in California. *Clim Dyn*. **38**: 1017–1029.

Kustas, W. and Anderson, M. (2009). Advances in thermal infrared remote sensing for land surface modeling. *Agric Meteorol*. **149**: 2071– 2081.

Lambin, E.F. and Geist, H.J. (2006). Land use and land cover change: local processes and global impacts. Springer Berl.

Lambin, E.F., Geist, H.J. and Lepers, E. (2003). Dynamics of land-use and landcover change in tropical regions. *Annu. Rev. Environ. Resour*. **28**: 205–41.

Lambin, E.F. and Meyfroidt, P. (2011). Global land use change, economic globalization, and the looming land scarcity. Proc Natl Acad Sci USA 108, 3465–3472.

Lambin, E.F., Turner, B.L., Geist, H.J., Agbola, S.B., Angelsen, A., Bruce, J.W., Coomes, O.T., Dirzo, R., Fischer, G. and Folke, C. (2001). The causes of land-use and land-cover change: Moving beyond the myths. *Glob Env. Chang*. **11**: 261–269.

Lazzarini, M., Marpu, P.R. and Ghedira, H. (2013). Temperature-land cover interactions: The inversion of urban heat island phenomenon in desert city areas. *Remote Sens. Environ*. **130**: 136–152.

Li, Z.L., Tang, B.H., Wu, H., Ren, H., Yan, G. and Wan, Z. (2013). Satellite-derived land surface temperature: current status and perspectives. *Remote Sens Env*. **131**: 14–37.

Li, Z.L., Tang, R., Wan, Z., Bi, Y., Zhou, C. and Tang, B. (2009). A review of current methodologies for regional evapotranspiration estimation from remotely sensed data. *Sensors*. **9**: 3801–3853.

Lillesand, T.M., Kiefer, R.W. and Chipman, J.W. (2004). Remote Sensing and Image Interpretation, 5th ed. John Wiley & Sons, New York.

Liu, H., Zhang, S., Li, Z., Lu, X. and Yang, Q. (2004). Impacts on wetlands of large-scale land-use changes by agricultural development: the small sanjiang plain, China. *Ambio*. **33**: 306–310.

Liu, S., Sylvia, P. and Li, X. (2002). Spatial patterns of urban land use growth in Beijing. *J. Geogr. Sci*. **12**: 266–274.

Liu, Y., Zha, Y. and Ni, S. (2004). Assessment of grassland degradation near Lake Qinghai, West China, using Landsat TM and in situ reflectance spectra data. *Int. J. Remote Sens*. **25**: 4177–4189.

Luber, G. and McGeehin, M. (2008). Climate change and extreme heat events. *Am. J. Prev. Med*. **35**: 429–435.

Lunetta, R.S., Knight, J.F., Ediriwickrema, J., Lyon, J.G. and Worthy, L.D. (2006). Land-cover change detection using multi-temporal MODIS NDVI data. *Remote Sens. Environ*. **105**: 142–154.

Maimatiyiming, M., Ghulam, A., Tiyip, T., Pla, F., Latorre-Carmona, P., Sawut, M., Halik, U. and Caetano, M. (2014). Effects of spatial pattern of green space on land surface temperature: implications for sustainable urban planning and climate change adaptation. *ISPRS J Photogramm Remote Sens*. **89**: 59–66.

Maitima, J.M., Mugatha, S.M., Reid, R.S., Gachimbi, L.N., Majule, A., Lyaruu, H., Pomery, D., Mathai, S. and Mugisha, S. (2009). The linkages between land use change, land degradation and biodiversity across East Africa. *Afr J Env. Sci Technol*. **3**: 310–325.

Mallick, J., Singh, C.K., Shashtri, S., Rahman, A. and Mukherjee, S. (2012). Land surface emissivity retrieval based on moisture index from LANDSAT TM satellite data over heterogeneous surfaces of Delhi city. *Int J Appl Earth Obstet*. **19**: 348–358.

Manea, D.L., Manea, E.E. and Robescu, D.N. (2013). Study on greenhousegas emissions from wastewater treatment plants. *Environ. Eng. Manag. J*. **12**: 59–63.

Markham, B.L. and Barker, J.L. (1986). Landsat-MSS and TM post calibration dynamic ranges, atmospheric reflectance and at-satellite temperature. EOSAT Landsat Technical Notes 1, (Lanham, Maryland: Earth Observation Satellite Company), pp. 3–8.

McCarthy, M.P., Best, M.J. and Betts, R.A. (2010). Climate change in cities due to global warming and urban effects. *Geophys Res Lett*. **37**: L09705.

Meijun, J., Junming, L., Caili, W. and Ruilan, S. (2015). A Practical Split-Window Algorithm for Retrieving Land Surface Temperature from Landsat-8 Data and a Case Study of an Urban Area in China. *Remote Sens*. **7**: 4371–4390.

Mekuria, A.D. (2005). Forest conversion–soil degradation–farmers' perception nexus: implications for sustainable land use in the southwest of Ethiopia.

Mohammed, A. (2011). Land use/cover dynamics and its implications in the dried lake Alemaya watershed, eastern Ethiopia. *J Sustain Dev Afr*. **13**: 1–18.

Mohammed, A., Le Roux, P.A., Barker, C.H. and Heluf, G. (2005). Soils of Jelo micro-catchment in the chercher highlands of eastern Ethiopia: I morphological and physicochemical properties. Alemaya Ethiop.

Mohan, M. and Kandya, A. (2015). Impact of urbanization and land-use/landcover change on diurnal temperature range: a case study of tropical urban airshed of India using remote sensing data. *Sci Total Env*. **506**: 453–465.

Mundia, C.N. and Aniya, M. (2005). Analysis of land use/cover changes and urban expansion of Nairobi city using remote sensing and GIS. *Int. J. Remote Sens*. **26**: 2831–2849.

Mustard, J.F., Defries, R.S., Fisher, T. and Moran, E. (2012). Land-use and land-cover change pathways and impacts. *Land Change Sci*. Springer Dordr. Neth. 411–429.

Niamir-Fuller, M., Kerven, C., Reid, R. and Milner-Gulland, E. (2012). Co-existence of wildlife and pastoralism on extensive rangelands: Competition or compatibility? *Pastor Res Policy Pr*. **2**: 1–14.

National Meteorological Agency of Ethiopia (NMA). (1996). National Meteorological Services Agency NMA. 1996. Climate and agro climatic resources of Ethiopia, Meteorological Research Report Series.Vol.1, No.1, Addis Ababa. pp137. Addis Ababa.

Norman, J.M. and Becker, F. (1995). Terminology in thermal infrared remote sensing of natural surfaces. *Agric. For. Meteorol*. **77**: 153–166.

Ottle', C. and Vidal-Madjar, D. (1992). Estimation of land surface temperature with NOAA 9 data. *Remote Sens. Environ*. **40**: 27–41.

Peter, M.V. (1994). Beyond Global Warming: Ecology and Global Change. *Ecol. Soc. Am*. **75**: 1861–1876.

Pham, H.M. and Yamaguchi, Y. (2011). Urban growth and change analysis using remote sensing and spatial metrics from 1975 to 2003 for Hanoi, Vietnam. *Int. J. Remote Sens*. **32**: 1901–1915.

Pomeroy, D., Tukahirwa, J., Mugisha, S., Nanyunja, R., Namaganda, M. and Chelimo, N. (2003). Linkages between Change in Land Use, Land Degradation and Biodiversity in SW Uganda.

Prata, A.J., Caselles, V., Coll, C., Sobrino, J.A. and Ottle, C. (1995). Thermal remote sensing of land surface temperature from satellites: current status and future prospects. *Remote Sens. Rev*. **12**: 175–224.

Price, J.C. (1984). Land surface temperature measurements from the split window channels of the NOAA 7 AVHRR. *J Geophys Res*. **89**: 7231–7237.

Price, J.C. (1983). Estimating surface temperatures from satellite thermal infrared data: A simple formulation for the atmospheric effect. *Remote Sens. Environ*. **13**: 353–361.

Pu, R., Gong, P., Michishita, R. and Sasagawa, T. (2006). Assessment of multi-resolution and multi-sensor data for urban surface temperature retrieval, Thermal Remote Sensing of Urban Areas. *Remote Sens. Environ*. **104**: 211–225.

Qijiao, X. and Zhixiang, Z. (2015). Impact of urbanization on urban heat island effect based on TM imagery in Wuhan, China. *Environ. Eng. Manag. J*. **14**: 647–655.

Qin, Z., Dall'Olmo, G., Karnieli, A. and Berliner, P. (2001b). Derivation of split window algorithm and its sensitivity analysis for retrieving land surface temperature from NOAA-advanced very high resolution radiometer data. *J. Geophys. Res. Atmos*. **106**: 22655–22670.

Qin, Z., Karnieli, A. and Berliner, P. (2001a). A mono-window algorithm for retrieving land surface temperature from Landsat TM data and its application to the Israel-Egypt border region. *Int. J. Remote Sens*. **21**: 3719–3746.

Quentin, F.B., Jim, C., Julia, C., Carole, H. and Andrew, S. (2006). Drivers of land use change, Final report: Matching opportunities to motivations (ESAI project 05116). Department of Sustainability and Environment and primary industries,Royal Melbourne Institute of Technology, Australia.

Rajeshwari, A. and Mani, N.D. (2014). Estimation of Land Surface Temperature of Dindigul District Using Landsat 8 Data. *Int. J. Res. Eng. Technol*. **3**: 122–126.

Reenberg, A. (2006). Land systems research in Denmark: Background and perspectives. *Geogr. Tidsskr. Dan. J. Geogr*. **106**: 1–6.

Richards, J.A. and Jia, X. (2006). Remote Sensing Digital Image Analysis: An introduction, 4th ed. Springer-Verlag Berlin Heidelberg 2006, Germany.

Rozenstein, O., Qin, Z., Derimian, Y. and Karnieli, A. (2014). Derivation of land surface temperature for Landsat-8 TIRS using a split window algorithm. *Sensors*. **14**: 5768–5780.

Sandra, E., Boniface, K., Evanson, N., Julie, G.Z. (2017). Agricultural Expansion and Intensification in the Foothills of Mount Kenya: A Landscape Perspective. *Remote Sens*. **9**: 784.

Sarma, P.K., Lahkar, B.P., Ghosh, S., Rabha, A., Das, J.P., Nath, N.K. and Brahama, N. (2008). Landuse and Landcover change and future implication analysis in Manas National Park, India using multi temporal satellite data. *Curr. Sci*. **95**: 1–5.

Sevgi, Y., Süleyman, T., Nalan, D.Y. and Hasan, Y. (2009). Human population growth and temperature increase along with the increase in urbanisation, motor vehicle numbers and green area amount in the sample of Erzurum city, Turkey. *Env. Monit Assess*. **148**: 205–213.

Sharma, A., Tiwari, K.N. and Bhadoria, P.B.S. (2011). Effect of land use land cover change on soil erosion potential in an agricultural watershed. *Env. Monit Assess*. **173**: 789–801.

Shukla, J., Nobre, C. and Sellers, P. (1990). Amazon Deforestation and Climate Change. *Am. Assoc. Adv. Sci*. **247**: 1322–1325.

Small, C. (2004). Global population distribution and urban land use in geophysical parameter space. *Earth Interact*. **8**: 1–18.

Sobrino, J.A., Coll, C. and Caselles, V. (1991). Atmospheric correction for land surface-temperature using NOAA-11 AVHRR channel-4 and channel-5. *Remote Sens Env*. **38**: 19–34.

Sobrino, J.A., Jimenez-Munoz, J.C. and Paolini, L. (2004a). Land surface temperature retrieval from LANDSAT TM5. *Remote Sens. Environ*. **90**: 434–440.

Sobrino, J.A., Jimenez-Munoz, J.C., El-Kharraz, J., Gomez, M., Romaguera, M. and Soria, G. (2004b). Single-channel and two-channel methods for land surface temperature retrieval from DAIS data and its application to the Barrax site. *Int. J. Remote Sens*. **25**: 215–230.

Sobrino, J.A., Jimenez-Munoz, J.C., Zarco-Tejada, P.J., Sepulcre-Canto, G., de Miguel, E., Soria, G., Romaguera, M., Julien, Y., Cuenca, J., Hidalgo, V., Franch, B., Mattar, C., Morales, L., Gillespie, A., Sabol, D., Balick, L., Su, Z., Jia, L., Gieske, A., Timmermans, W., Olioso, A., Nerry, F., Guanter, L., Moreno, J. and Shen, Q. (2009). Thermal remote sensing from airborne hyperspectral scanner data in the framework of the SPARC and SEN2FLEX projects: an overview. *Hydrol Earth Syst Sc*. **13**, 2031– 2037.

Sobrino, J.A. and Raissouni, N. (2000). Toward remote sensing methods of land cover dynamic monitoring: Application to Morocco. *Int. J. Remote Sens*. **21**: 353–366.

Sobrino, J.A., Raissouni, N. and Li, Z.L. (2001). A comparative study of land surface emissivity retrieval from NOAA data. *Remote Sens. Environ*. **75**: 256–266.

Srivastava, P.K., Majumdar, T.J. and Bhattacharya, A.K. (2010). Study of land surface temperature and spectral emissivity using multi-sensor satellite data. *J Earth Syst Sci*. **119**: 67–74.

Sun, Q., Wu, Z. and Tan, J. (2012). The relationship between land surface temperature and land use/land cover in Guangzhou, China. *Environ. Earth Sci*. **65**: 1687–1694.

Susskind, J., Rosenfield, J., Reuter, D. and Chahine, M.T. (1984). Remote sensing of weather and climate parameters from HIRS2/Msu on TIROS-N. *J. Geophys. Res*. **89**: 4677–4697.

Tang, Z., Shi, C.B. and Bi, K.X. (2014). Impacts of land cover change and socioeconomic development on ecosystem service values. *Environ. Eng. Manag. J*. **13**: 2697–2705.

Taubenböck, H., Esch, T. and Felbier, A. (2012). Monitoring urbanization in mega cities from space. *Remote Sens. Environ*. **117**: 162–176.

Temesgen, G., Amare, B. and Abraham, M. (2014). Evaluations of Land Use/Land Cover Changes and Land Degradation in Dera District, Ethiopia: GIS and Remote Sensing Based Analysis. *Int. J. Sci. Res. Environ. Sci*. **2**: 199–208.

Temesgen, M., Hoodmold, W., Rockstrom, G. and Savenije, H.H. (2009). Conservation tillage implements and system for smallholder farmers in some arid Ethiopia. *Soil Tillage Res*. **104**: 185–191.

Tilahun, A., Takele, B. and Endrias, G. (2001). Reversing the degradation of arable land in the Ethiopian Highlands. **In**: Preceding. International center for research in agro-forestry. (Managing Africa's Soils No. 23)

Tsehaye, G. and Mohammed, A. (2013). Effects of slope aspect and vegetation types on selected soil properties in a dryland Hirmi watershed and adjacent agro-ecosystem, northern highlands of Ethiopia. *Afr J Ecol*. **52**: 1–8.

UN-HABITAT. (2013). State of the World's Cities 2012/2013: Prosperity of Cities. Routledge Taylor & Francis Group, United Nations Human Settlements Programme, New York.

UN-HABITAT. (2010). State of the World's Cities 2010/2011: Prosperity of Cities. Earthscan, UK, United Nations Human Settlements Programme.

United Nations. (2014). World Urbanization Prospects: The 2014 Revision, Highlights (No. ST/ESA/SER.A/352). United Nations, Department of Economic and Social Affairs, Population Division, New York.

United States Environmental Protection Agency (EPA). (1999). Land Cover Trends: Rates, Causes, and Consequences of Late-Twentieth Century U.S. Land Cover Change.

USGS. (2016). Landsat 8 (L8) Data Users Handbook. Department of the Interior U.S. Geological Survey.

Valor, E. and Caselles, V. (1996). Mapping land surface emissivity from NDVI: Application to European, African, and South American areas. *Remote Sens. Environ*. **57**: 167–184.

Van De Griend, A.A. and Owe, M. (1993). On the relationship between thermal emissivity and the normalized diVerence vegetation index for natural surfaces. *Int. J. Remote Sens*. **14**: 1119–1131.

Veldkamp, A. and Lambin, E.F. (2001). Predicting land-use change. *Agric Ecosyst Env*. **85**: 1–6.

Verheye, W.H. (2007). Factors affecting land use and land cover change. **In**: Preceding of Briassoulis, Land Use, Land Cover and Soil Sciences (9). Mytilini.

Vlassova, L., Perez-Cabello, F., Nieto, H., Martín, P., Riaño, D. and de la Riva, J. (2014). Assessment of methods for land surface temperature retrieval from Landsat-5 TM images applicable to multiscale tree-grass ecosystem modeling. *Remote Sens*. **6**: 4345–4368.

Voolgt, J. and Oke, T. (2003). Thermal remote sensing of urban climates. *Remote Sens. Environ*. **86**: 370–384.

Wang, F., Qin, Z., Song, C., Tu, L., Karnieli, A. and Zhao, S. (2015). An improved mono-window algorithm for land surface temperature retrieval from landsat 8 thermal infrared sensor data. *Remote Sens*. **7**: 4268–4289.

Wang, M., Yan, X., Liu, J. and Zhang, X. (2013). The contribution of urbanization to recent extreme heat events and a potential mitigation strategy in the Beijing-Tianjin-Hebei metropolitan area. *Theor Appl Clim*. **114**: 407–416.

Warra, H.H., Mohammed, A.A. and Nicolau, M.D. (2013). Spatio-temporal impact of socio-economic practices on land use/land cover in the kasso catchment, bale mountains, Ethiopia. **In**: Scientific Annals of "Alexandru Ioan Cuza" University of IASI, Volume LIX, no.1, S. II C, Geography Series, 1–26.

Wei, H., Yongnian, Z. and Songnian, L. (2015). An analysis of urban expansion and its associated thermal characteristics using Landsat imagery. *Geocarto Int*. **30**: 93–103.

Weng, Q. (2012). Remote sensing of impervious surfaces in the urban areas: requirements, methods, and trends. *Remote Sens. Environ*. **117**: 34–49.

Weng, Q. (2003). Fractal analysis of satellite-detected urban heat island effect. *Photogramm. Eng. Remote Sens*. **69**: 555–565.

Weng, Q. (2001). A remote sensing? GIS evaluation of urban expansion and its impact on surface temperature in the Zhujiang Delta, China. *Int. J. Remote Sens*. **22**: 1999–2014.

Weng, Q., Lu, D. and Schubring, J. (2004). Estimation of land surface temperature-vegetation abundance relationship for urban heat island studies. *Remote Sens. Environ*. **89**: 467–483.

Weng, Q.H. (2009). Thermal infrared remote sensing for urban climate and environmental studies: methods, applications, and trends. *Isprs J Photogramm*. **64**: 335–344.

William, B.M. and Turner, B.L. (1992). Human Population Growth and Global Land-Use/Cover Change. *Annu. Rev. Ecol. Syst*. **23**: 39–61.

Wilson, E.H., Hurd, J.D., Civco, D.L., Prislof, M.P. and Arnold, C. (2003). Development of a geospatial model to quantify, describe and map urban growth. *Remote Sens. Environ*. **86**: 275–285.

Woldeamlak, B. (2002). Land cover dynamics since the 1950s in chemoga watershed, Blue Nile Basin. *Mt Res Dev*. **22**: 263–269.

Woldeamlak, B. and Sterk, G. (2005). Dynamics in land cover and its effect on stream flow in the chemoga watershed, blue Nile basin, Ethiopia. *Hydrol Process*. **19**: 445–458.

Woldemichael, A.T., Hossain, F., Pielke, R. and Beltrán-Przekurat, A. (2012). Understanding the impact of dam-triggered land use/land cover change on the modification of extreme precipitation. *Water Resour Res*. **48**: 1–16.

Woodcock, C.E., Macomber, S.A. and Kumar, L. (2002). Vegetation Mapping and Monitoring. In: Skidmore, A.K. Environmental Modelling with GIS and Remote Sensing. Taylor and Francis, London, UK.

Wu, C.D., Lung, S.C.C. and Jan, J.F. (2013). Development of a 3-D urbanization index using digital terrain models for surface urban heat island effects. *ISPRS J. Photogramm. Remote Sens*. **81**: 1–11.

Wubalem, T. (2012). The status of forestry development in Ethiopia: challenges and opportunities. **In**: Preceding of National Dialog on Sustainable Agricultural Intensification in Ethiopia and Its Role on the Climate Resilient Green Economy Initiative in Ethiopia July 23rd and 24th, 2012, ILRI Campus. Addis Ababa, Ethipia.

Xiaolei, Y., Xulin, G. and Zhaocong, W. (2014). Land Surface Temperature Retrieval from Landsat 8 TIRS: Comparison between Radiative Transfer Equation-Based Method, Split Window Algorithm and Single Channel Method. *Remote Sens*. **6**: 9829–9852.

Yadvinder, M., J. Timmons, R., Richard, A.B., Timothy, J.K., Wenhong, L. and Carlos, A.N. (2008). Climate Change, Deforestation, and the Fate of the Amazon. *Science*. **319**: 169–172.

Yanagi, T. (2008). Water temperature changes of 1.5 ℃ per decade in Tokyo Bay, Japan: its causes and consequences. *J. Disaster Res*. **3**: 113–118.

Yeshaneh, E., Wolfgang, W., Michael, E., Legesse, D. and Günter, B. (2013). Identifying land use/cover dynamics in the koga catchment, Ethiopia, from multi-scale data, and implications for environmental change. *ISPRS Int J Geo Inf*. **2**: 302–323.

Yuan, F. and Bauer, M.E. (2007). Comparison of impervious surface area and normalized difference vegetation index as indicators of surface urban heat island effects in Landsat imagery. *Remote Sens. Environ*. **106**: 375–386.

Yue, W., Xu, J., Tan, W. and Xu, L. (2007). The relationship between land surface temperature and NDVI with remote sensing: application to Shanghai Landsat 7 ETM+ data. *Int. J. Remote Sens*. **28**: 3205–3226.

Zhao, M., Cai, H., Qiao, Z. and Xu, X. (2016). Influence of urban expansion on the urban heat island effect in Shanghai. *Int. J. Geogr. Inf. Sci*. **30**: 2421–2441.

Zhao, S. and Lai, P. (2007). Millennium Ecosystem Assessment.

Zheng, B.J., Myint, S.W. and Fan, C. (2014). Spatial configuration of anthropogenic land cover impacts on urban warming. *Landsc. Urban Plan*. **130**: 104–111.

Zhenglei, X., Xuegong, X. and Lei, Y. (2009). Analyzing qualitative and quantitative changes in coastal wetland associated to the effects of natural and anthropogenic factors in a part of Tianjin, China. *Estuar. Coast. Shelf Sci*. **86**: 379–386.

Zhou, D., Zhao, S., Liu, S., Zhang, L. and Zhu, C. (2014). Surface urban heat island in China's 32 major cities: Spatial patterns and drivers. *Remote Sens. Environ*. **152**: 51–61.

Zhu, J., Tian, S., Tan, K. and Du, P. (2016). Human Settlement Analysis Based on Multi-temporal Remote Sensing Data: A Case Study of Xuzhou City, China. *Chin. Geogr. Sci*. **26**: 389–400.

Zubair, A.O. (2006). Change detection in land use and Land cover using remote sensing data and GIS (A case study of Ilorin and its environs in Kwara State) (MSc. Thesis). University of Ibadan, Nigeria.

Appendices

Appendix 1: Sample LULC photographs

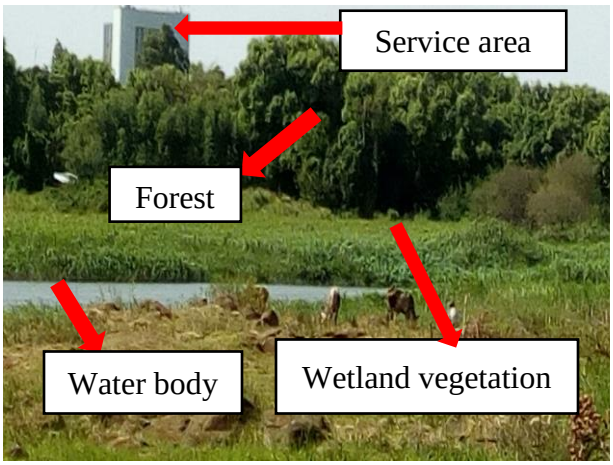


Shrubland

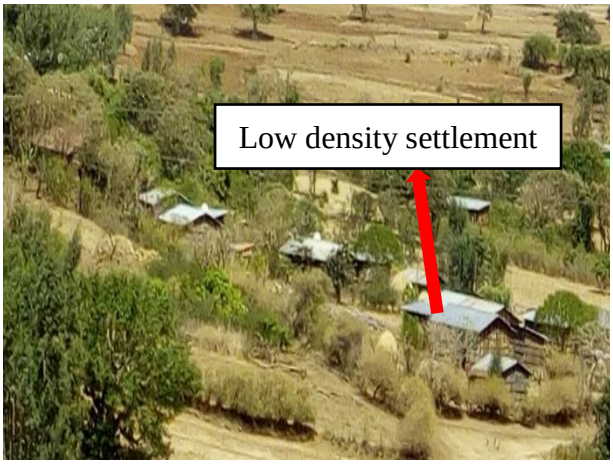
Low density settlement


Green area


Grassland

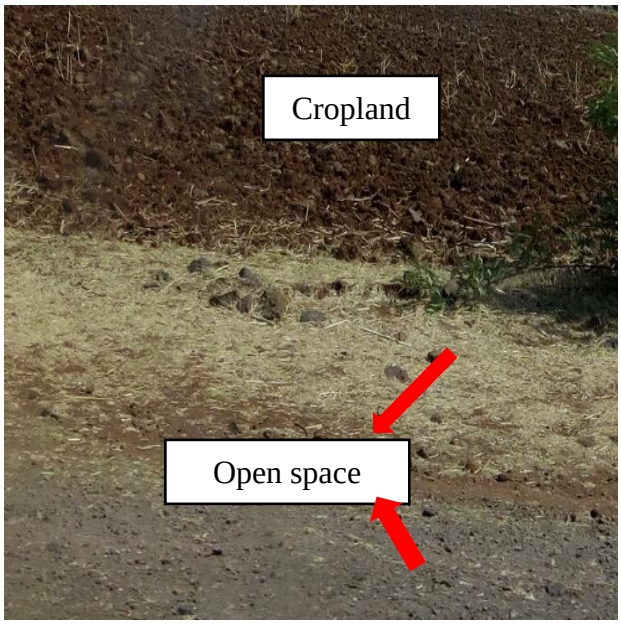
Cropland
Open space


Recreation

Appendix 2: 2017 Landsat image with its LULC photo

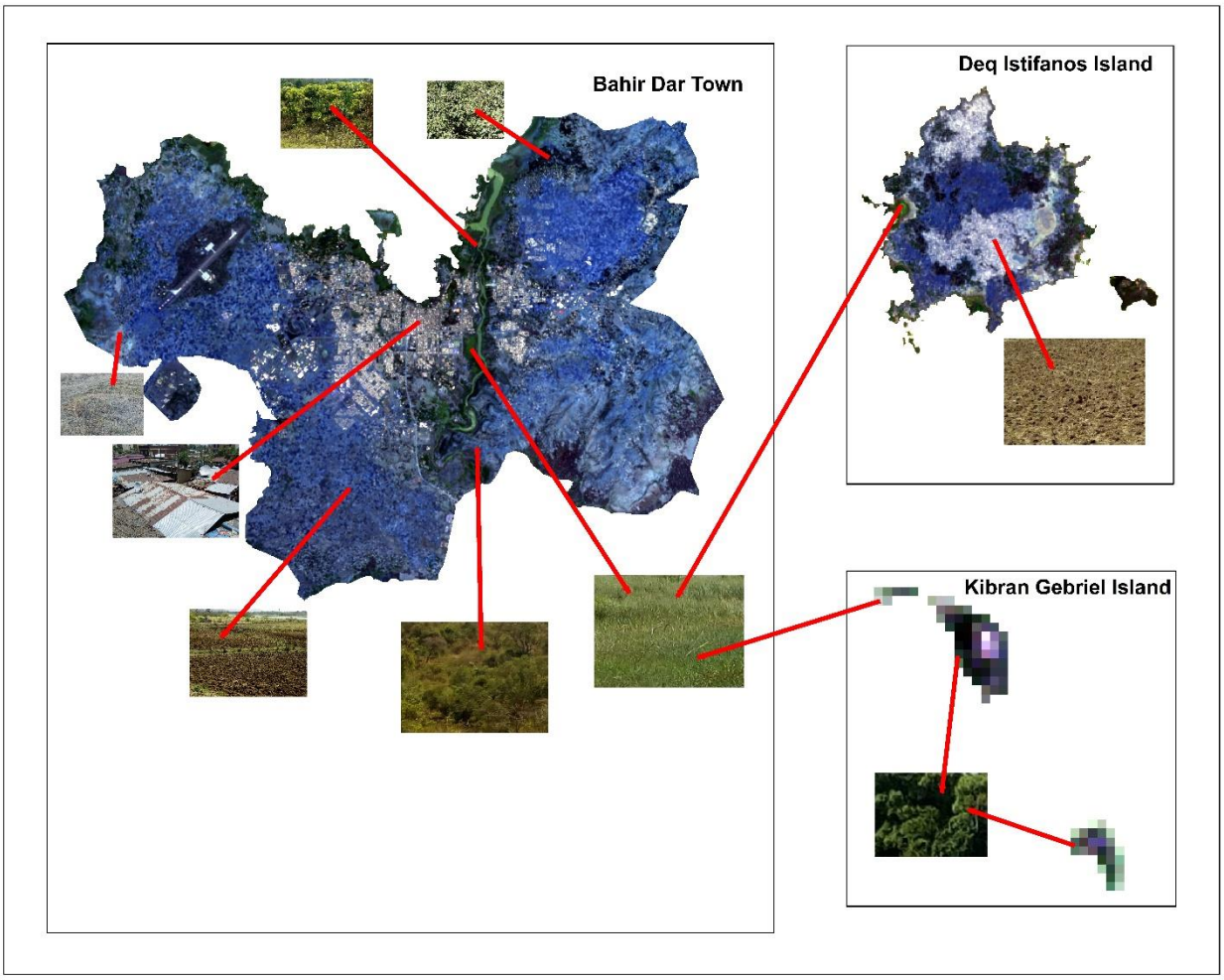

Appendix 3: Ground truth points map

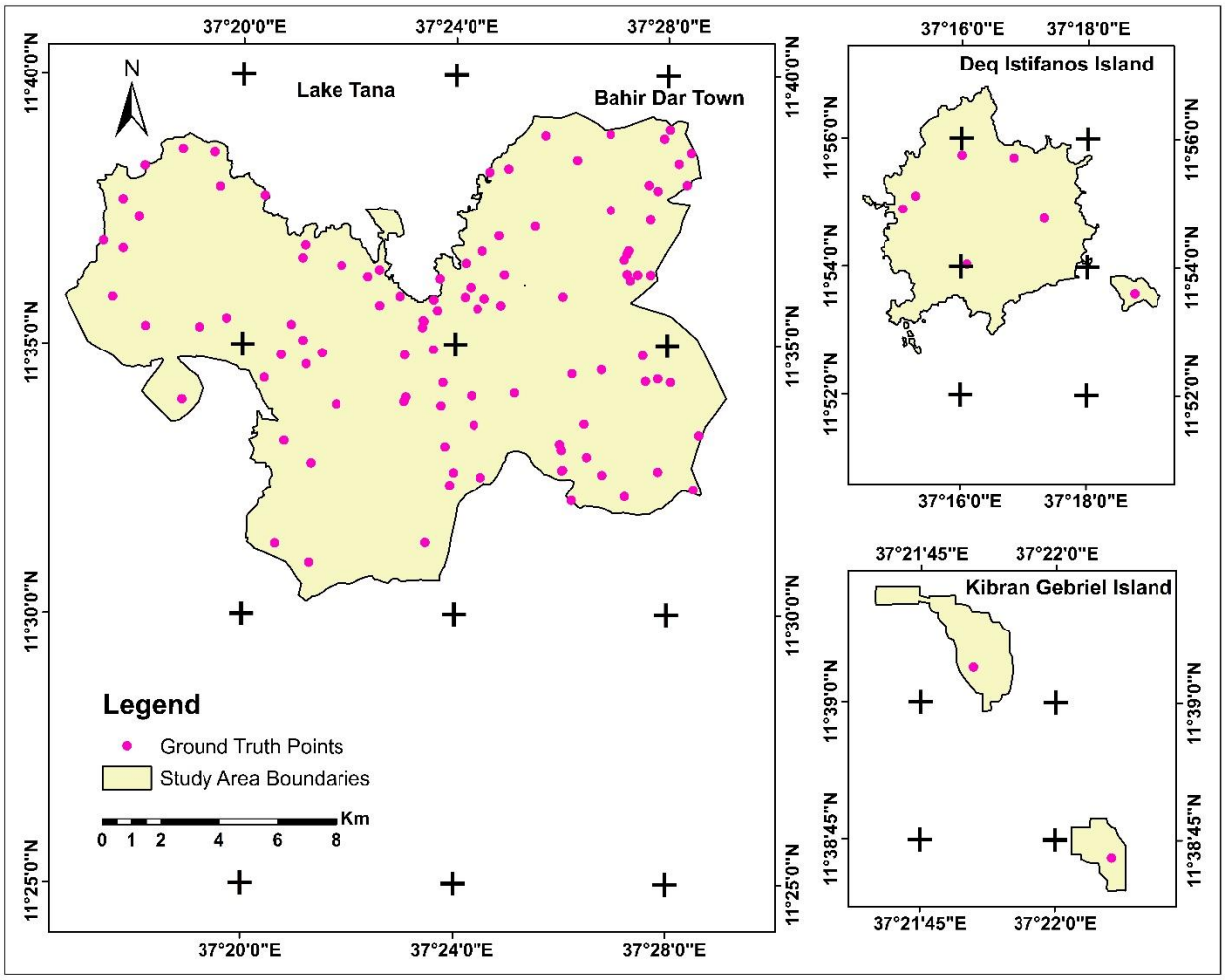

Appendix 4: Accuracy assessment for 1987

		Reference Data															
		CL	**FO**	**GL**	**HDS**	**IN**	**LDS**	**OP**	**PL**	**PS**	**RV**	**SA**	**SH**	**WB**	**WV**	**RT**	**UA**
Classified Data	**CL**	**6**	0	1	0	0	0	0	1	0	0	0	0	0	0	**8**	75
	FO	0	**8**	0	0	0	0	0	0	0	0	0	0	0	0	**8**	100
	GL	1	0	**7**	0	0	0	0	0	0	0	0	0	0	0	**8**	87.5
	HDS	0	0	0	**8**	0	0	0	0	0	0	0	0	0	0	**8**	100
	IN	0	0	0	0	**8**	0	0	0	0	0	0	0	0	0	**8**	100
	LDS	2	0	0	0	0	**6**	0	0	0	0	0	0	0	0	**8**	75
	OP	0	0	1	0	0	0	**7**	0	0	0	0	0	0	0	**8**	87.5
	PL	0	0	0	0	0	0	0	**8**	0	0	0	0	0	0	**8**	100
	PS	0	0	0	0	2	0	0	0	**6**	0	0	0	0	0	**8**	75
	RV	0	0	0	0	0	0	0	0	0	**5**	0	3	0	0	**8**	62.5
	SA	0	0	0	3	0	0	0	0	0	0	**5**	0	0	0	**8**	62.5
	SH	0	1	0	0	0	0	0	0	0	0	0	**7**	0	0	**8**	87.5
	WB	0	0	0	0	0	0	0	0	0	0	0	0	**7**	1	**8**	87.5
	WV	0	0	0	0	0	0	0	0	0	0	0	0	0	**8**	**8**	100
	CT	**9**	**9**	**9**	**11**	**10**	**6**	**7**	**9**	**6**	**5**	**5**	**10**	**7**	**9**	**112**	
	PA	66.67	88.89	77.78	72.73	80	100	100	88.9	100	100	100	70	100	88.89		
	OA	85.71															
	$\hat{K}$	0.854															

Where: CL=cropland, FO= forest, GL=grassland, HDS=high density settlement, IN=industrial area, OP=open space, PL=plantation, PS=paved surface, RV=riparian vegetation, SA=service area, SH=shrubland, LDS=low density settlement, WB=water body, WV=wetland vegetation, PA=producer accuracy, UA=user accuracy, OA= overall accuracy, $\hat{K}$ *= kappa coefficient*

Appendix 5: Accuracy assessment for 2002

		Reference Data														
		CL	**FO**	**GL**	**HDS**	**IN**	**LDS**	**OP**	**PL**	**PS**	**RV**	**SA**	**SH**	**WB**	**WV**	**RT**	**UA**
Classified Data	**CL**	**6**	0	1	0	0	0	0	1	0	0	0	0	0	0	**8**	75
	FO	0	**8**	0	0	0	0	0	0	0	0	0	0	0	0	**8**	100
	GL	0	0	**5**	0	0	0	3	0	0	0	0	0	0	0	**8**	62.5
	HDS	0	0	0	**8**	0	0	0	0	0	0	0	0	0	0	**8**	100
	IN	0	0	0	0	**8**	0	0	0	0	0	0	0	0	0	**8**	100
	LDS	2	0	0	0	0	**5**	0	0	0	0	1	0	0	0	**8**	62.5
	OP	0	0	0	0	0	0	**8**	0	0	0	0	0	0	0	**8**	100
	PL	0	0	0	0	0	0	0	**8**	0	0	0	0	0	0	**8**	100
	PS	0	0	0	0	2	0	0	0	**6**	0	0	0	0	0	**8**	75
	RV	0	0	0	0	0	0	0	0	0	**5**	0	3	0	0	**8**	62.5
	SA	0	0	0	0	0	0	0	0	0	0	**8**	0	0	0	**8**	100
	SH	0	1	0	0	0	0	0	0	0	0	0	**7**	0	0	**8**	87.5
	WB	0	0	0	0	0	0	0	0	0	0	0	0	**7**	1	**8**	87.5
	WV	0	0	0	0	0	0	0	0	0	0	0	0	0	**8**	**8**	100
	CT	**8**	**9**	**6**	**8**	**10**	**5**	**11**	**9**	**6**	**5**	**9**	**10**	**7**	**9**	**112**	
	PA	75	88.89	83.33	100	80	100	72.73	88.9	100	100	88.89	70	100	88.89		
	OA	86.61															
	$\widehat{K}$	0.864															

Where: CL=cropland, FO= forest, GL=grassland, HDS=high density settlement, IN=industrial area, OP=open space, PL=plantation, PS=paved surface, RV=riparian vegetation, SA=service area, SH=shrubland, LDS=low density settlement, WB=water body, WV=wetland vegetation, PA=producer accuracy, UA=user accuracy, OA= overall accuracy, $\widehat{K}$ *= kappa coefficient*

Appendix 6: Accuracy assessment for 2017

		Reference Data														
		CL	**FO**	**GL**	**HDS**	**IN**	**LDS**	**OP**	**PL**	**PS**	**RV**	**SA**	**SH**	**WB**	**WV**	**RT**	**UA**
Classified Data	**CL**	**7**	0	1	0	0	0	0	0	0	0	0	0	0	0	**8**	87.5
	FO	0	**6**	0	0	0	1	0	0	0	0	0	1	0	0	**8**	75
	GL	0	0	**5**	0	0	0	2	0	0	0	0	0	0	1	**8**	62.5
	HDS	0	0	0	**8**	0	0	0	0	0	0	0	0	0	0	**8**	100
	IN	0	0	0	0	**8**	0	0	0	0	0	0	0	0	0	**8**	100
	LDS	0	0	0	0	0	**7**	0	0	0	0	1	0	0	0	**8**	87.5
	OP	0	0	0	0	0	0	**8**	0	0	0	0	0	0	0	**8**	100
	PL	0	0	0	0	0	0	0	**8**	0	0	0	0	0	0	**8**	100
	PS	0	0	0	0	1	0	0	0	**7**	0	0	0	0	0	**8**	87.5
	RV	0	0	0	0	0	0	0	0	0	**8**	0	0	0	0	**8**	100
	SA	0	0	0	0	0	0	0	0	0	0	**8**	0	0	0	**8**	100
	SH	0	1	0	0	0	0	0	0	0	0	0	**7**	0	0	**8**	87.5
	WB	0	0	0	0	0	0	0	0	0	0	0	0	**8**	0	**8**	100
	WV	0	0	0	0	0	0	0	0	0	0	0	0	0	**8**	**8**	100
	CT	**7**	**7**	**6**	**8**	**9**	**8**	**10**	**8**	**7**	**8**	**9**	**8**	**8**	**9**	**112**	
	PA	100	85.7	83.3	100	88.889	87.5	80	100	100	100	88.889	87.5	100	88.8889		
	OA	92															
	$\widehat{K}$	0.92															

Where: CL=cropland, FO= forest, GL=grassland, HDS=high density settlement, IN=industrial area, OP=open space, PL=plantation, PS=paved surface, RV=riparian vegetation, SA=service area, SH=shrubland, LDS=low density settlement, WB=water body, WV=wetland vegetation, PA=producer accuracy, UA=user accuracy, OA= overall accuracy, $\widehat{K}$ *= kappa coefficient*

Declaration

I hereby declare that this MSc. thesis paper for the partial fulfillment of the requirements for the degree of Master of Science in Remote Sensing and Geo-informatics entitled “Impacts of Land-use and Land-cover Changes on Land Surface Temperature Distribution in Bahir Dar Town and its Surrounding Using Remote Sensing” is my original research work prepared independently by my own effort with the close advice and guidance of my adviser. I have not submitted it or any of its part to any other academic institutions for any degree and all sources that I have used have been indicated and acknowledged by means of complete references.

Abel Balew _____ _____/_____/_____

Signature Date

I thesis has been submitted for examination with my approval as university advisor.

Dr. Tesfaye Korme _____ _____/_____/_____

Signature Date